Dissertation

with the aim of achieving the degree

doctor rerum naturalium

Role of the γ-subunit of GlcNAc-1-phosphotransferase in the pathogenesis of mucolipidosis type III

submitted by

Giorgia Di Lorenzo

from Giulianova (TE) Italy

at the Department of Biology,

Faculty of Mathematics, Informatics and Natural Sciences,

University of Hamburg

Hamburg, 2018

To my family

Academic advisor: Prof. Dr. Thomas Braulke

Co-advisors: Prof. Dr. Tim-Wolf Gilberger

Date of disputation: 22nd June 2018

Index

1. Introduction

1.1 Synthesis and transport of lysosomal protein

Eukaryotic cells contain numerous membrane bound organelles of different functions. More than 60 years ago, Christian de Duve has discovered the lysosomes (De Duve *et al*, 1955), which play a crucial role in cell metabolism. Lysosomes have a single-lipid bilayer membrane limiting an acidic lumen (pH < 5), that is maintained by the V-type H^+-ATPase which transports protons from the cytosol into the lysosomal lumen. The low pH is essential for the activity of 70 lysosomal enzymes required for degradation of intracellular and extracellular macromolecules. Extracellular materials reach the lysosomes mainly through endocytic pathway, while intracellular components are delivered to lysosomes by autophagy. After degradation of lipids, polysaccharides, proteins and nucleic acids, the catabolites are translocated from the lumen of lysosomes into the cytosol by specific transporters and reused by the cell (Saftig and Klumperman 2009).

1.1.1 Biosynthesis of soluble lysosomal proteins

Soluble lysosomal proteins are synthesised at ribosomes of the endoplasmic reticulum (ER). They contain an *N*-terminal sequence of 20-25 amino acids that drives the translocation of the precursor proteins into the ER lumen. In a first step a signal peptide of the nascent proteins bind to signal recognition particles (SRP) which are then recruited to the SRP receptors and translocated into the ER lumen (Saraogi & Shan, 2011). The signal peptides are cleaved by signal peptidases and the remaining proteins undergo posttranslational *N*-glycosylation. First, a preformed oligosaccharide core $Glc_3Man_9GlcNAc_2$ is added to selected asparagine residues that are part of the Asn-X-Ser/Thr consensus sequence (X can be any amino acid except proline or asparagine) of the polypeptides (Ruddock & Molinari, 2006). The *N*-glycan structure is further modified by glycosidases ("trimming") in the ER lumen such as α-glucosidase I and II that removes the terminal and the two inner glucose residues, respectively. The chaperones calreticulin or calnexin can bind to the resulting Man_9GlcAc_2 high-mannose-type glycans until the folding of the newly synthesized proteins is completed.

Upon arrival in the Golgi apparatus the oligosaccharides can be further modified by transfer of complex sugars like fucose, galactose, *N*-acetylglucosamine (GlcNAc) and sialic acid (Helenius & Aebi, 2001).

1.1.2   Generation of mannose 6-phosphate residues on lysosomal enzymes

The formation of mannose 6-phosphate (M6P) residues on selected mannoses of high-mannose type oligosaccharides on newly synthesized soluble lysosomal enzymes is required for their effective targeting to the endosomal/lysosomal compartment. This specific M6P modification is generated in a two-step reaction. In the *cis*-Golgi apparatus GlcNAc-1-phosphotransferase recognizes lysosomal enzymes and catalyses the transfer of GlcNAc-1-phosphate from the donor UDP-GlcNAc to the C6 hydroxyl groups of selected mannose residues. The first phosphodiester modification takes place in the α-1,6 branch of the high mannose-type glycan and a further phosphorylation can occurs in the α-1,3 branch (Pohl *et al*, 2009a). In the second step the GlcNAc-1-phosphodiesterase (uncovering enzyme) localized in the *trans*-Golgi network (TGN) hydrolyse the covering GlcNAc residue from the *N*-linked glycan exposing the M6P marker.

In the TGN, M6P-containing proteins are recognized by two M6P receptors (MPRs), the 46 kDa cation-dependent MPR46 and the 300 kDa cation-independent MPR300 (Braulke & Bonifacino, 2009). The MPR-enzyme complexes are transported to early endosomes in clathrin-coated vesicles (Fig. 1.1). In late endosomes, the acidic pH leads to the dissociation of the lysosomal enzymes from the MPRs. The lysosomal enzymes reach their final destination by fusion of endosomes and lysosomes. The MPRs cycle back to the TGN, where they start a new sorting cycle (Fig. 1.1).

A portion of newly synthesized lysosomal enzymes (5-10%) escape the binding to MPR in the TGN and are secreted to the extracellular space, where they can be partially recaptured by MPR300 located at the plasma membrane. These MPR-enzyme complexes are internalized by clathrin-dependent endocytosis and transported to lysosomes via the endosomal compartment (Braulke & Bonifacino, 2009; Fig. 1.1).

Usually, in the lumen of lysosomes the enzymes are dephosphorylated by the concerted action of Acp2 (lysosomal acid phosphatase) and Acp5 (tartrate-resistant acid phosphatase) (Makrypidi *et al*, 2012).
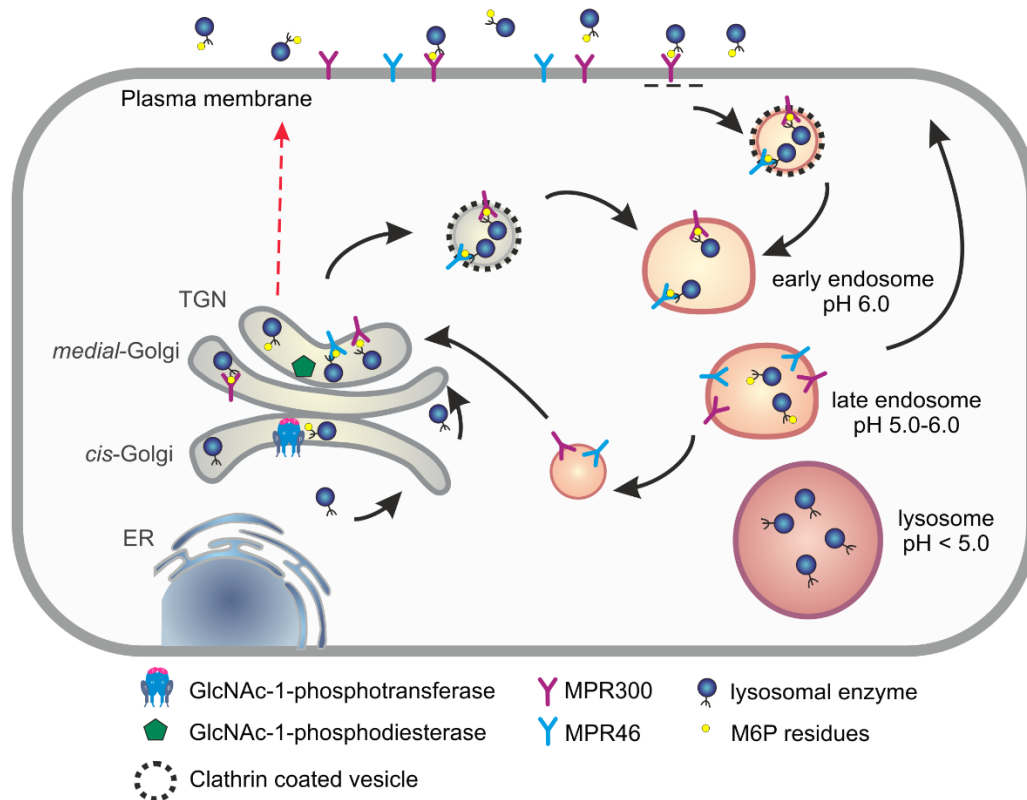
Figure 1.1. Schematic representation of M6P-dependent transport of soluble lysosomal enzymes. In the Golgi apparatus GlcNAc-1-phoshotransferase and -diesterase synthesize M6P residues on newly synthesized lysosomal enzymes. In the TGN MPR46 and MPR300 recognize M6P-containing lysosomal enzymes, and these complexes are transported via clathrin-coated vesicles to early endosomes. In late endosomes the release of MPRs is induced by reduced pH, followed by retrograde MPR transport to the TGN and delivery of enzymes into lysosomes. Secreted M6P-containing lysosomal enzymes can be partially recaptured by MPR300 at the plasma membrane, re-internalized and transported to lysosomes.

1.1.3   GlcNAc-1-phosphotransferase

The GlcNAc-1-phosphotransferase is a 540 kDa heterohexameric complex consisting of two membrane-bound α- and β-subunits and two soluble γ-subunits ($\alpha_2\beta_2\gamma_2$) (Bao *et al*, 1996; Fig. 1.2A). The human α- and β-subunits are encoded by the *GNPTAB* gene and are synthesized as a common type III precursor membrane protein of 1,256 amino acids with a hairpin orientation projecting both N- and C-terminus into the cytosol (Tiede *et al*, 2005). The covalent dimerization of the α/β-precursor is mediated by cysteine residue C70 located in the α-subunit (De Pace *et al*, 2015).

The human soluble γ-subunit is composed of 305 amino acids which contains an N-terminal signal peptide of 24 amino acids for translocation into the ER. The γ-subunit has two *in-vivo* used *N*-glycosylation sites at positions N88 and N115 (Fig. 1.2B) modified with high mannose- and hybrid-type oligosaccharides, which was found to be crucial for ER exit and the stability of the protein. Moreover, the cysteine residue C245 is responsible for disulfide-linked homodimer formation of the γ-subunits (Encarnação *et al*, 2011). Of note, the soluble γ-subunit was also found to be secreted (Encarnação *et al*, 2011).

After assembly of the α/β-subunit precursors with the γ-subunits of the GlcNAc-1-phosphotransferase in the ER, the inactive enzyme complex is transported to the Golgi apparatus mediated by a combinatorial cytoplasmic sorting motif of the α/β-subunit precursor protein (Encarnação *et al*, 2011; Franke *et al*, 2013). Upon arrival in the *cis*-Golgi apparatus, the α/β-subunit precursor is proteolytically cleaved by the site-1 protease into the individual α- and β-subunits, which is prerequisite for catalytic GlcNAc-1-phosphotransferase activity (Marschner *et al*, 2011). Recently, the γ-subunit binding domain was identified in a region of the α-subunit that is required for maximum GlcNAc-1-phosphotransferase activity (De Pace *et al*, 2015; Velho *et al*, 2016a). Whereas the α- and β-subunit harbour the substrate binding sites and the catalytic center of the GlcNAc-1-phosphotransferase, the functions of the γ-subunits are poorly defined. Since direct interactions of γ-subunits with lysosomal enzymes were excluded (Tiede *et al*, 2005; Pohl *et al*, 2009b), the current view suggests the enhanced recognition and binding of lysosomal enzymes to the α-subunits by γ-subunits (Qian *et al*, 2010).
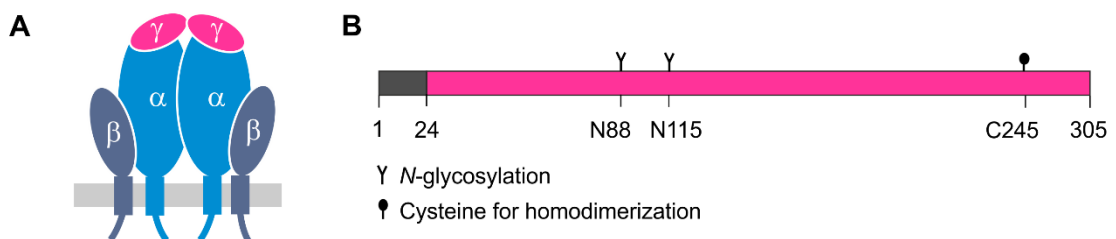
Figure 1.2. Schematic representation of the GlcNAc-1-phosphotransferase. A) GlcNAc-1-phosphotransferase consists of two membrane bound α- and β-subunits and two soluble γ-subunits ($\alpha_2\beta_2\gamma_2$). Both α- and γ-subunits forms covalently linked homodimers. **B)** Schematic representation of human γ-subunits composed by 305 amino acids containing an N-terminal signal peptide of 24 amino acids, two *N*-glycosylation sites at positions N88 and N115 and the cysteine residue C245 responsible for dimerization.

1.2 Mucolipidosis type II and III

Mucolipidosis (ML) type II and III are autosomal recessive inherited lysosomal storage disorders (Cathey *et al*, 2008). Mutations in the *GNPTAB* gene, encoding the α/β-precursor of GlcNAc-1-phosphotransferase, cause MLII that result in the complete loss of GlcNAc-1-phosphotransferase activity (Tiede *et al*, 2005). In addition, mutation in the *GNPTG* gene encoding the γ-subunit results in MLIII characterized by reduced GlcNAc-1-phosphotransferase activity (Raas-Rothschild *et al*, 2000). Biochemically in cells from MLII and MLIII patients the formation of M6P residues on newly synthesized lysosomal enzymes is lacking or strongly reduced, respectively. This prevents or reduces the recognition by MPR in the TGN which consequently leads to their missorting and hypersecretion into the extracellular space (Kollmann *et al*, 2010). The subsequent deficiencies of intracellular lysosomal enzymes result in cell- and tissue-specific accumulation of non-degradable macromolecules in lysosomes and in lysosomal dysfunction. The diagnosis of MLII and MLIII patients is confirmed by elevated lysosomal enzyme activities in the serum, and decreased activities of lysosomal enzymes in cultured fibroblasts (Raas-Rothschild *et al*, 2012). Of note, this analysis does not allow the distinction between MLII and MLIII. Therefore sequencing of the *GNPTAB* and *GNPTG* genes is required (Pohl *et al*, 2010a).

Clinically, MLII patients are characterized by severe psychomotor retardation, skeletal abnormalities, organomegaly, immune defects, coarse facial features, and death in the first decade of life (Braulke *et al*, 2013; Otomo *et al*, 2015). In particular, the skeletal abnormalities in MLII patients comprise growth defects, osteopenia, wide ribs and vertebral bodies, marked scoliosis, short diameter of the vertebral bodies, narrowed ilia, broad phalanges and facial coarseness with a depressed nasal bridge (Cathey *et al*, 2010; Raas-Rothschild *et al*, 2012; Braulke *et al*, 2013).

MLIII is a more slowly progressive disorder than the MLII disease and characterized by a less progressive phenotype affecting mainly the skeleton, joints and connective tissues. The first clinical symptoms of MLIII patients are joint stiffness of fingers, shoulders as well as hip, elbow, wrist and ankle stiffness in an age between 5 and 10 years of life, and represent cardinal features of the disease (Raas-Rothschild *et al*, 2012). However, MLIII patients are often initially misdiagnosed for juvenile idiopathic arthritis or chronic arthritis (Tüysüz *et al*, 2018).

The weight and length at birth are within the normal range but gradual slowing of growth rate begins in early childhood. The short stature, bowed limbs, dysplasia of the femoral epiphyses, progressive joint stiffness, hip and knee contractures, thoracic asymmetry, wide ribs, congenital hip dislocation associated with shallow acetabula and flared iliac wings, flattened vertebral bodies, kyphoscoliosis, scoliosis and hyperlordosis have been summarized as *dysostosis multiplex*. These clinical features are associated with chronic pain and progressive decline of mobility, strongly reducing the quality of life of MLIII patients (Raas-Rothschild *et al*, 2012). In late childhood skeletal radiographs shows osteopenia characterized by reduced bone density (Raas-Rothschild *et al*, 2012). Moreover, bilateral hip and knee joint replacements are common surgeries in adolescent and adult affected individuals. Some MLIII patients have mild facial dysmorphism and mild to moderate corneal clouding (Raas-Rothschild *et al*, 2004; Raas-Rothschild *et al*, 2012; Tüysüz *et al*, 2018). Neurological symptoms such as carpal tunnel syndrome caused by compression of the median nerve of the wrist have been reported in MLIII patients, which can be treated by surgery (Tylki-Szymanska *et al*, 2002; Smuts *et al*, 2009; Tüysüz *et al*, 2018). Generally MLIII patients appeared to have a normal mental development and cognitive function including language and learning skills. Affected children may require school assistance but mostly because of physical limitations. Some patients are affected by cardiac complications caused by thickening and insufficiency of the mitral and aortic valves (Raas-Rothschild *et al*, 2004; Tüysüz *et al*, 2018). Other organs are usually not affected and MLIII patients do not present hepatosplenomegaly. However, abnormalities of the spine and ribs, a reduced tracheal suppleness from stiff connective tissue, and progressive narrowing of the airway from mucosal thickening may limit lung capacity (Raas-Rothschild *et al*, 2012).

The skin may become thickened with time. Recently scleroderma-like symptoms were described in MLIII patients (Zrhidri *et al*, 2017). In addition, mild hoarseness or metallic voice has been reported in some MLIII patients (Raas-Rothschild *et al*, 2004). Since skeletal dysplasia is the most prominent clinical complication in the MLIII disease, patients can survive into adulthood (Braulke *et al*, 2013). To date, world-wide 36 patient-associated *GNPTG* mutations were identified including missense, nonsense, deletion, frameshift and splice mutations (Table 1.1). However, a correlation between the severity of the disease and the type of mutation has not been reported.

Table 1.1: Summary of known *GNPTG* mutations identified in MLIII patients

Patient (Origin)	*GNPTG* mutation 1. Allele	2. Allele	Reference
1 (Turkey)	p.R66*	p.R66*	Tüysüz *et al*, 2018
2 (Netherlands)	p.R66*	c.318-1G>C[a]	Raas-Rothschild *et al*, 2004
3 (Marroco)	p.R66*	p.F213*	Zrhidri *et al*, 2017
4 (Chile)	c.233+5G>C[a]	c.233+5G>C[a]	Dr. R. V. Velho, unpublished
5-7[b] (China)	c.234-1G>C[a],	p.C157W*fs*5	Gao *et al*, 2011
8-11[b] (Canada)	p.K80_Y81del	p.K80_Y81del	Schrader *et al*, 2011
12 (Brazil)	p.F83*	p.E110*	Velho *et al*, 2014
13 (Turkey)	p.F96L*fs*32	p.F96L*fs*32	Tüysüz *et al*, 2018
14 (Israel)	p.G106S	p.G106S	Raas-Rothschild *et al*, 2004
15-16[b] (Italy)	p.G106S	c.610-2A>G[a]	Persichetti *et al*, 2009
17 (China)	p.W108*	?	Mistri *et al*, 2018
18-19[b] (Brazil)	p.E110*	p.E110*	Velho *et al*, 2016b
20-21[b] (Spain) 22 (USA)	p.W111*	p.W111*	Persichetti *et al*, 2009 Cagle, 2017
23-24[b] (Germany) 25 (Italy) 26-27[b] + 28 (Turkey)	p.N116del	p.N116del	Tiede *et al*, 2004 Persichetti *et al*, 2009 Tüysüz *et al*, 2018
29-30[b] (Turkey)	p.M123V	p.A149F*fs*13	Tüysüz *et al*, 2018
31 (USA)	p.G126S	p.G126S	Barea *et al*, 2015
32 (Finland)	p.D127P*fs*31	p.D127P*fs*31	Raas-Rothschild *et al*, 2004
33-34[b] (Netherlands)	c.411+8del27[a]	c.411+8del27[a]	Dr. S. Pohl, unpublished
35 (China)	p.C142V	p.C142V	Liu *et al*, 2014
36-37[b] (Iran) 38 (USA)	p.A149F*fs*12	p.A149F*fs*12	Raas-Rothschild *et al*, 2004 Zarghooni & Dittakavi, 2009
39-40 (Israel) 41-42 (Turkey)	p.L167P*fs*32	p.L167P*fs*32	Raas-Rothschild *et al*, 2000 Tüysüz *et al*, 2018
43-44[b], 45-46[b], 47 (Israel)	p.V168R*fs*29	p.V168R*fs*29	Raas-Rothschild *et al*, 2004
48-49[b] (India)	p.H172W*fs*28	p.H172W*fs*28	Dr. S. Alves, unpublished
50 (China)	p.H172P*fs*27	p.H172P*fs*27	Liu *et al*, 2014
51-53[b] (Afghanistan)	c.527-10G>A[a]	c.527-10G>A[a]	Pohl *et al*, 2010a
54-56[b] (Turkey)	p.Q203H*fs*4	p.Q203H*fs*4	Raas-Rothschild *et al*, 2004
57 (China)	c.609+1G>C[a]	c.609+1G>C[a]	Liu *et al*, 2014
58 (Italy)	c.609+28_610-16del33[a]	c.609+28_610-16del33[a]	Persichetti *et al*, 2009
59 (Portugal)	c.610-1G>T[a]	p.F213L*fs*7	Encarnação *et al*, 2009
60-61[b] (Italy)	c.611del[a]	c.611del[a]	Persichetti *et al*, 2009
62 (Germany)	p.K207I*fs*8	p.K207I*fs*8	Pohl *et al*, 2009b
63 (Spain)	p.E214K*fs*37	p.E214K*fs*37	Persichetti *et al*, 2009
64 (Turkey)	p.Y218*	p.Y218*	Tüysüz *et al*, 2018
65 (Italy)	p.T286M	?	Persichetti *et al*, 2009

[a] splicing defects, [b] patients from the same family, ? not identified mutation

So far only symptomatic therapies but no treatments are available for MLII and MLIII patients. However, some MLIII patients received treatment with intravenous infusions of the bisphosphonate drug pamidronate. Bisphosphonates bind to the mineralized bone matrix and inhibits osteoclast-mediated bone resorption (Russell, 2011), which was found to reduce bone pain, improve mobility and increase the bone density in MLIII patients (Tüysüz *et al*, 2018).

1.3 Bone formation and remodelling

Bone formation occurs through two distinct processes: intramembranous ossification that produces mainly craniofacial bones, and endochondral ossification which build the vertebrate skeleton (Cohen, 2000). Endochondral ossification is a tightly regulated process based on the transition from cartilage to bone and is performed by a cooperative work of chondrocytes, bone-resorbing osteoclasts and bone-forming osteoblasts. The primary ossification starts during embryonic development and the secondary ossification occurs after birth during skeletal development and takes place in the epiphysis of long bones (Kozhemyakina *et al*, 2015; Fig. 1.3). During embryonic development, mesenchymal progenitors condensate and induce chondrogenesis (Fig. 1.3A; Long & Ornitz, 2013). Chondrocytes produces their own extracellular matrix composed by 60% collagen fibres mainly composed of collagen type II and 25-35% proteoglycans.
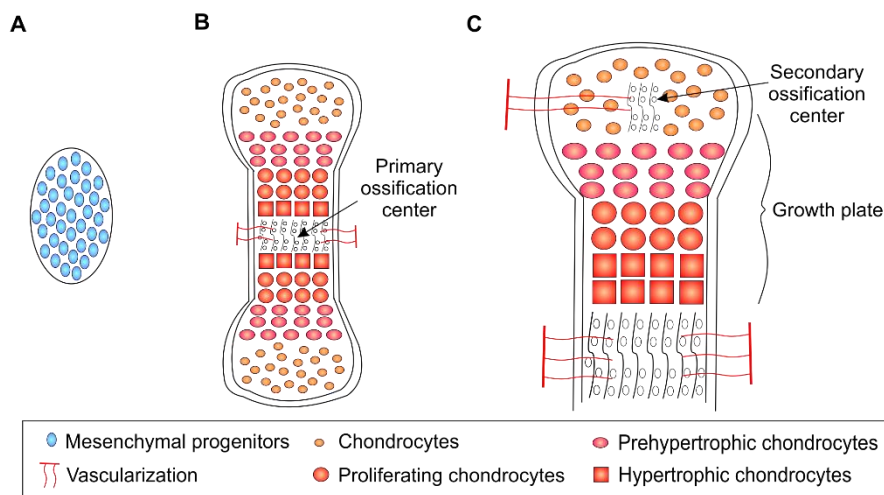
Figure 1.3. Schematic presentation of endochondral bone formation. A) Condensation of mesenchymal progenitors. **B)** Chondrocytes maturation and formation of the primary ossification centre. **C)** Formation of the growth plate chondrocytes and secondary ossification centre.

After the formation of the primordial cartilage, chondrocytes undergo a progressive maturation to proliferating, prehypertrophic and hypertrophic chondrocytes (Gentili & Cancedda, 2009; Fig. 1.3B and C). These cells comprise the growth plate chondrocytes which are located between the primary and the secondary ossification centre (Fig. 1.3C) and control the bone growth and length based on their width. In the center of the growth plate, hypertrophic chondrocytes finally undergo apoptosis which is followed by vascularization (Fig. 1.3B and C) leading to resorption of the residual cartilage matrix by osteoclasts and deposition of new trabecular bone by osteoblasts (Long & Ornitz, 2013). This process leads to the formation of the primary and secondary ossification centre (Fig. 1.3B and C). Once the growth plate is completely replaced by bone, the skeletal maturity is achieved. During adult age, chondrocytes build mainly articular cartilage which is the component of synovial joints surrounding the end of long bones (Gentili & Cancedda, 2009).

The trabecular bone matrix is continuously remodelled by osteoblasts and osteoclasts (Zaidi, 2007; Fig. 1.4). Osteoclasts are multinucleated giant cells derived from hematopoietic stem cells of the macrophage lineage in the bone marrow (Fig. 1.4). For bone resorption, the osteoclasts attach tightly to the bone surface. The plasma membrane of the osteoclast enlarges to generate the ruffled border (Cappariello *et al*, 2014) characterized by proton pumps such as V-ATPase and chloride exchanger mainly CLC-7 to generate an acidic extracellular environment called resorption lacuna or "extracellular lysosome" (Lacombe *et al*, 2013; Cappariello *et al*, 2014; Fig. 1.4).
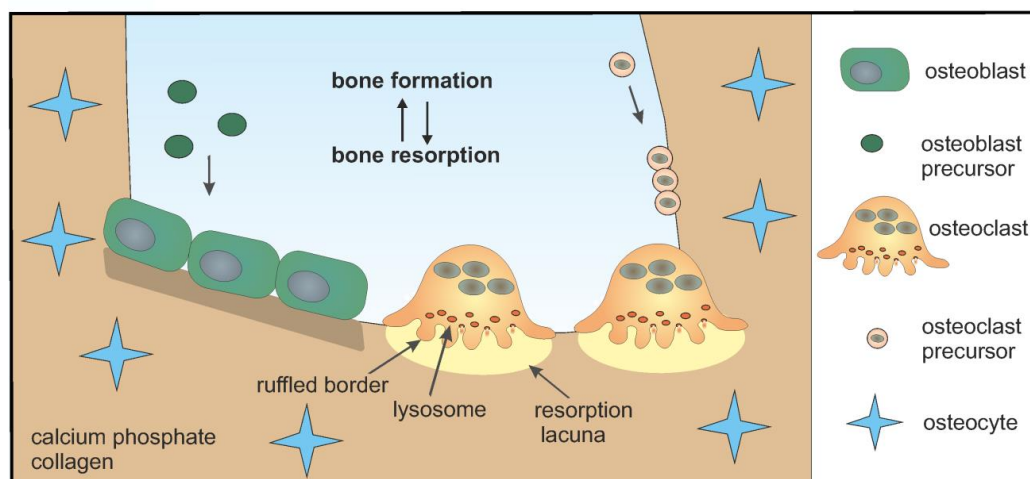
Figure 1.4. Schematic presentation bone remodelling: Bone-forming osteoblasts derive from osteoblast precursor and can further differentiate to osteocytes. Osteoclast precursor fusion result in mature osteoclasts that, building the resorption lacuna, accomplish their resorptive function.

Lysosomes release their luminal lysosomal enzymes by fusing with the ruffled border. Upon acidification, the inorganic part of the bone is dissolved. Moreover, the low pH of the resorption lacuna enhances the activity of lysosomal enzymes for degradation of the organic bone components (Cappariello *et al*, 2014). Cathepsin K is the prototypical lysosomal protease involved in osteoclast resorptive function by degradation of collagen I (Costa *et al*, 2011). Osteoblasts represent bone-forming cells and derive from mesenchymal progenitors, which differentiate to pre-osteoblasts and finally to mature osteoblasts. Osteoblasts generate the extracellular matrix composed by collagen fibres mainly collagen type I and proteoglycans named osteoid that gradually mineralizes by the deposition of calcium phosphate crystals (Karsenty *et al*, 2009). A subset of osteoblasts undergoes terminal differentiation into osteocytes, which form a cellular network within the mineralized bone matrix and regulate bone remodelling and mineral homeostasis (Dallas *et al*, 2013; Fig. 1.4).

1.4 Skeletal abnormalities in MLII mice

To maintain healthy and functional bone, a proper balance between osteoblasts and osteoclasts is required because combination of increased bone degradation and low bone formation or the opposite can alter the bone microarchitecture leading to pathological conditions (Zaidi, 2007). Many lysosomal storage disorders are characterized by defects of skeletal growth and bone abnormalities summarized as *dysostosis multiplex* (Clarke & Hollak, 2015; James *et al*, 2016). In particular, the MLII disease presents severe craniofacial and skeletal defects as demonstrated by deep skeletal phenotyping of MLII mice (Kollmann *et al*, 2013; Köhne *et al*, 2016). The skeleton of 1 week MLII old mice was substantially smaller than the wild-type skeleton, e.g. the lumbar spine and femoral length was significantly decreased (Fig. 1.5A). This resulted from widening of the growth plate of MLII mice (Fig. 1.5B). In addition, increased cortical porosity was observed, indicating enhanced bone resorption. Moreover, histomorphometric quantification of the bone volume per tissue volume revealed a strong reduction of the trabecular bone volume in 12 weeks old MLII mice (Fig. 1.5C). The bone loss was caused by an increased number of osteoclasts in MLII compared to wild-type mice (Fig. 1.5D).

The accumulation of lysosomal storage material in osteoblasts impairs their functionality and differentiation demonstrated by altered mineralization and decreased expression of osteoblastogenic differentiation markers of MLII osteoblasts i.e. *Ibsp*, *Dmp1*, *Col1a1*, *Bglap*, *Alpl*, *Sp7*, *Sost*, *Phex* (Fig. 1.5E). All these findings support the osteoporotic phenotype of MLII mice, which is present also in MLII patients.
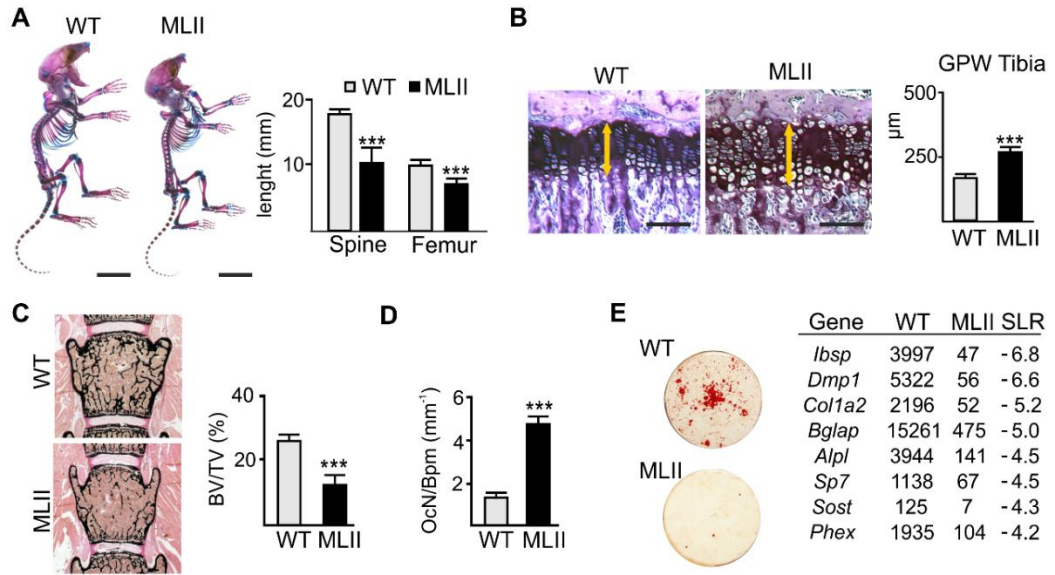
Figure 1.5. Bone phenotype of MLII mice. A) Alcian blue/alizarin red staining of the whole skeleton from 7 days old wild-type (WT) and MLII mice. Scale bar: 1 cm. Quantification of lumbar spine and femoral length of 12 weeks old mice. **B)** Toluidin blue-stained sections and quantification of the growth plate width (GPW) from tibia of 12 weeks old mice, white arrows indicate the growth plate. Scale bars: 100 µm. **C)** Von Kossa/van Gieson staining and histomorphometric quantification of bone volume per tissue volume (BV/TV) of non-decalcified sections from vertebral bodies of 12 weeks old mice. **D)** Quantification of osteoclasts number per bone perimeter (OcN/Bpm) in vertebral bodies of 12 weeks old mice. **E)** Alizarin red staining of primary osteoblast cultures and expression of osteoblastogenic markers in WT and MLII samples. The mean signal intensities and the signal log ratio (SLR) are shown. (modified from Kollmann *et al*, 2013)

1.5 Animal models for MLIII

In order to understand the role of the γ-subunits for GlcNAc-1-phosphotransferase activity and the M6P formation on lysosomal enzymes different *Gnptg*-targeted animal models were generated. In a γ-subunit-deficient mouse model (*Gnptg$^{-/-}$*) exons 4 to 11 of the *Gnptg* gene were deleted (Lee *et al*, 2007). Standard phenotypic characterization performed by the company *Lexicon Pharmaceuticals* revealed no differences between wild-type and *Gnptg$^{-/-}$* mice at the age of 8 to 14 weeks. In follow-up analyses normal growth, behaviour, reproduction and lifespan of 2 years old *Gnptg$^{-/-}$* mice were observed.

The examination of bone density and bone mineral content revealed no skeletal and joint abnormalities in *Gnptg*^{-/-} mice (Vogel *et al*, 2009), which are typical symptoms for the human MLIII disease. However, it has been reported that the *Gnptg*^{-/-} mice exhibit mild impaired sensor and motor function starting with 6 to 12 month of age (Idol *et al*, 2014). Biochemically, increased levels of lysosomal enzymes were found in the serum of *Gnptg*^{-/-} mice compared to wild-type mice (Vogel *et al*, 2009). The analysis of the brain M6P proteome of *Gnptg*^{-/-} mice using an MPR affinity chromatographic approach followed by mass spectrometry revealed that 25% of the lysosomal enzymes were poorly phosphorylated (Qian *et al*, 2010). In particular, γ-subunits enhance the M6P formation of a subset of lysosomal enzymes such as α-mannosidase, arylsulfatase A, α-galactosidase, cathepsin C, dipeptidyl-peptidase 7, iduronate 2-sulfatase and tripeptidyl peptidase I. However, since non-fractionated brain homogenates were used for these experiments, no information about the intra- or extracellular localization of the lysosomal enzymes is available. The missorting of specific lysosomal enzymes results in the accumulation of storage material in lysosomes, which was detectable in secretory epithelial cells of several exocrine glands. Acinary cells in the pancreas and parotid salivary glands of 2 years old *Gnptg*^{-/-} mice showed disruption of the cellular and tissue structure due to enlarged vacuoles filled with storage material (Vogel *et al*, 2009). Moreover, submandibular glands of these mice were enlarged due to cytoplasmic microvacuoles. In contrast, chondrocytes appeared to be completely normal, even in aged *Gnptg*^{-/-} mice, indicating the absence of joint defects which are typical characteristic features of MLIII patients.

The phenotypic analysis of *gnptg*^{-/-} zebrafish revealed no morphological or behavioural defects (Flanagan-Steet *et al*, 2016). In particular, the development of the cartilage was not affected in *gnptg*^{-/-} zebrafish. The *gnptg*^{-/-} chondrocytes showed a normal morphology and an unchanged expression of chondrogenic markers. For biochemical analysis, *gnptg*^{-/-} and wild-type embryo lysates were fractionated by MPR300 affinity chromatography and revealed that many glycosidases were not M6P-modified in *gnptg*^{-/-} zebrafish such as β-galactosidase, β-glucuronidase, α-hexosaminidase, α-mannosidase and α-iduronidase. In contrast, the M6P formation of cathepsin K, L, S and D was not impaired in *gnptg*^{-/-} zebrafish (Flanagan-Steet *et al*, 2016).

Since the *Gnptg*^{-/-} mice from the Kornfeld group are not available, the group of Dr. S. Pohl generated *Gnptg*[lacZ] and *Gnptg*[ko] mice used for all experiments performed in this thesis. *Gnptg*[lacZ] mice carry a floxed IRES lacZ cassette in the intron 3 of *Gnptg* gene allowing the *Gnptg* promoter driven expression of bacterial β-galactosidase (Fig. 1.6A).

The *Gnptg^ko* mice were generated by sequential crossing with mice expressing Flp and Cre-recombinase which led to the deletion of exon 4-11 of *Gnptg* (Fig. 1.6A). The targeted deletion leads to a C-terminally truncated γ-subunit of 59 amino acids (p.S59X).
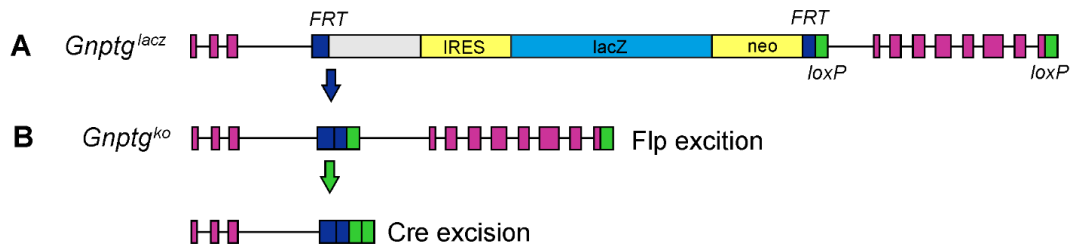
Figure 1.6. Schematic presentation of *Gnptg^ko*. **A)** *Gnptg^lacZ* mice a floxed promotor-driven IRES lacZ neomycin cassette flanked by FRT sites into intron 3 of *Gnptg* gene was inserted. **B)** Subsequential crossing of *Gnptg^lacZ* mice with Flp and Cre recombinase expressing mice leads to deletion of *Gnptg* exons 4-11 in *Gnptg^ko* mice using *FRT* and *loxP* sites, respectively.

2. Aim of the study

The hexameric GlcNAc-1-phosphotransferase complex ($\alpha_2\beta_2\gamma_2$) catalyses the generation of mannose 6-phosphate (M6P) recognition markers on lysosomal enzymes, which is fundamental for their proper targeting to lysosomes. The membrane-bound α- and β-subunits exhibit the substrate binding sites and the catalytic center, whereas the functions of the soluble γ-subunits are poorly defined. Mutations in the *GNPTG* gene encoding the γ-subunits cause the lysosomal storage disorder mucolipidosis type III (MLIII) that is mainly characterized by i) missorting of selected lysosomal enzymes and ii) bone and cartilage abnormalities in affected patients. The experiments performed in this thesis aimed to understand the role of γ-subunits of GlcNAc-1-phosphotransferase in the pathogenesis of the MLIII disease.

1. To analyse the *in-vitro* expression profile of γ-subunits in different tissues and cell types which might provide information on biological significance and organ/cell specificity of γ-subunits, the mRNA and protein of the γ-subunit was analysed in tissues and cells from wild-type and *Gnptg^{lacZ}* reporter mice.

2. To determine the role of γ-subunits in M6P formation on selected lysosomal enzymes, quantitative lysosomal proteomics and analysis of M6P secretome was performed in *Gnptg^{ko}* mouse fibroblasts.

3. Based on the clinical phenotype of MLIII patients, the role of γ-subunits in bone homeostasis was investigated *in vivo* and in primary cultured bone and cartilage cells from *Gnptg^{ko}* mice.

4. Depending on the identification of missorted lysosomal enzymes in the absence of γ-subunits, potential enzyme replacement therapies were evaluated as proof-of-principle to reduce the accumulation of non-degraded storage material such as glycosaminoglycans in *Gnptg^{ko}* fibroblasts.

3. Materials and Methods

3.1 Materials

Standard lab reagents (such as salts, solvents, acids and bases) were purchased from Sigma, VWR and Merck.

3.1.1 Chemicals

Chemical	Company
[^{35}S]sulfuric acid (activity 1 mCi/mmol)	Hartmann Analytik
2-Mercaptoethanol	Sigma
4-(2-Hydroxyethyl)-1-piperazineethanesulfonic acid (HEPES)	Sigma
4-methylumbelliferone (4-MU)	Sigma
Acrylamide	Roth
Agarose	Thermo Fisher Scientific
Albumin standards	Thermo Fisher Scientific
Aqua-Poly/Mount®	Polysciences
Bovine serum albumin (BSA)	Serva
Coomassie® Blue R250	Serva
Concanavalin A-sepharose	GE Healthcare
Diethylaminoethyl (DEAE) - Sepharose	GE Healthcare
Diethylpyrocarbonat (DEPC)	Sigma
Dithiothreitol (DTT)	Sigma
DNA loading dye	Thermo Fisher Scientific
DNA standard 1kb ladder	Thermo Fisher Scientific
Ethidium bromide	Sigma
Glycine	Roth
L-Arginin (light)	Thermo Fisher Scientific
L-Arginin^{13}C$_6$^{15}N$_4$	Thermo Fisher Scientific
L-Lysin (light)	Thermo Fisher Scientific
L-Lysin^{13}C$_6$^{15}N$_2$	Thermo Fisher Scientific
L-Lysin^{13}C$_6$	Thermo Fisher Scientific
Luminol	Roth
Milk powder	Roth
NNN′N′-Tetramethylethylenediamine (TEMED)	Sigma
p-Cumaric acid	Sigma
PageRuler™	Thermo Fisher Scientific
Protease inhibitor cocktail	Sigma
Sephadex PD-10	GE Healthcare
Scintillation cocktail	Roth
Sucrose	Sigma

TissueTek®	Sakura
TriReagent®	Sigma
Tris(hydroxymethyl)aminomethane (Tris)	Sigma
Triton X-100	Sigma
Tween 20	Roth

3.1.2 Equipment

Equipment (Model)	Company
Balances (AC100, TE2101)	Mettler Toledo, Sartorius
Thermoblock (MHR23)	HLC
Centrifuges (5424, 5415R and 5804R, MC6)	Eppendorf, Sarstedt
Cryogenic freezing unit (CoolCell® alcohol-free)	Biocision
Camera EOS 10D	Canon
Electrophoresis chambers (Agagel Midi Wide, SE600)	PeqLab, GE Healthcare
Fluorometer (Fluoroskan Ascent)	Thermo Scientific
Gel documentation (E Box V2)	PeqLab
Horizontal shaker	Labotect
Imager (Chemi Doc XRS)	Bio-Rad
Ice machine (AF 10)	Scotsman
Incubators (Gasboy C20A,BB15)	Labotect, Thermo Scientific
Inverted microscope (Axiovert 25)	Zeiss
Liquid nitrogen container (Airpege 55)	Air Liquide
Magnetic stirrer (MR Hei-Mix)	Heidolph
Microtome	Leica 9000
Microwave (Promicro)	Whirlpool
pH meter (Five Easy FE20)	Mettler-Toledo
Photometer (Multiscan GO)	Thermo Scientific
Pipette controller (Pipetus®)	Hirschmann
Pipettes	Eppendorf
Real-time PCR Thermocycler (MxPro3000)	Agilent
Scintillation counter (Tri-carb 2900TR)	Perkin Elmer
Shaker	GFL
Safety Cabinet (Hera Safe)	Thermo Scientific
Thermocyclers (TPersonal)	Biometra
Transfer chamber (TE62 & TE22)	GE Healthcare
Vacuum pump (PC 2002 VARIO)	Vacuubrand
Vortex Mixer (Genie1™)	Scientific Industries
Ultra Turrax Dremel®	Bio Spec Products
Water bath	Schütt Labortechnik

3.1.3 Consumables

Consumable	Company
Amicon Ultra-0.5 ml centrifugal filters (3 kDa)	Merck
Cuvettes	Sarstedt
Disposable lab consumables	BD Falcon, Sarstedt, Nunc
Needles Sterican 27 G)	Braun
Nitrocellulose membrane	GE Healthcare
Parafilm	Bemis Company
Precast gel (ServaGel™ TG Prime™) (0.70 μm)	Serva
Scalpels	Braun
Scintillation tubes	Perkin-Elmer
Sterile syringe filter (0.22 μm)	VWR
Sterile surgical blade	Vayha
Strainer	VWR
Syringes	Braun
Blotting paper	Roth
Microplate 96 well, black	Greiner Bio-One International
Microplate 96 well, half area, transparent	Greiner Bio-One International

3.1.4 Kits and assay

Kit and assay	Company
AccuStart II PCR Genotyping Kit	Quanta BioSciences
Protein Assay Dye Reagent	Biorad
High-Capacity cDNA reverse transcription Kit	Thermo Fisher Scientific
Perfecta FastMix II	VWR
PeqGold Total RNA Kit	VWR

3.1.5 Enzymes

Enzymes	Company, Reference
Arylsulfatase B (Naglazyme®)	Biomarin
Chondroitinase ABC	Sigma
Collagenase I	Sigma
Dispase I	Sigma
Heparinase I	Sigma
Heparinase II and III	Dr. J. Esko, University of California
Pronase	Roche

3.1.6 Enzyme substrates

Enzyme substrates	Company
5-Bromo-4-chloro-indolyl-β-D-galactopyranoside (X-Gal)	Thermo Fisher Scientific
4-Nitrocatechol sulfate	Sigma
4-Nitrophenyl-N-acetyl-β-D-glucosaminide	Sigma
4-Nitrophenyl-α-D-mannopyranoside	Sigma
4-MU-α-L-fucopyranoside	Sigma
4-MU-β-D-galactopyranoside	Sigma
4-MU-α-D-mannopyranoside	Sigma
4-MU-β-D-galactosid-6-sulfate	Moscerdam

3.1.7 Primera and TaqMan™ assays

Primers for genotyping

Name	Sequence 5′ – 3′
*Gnptg*_F3 forwards	GCTCCTGGCTTCGGTTATCA
*Gnptg*_F2A forwards	CACTCACTCTCAGCACCTGG
*Gnptg*_R2A revers	CCAGCAGGTCCCTCTTGTTT
*Gnptg*_R3 revers	TTGTCTGTGGCAGGATTCCC
LacZ-F1 forwards	GTT GCA GTG CAC GGC AGA TAC ACT TGC TGA
LacZ-R1 revers	GCC ACT GGT GTG GGC CAT AAT TCA ATT CGC

TaqMan™ assays

Gene	Protein	Assay Number
Acan	Aggrecan	Mm00545794_m1
Actb	β-Actin	Mm00607939_s1
Aga	Aspartylglucosaminidase	Mm01208043_m1
Arsa	Arylsulfatase A	Mm00802173_g1
Arsb	Arylsulfatase B	Mm00802167_m1
Asah1	N-Acylsphingosine amidohydrolase 1	Mm00480021_m1
Bglap	Osteocalcin	Mm03413826_mH
Calcr	Calcitonin receptor	Mm00432282_m1
Clcn7	Chloride channel 7	Mm00442400_m1
Cln5	Ceroid-lipofuscinosis, neuronal 5	Mm01224444_m1
Col1a1	Collagen type I, alpha 1	Mm00801666_g1
Creg1	Creg1 protein	Mm00516189_m1
Ctbs	Di-N-acetylchitobiase	Mm00547006_m1
Ctsa	Cathepsin A	Mm00447197_m1
Ctsb	Cathepsin B	Mm01310506_m1
Ctsc	Cathepsin C	Mm00515580_m1

Ctsd	Cathepsin D	Mm00515587_m1
Ctsk	Cathepsin K	Mm00484039_m1
Ctsl	Cathepsin L	Mm00515597_m1
Ctss	Cathepsin S	Mm01255859_m1
Ctsz	Cathepsin Z	Mm00517697_m1
Dpp7	Dipeptidylpeptidase 7	Mm00473420_m1
Epdr1	Ependymin related protein 1	Mm00840848_m1
Galns	N-acetylgalactosamine 6-sulfatase	Mm00489576_m1
Gapdh	Glyceraldehyde 3-phosphate dehydrogenase	Mm99999915_g1
Gba	β-glucocerebrosidase	Mm00484700_m1
Ggh	γ-Glutamyl hydrolase	Mm01222952_m1
Glb1	β-Galactosidase	Mm00515342_m1
Gnptab	GlcNAc-1-phosphotransferase (α/β-precursor)	Mm01773334_m1
Gnptg	GlcNAc-1-phosphotransferase (γ-subunit)	Mm01330321_g1
Gusb	β-Glucuronid	Mm00446956_m1
HexB	β-Hexosaminidase, subunit B	Mm00599880_m1
Lamp1	Lysosomal-associated membrane protein 1	Mm00495262_m1
Scarb2	Scavenger receptor class B, member 2 (*Limp2*)	Mm00446978_m1
Lipa	Lysosomal acid lipase A	Mm00498820_m1
Man2b1	α-Mannosidase	Mm00487585_m1
Manba	β-Mannosidase	Mm00466160_m1
Naaa	N-Acylethanolamine acid amidase	Mm01341699_m1
Naga	α-N-acetylgalactosaminidase	Mm00476274_m1
Neu1	Neuraminidase 1	Mm00456846_m1
Npc2	Niemann-Pick type C2 protein	Mm00499230_m1
Pla2g15	Phospholipase A2, group XV	Mm00505425_m1
Plbd2	Phospholipase B domain containing 2	Mm00469973_m1
Ppt1	Palmitoyl-protein thioesterase 1	Mm00477078_m1
Prcp	Prolylcarboxypeptidase	Mm00804502_m1
Psap	Prosaposin	Mm00478327_m1
Siae	Sialic acid acetylesterase	Mm00496036_m1
Sost	Sclerostin	Mm00470479_m1
Sp7	Sp7 transcription factor	Mm00504574_m1
Tpp1	Tripeptidyl peptidase 1	Mm00487016_m1

3.1.8 Media and supplements for cell culture

Media and supplements	Company
Minimal essential medium (α-MEM)	Sigma
Dulbecco's modified Eagle Medium (DMEM)	Thermo Fisher Scientific
DMEM/HAM´s F-12	Biochrom AG
Fetal calf serum (FCS)	Thermo Fisher Scientific
GlutaMAX™ (100×)	Thermo Fisher Scientific

Penicillin (Pen, 10000 U/ml), streptomycin (Strep, 10 mg/ml)	Thermo Fisher Scientific
PBS (10×)	Thermo Fisher Scientific
Opti-MEM™	Thermo Fisher Scientific
Trypsin/EDTA solution (0.05%)	Thermo Fisher Scientific
1,25-dihydroxyvitamin-D3	Sigma
Macrophage colony stimulating factor (M-Csf)	Peprotech
Receptor activator of nuclear factor kappa-B ligand (Rankl)	Peprotech
Ascorbic acid	Sigma
β-glycerophosphate	Sigma

3.1.9   Antibodies

Primary antibodies	Species	Dilution	Cat. No.	Company/Reference
ARSB	mouse	1:500	MAB4415	R&D
Creg1	goat	1:1000	AF1697	R&D
Ctsb	goat	1:1000	GT15047	Neuromics
Ctsc	goat	1:300	AF1034	R&D
Ctsd	goat	1:200	sc6486	Santa Cruz
Ctsk	mouse	1:100	sc48353	Santa Cruz
Ctsl	goat	1:500	AF1515	R&D
Ctss	mouse	1:200	sc6503	Santa Cruz
Ctsz	goat	1:1000	AF1033	R&D
Dpp7	goat	1:500	AF3436	R&D
Gapdh	rabbit	1:1000	sc25778	Santa Cruz
Gba	rabbit	1:250	G4171	Sigma
Gnptg	rabbit	1:100		Encarnação *et al*, 2011
single-chain M6P antibody fragment		1:100		Müller-Loennies *et al*, 2010
Npc2	rabbit	1:100	sc33776	Santa Cruz
Pla2g15	rabbit	1:300	HPA041702	Sigma
Plbd2	rabbit	1:500		Deuschl *et al*, 2006
Ppt1	rabbit	1:1000		Dr. S. Hofmann University of Texas
Transferrin	goat	1:200	T6265	Sigma
α-tubulin	mouse	1:1000	T9026	Sigma

Secondary antibodies	Dilution	Company
HRP-conjugated goat anti-rabbit IgG	1:5000	Dianova
HRP-conjugated rabbit anti-goat IgG	1:3000	Dianova
HRP-conjugated goat anti-rat IgG	1:3000	Dianova
HRP-conjugated goat anti-mouse IgG	1:3000	Dianova

3.1.10 Software

Software	Company/Institution
Adobe Photoshop 7.0	Adobe
Corel Draw®	Corel
ECapt, ND-1000 V3.5.2	PeqLab
Endnote X3	Thomson Reuter
Image Lab 3.0.1, Quantity One-4.6.7	Bio-Rad
Microsoft Office	Microsoft
MxPro-QPCR software	Agilent
Quanta Smart, Volocity Demo 6.1.1	Perkin Elmer

3.2 Molecular biology methods

3.2.1 Genotyping of mice

DNA extraction from tail biopsies of offspring from heterozygous matings of $Gnptg^{ko}$ and $Gnptg^{lacZ}$ mice and subsequent polymerase chain reaction (PCR) was performed using the AccuStart II PCR Genotyping Kit according to the manufacturer's instructions. The amplified DNA region and the binding of the respective primers are indicated in the scheme (Fig. 3.1).
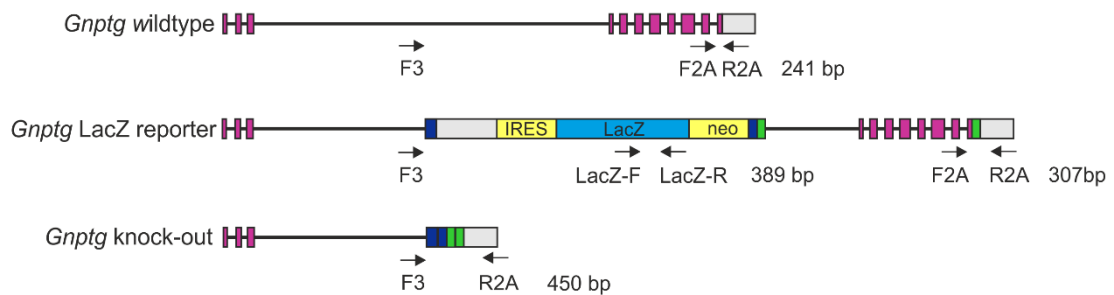
Figure 3.1 Genotyping scheme. Wild-type mice were genotyped using F2A and R2A primers that resulted in a PCR product of 241 bp. $Gnptg^{lacZ}$ mice were genotyped via multiplex PCR using LacZ-F and -R primers that amplified a product of 389 bp and primers F2A and R2A which resulted in 307 bp product. For $Gnptg^{ko}$ genotyping primers F3 and R2A were used, resulting in a PCR product of 450 bp.

The following PCR program was used for both genotyping:

1. 95 °C   3 min
2. 95 °C   15 s
3. 59 °C   15 s
4. 72 °C   15 s [2-4] × 40 cycles
5. 72 °C   4 min

21

3.2.2 Agarose gel electrophoresis

For separation of DNA and RNA, 1.5% agarose gels were prepared. The agarose was boiled in TAE buffer (40 mM Tris/HCl (pH 8.5), 20 mM acetic acid, 2 mM EDTA). After cooling down ethidium bromide (0.5 µg/ml) was added and the solution placed in a chamber. After 30 min the polymerized gel was transferred into an electrophoresis chamber filled with TAE buffer. The samples and a molecular weight ladder were loaded into the pockets and electrophoresis was performed at 120 V for 40 min. The gel bands were detected by UV illumination using a gel documentation system.

3.2.3 RNA extraction and cDNA synthesis

RNA was extracted from MEF, osteoclasts, osteoblasts and chondrocytes using the PeqGOLD total RNA purification kit according to the manufacturer's instructions.

To isolate RNA from tissue, 100 mg mouse tissue was homogenized with 1 ml Tri-Reagent using an Ultra Turrax. After 5 min incubation at room temperature (RT), 500 µl chloroform was added and mixed for 15 seconds by vortexing followed by 10 min incubation at RT. After centrifugation at $12,000 \times g$ for 15 min at 4 °C the uppermost RNA-containing phase was transferred to a 1.5 ml tube. To precipitate the RNA, 500 µl isopropanol was added and mixed by vortexing. After 10 min incubation at RT the sample was centrifuged at $12,000 \times g$ for 10 min at 4 °C and the RNA pellet washed with 500 µl 70% EtOH. After centrifugation at $12,000 \times g$ for 10 min at 4 °C the EtOH was decanted and the pellet was air dried to remove remaining EtOH. The RNA was resuspended in 100 µl DEPC water. The RNA quality was controlled by agarose gel electrophoresis. The RNA concentration was measured using a spectrophotometer. The concentration was determined in base of the absorbance at 260 nm (OD_{260}). The RNA samples were stored at -80 °C. The cDNA was synthesized from 1 µg RNA using the High-Capacity cDNA reverse transcription kit according to the manufacturer´s protocol.

3.2.4 Quantitative real-time PCR

To determine the RNA expression level of genes, the TaqMan® gene expression assays were used. PCR reaction:

- 10 µl 2× Perfecta FastMix II
- 7 µl Nuclease-free water
- 2 µl cDNA
- 1 µl TaqMan® assay

Cycling condition for Real-time PCR reaction:

1. 95 °C   10 min
2. 95 °C   30 sec
3. 60 °C   1 min [2-3]× 40 cycles

The analysis of the data was performed according to the $2^{-\Delta\Delta CT}$-method (Schmittgen & Livak, 2008). The difference between the C_T value of the gene of interest and the control gene (*Actb* or *Gapdh*) was calculated. The relative expression was determined comparing each group (knock-out versus wild-type) according to the following equation: $2^{-\Delta\Delta CT}$

$\Delta C_T = C_{T\,gene} - C_{T\,control\,gene}$

$\Delta\Delta C_T = \Delta C_{T\,knock-out} - \Delta C_{T\,wild-type}$

3.3   Cell biology methods

3.3.1   Isolation and culture of mouse embryonic fibroblasts

To isolate primary mouse embryonic fibroblasts (MEF), animals were prepared on day 12.5 of embryonic development. The pregnant female mouse was sacrificed in a CO_2 chamber, the abdomen was disinfected with 70% EtOH. The uterus were removed and placed in a 10 cm cell culture dish. Every embryo was extracted from the embryonic sac and individually placed in a 6 well culture dish containing PBS. Afterwards the PBS was removed and every embryo was dissected into small pieces to facilitate the digestion. A small part of each embryo was kept for genotyping. Subsequently the embryo was transferred to a 15 ml falcon tube containing 4 ml of trypsin/EDTA solution and mixed by pipetting. The samples were incubated at 37 °C in a water bath for 10 min to release individual cells.

The reaction was stopped by the addition of 10 ml DMEM culture medium containing 10% FCS, 1% Pen/Strep, 1% GlutaMAX™ and the cells were plated in a 10 cm cell culture flask. To remove the trypsin/EDTA, after 24 h the medium was replaced with fresh DMEM culture medium. MEF were cultured at 37 °C and 5% CO_2 in pre-warmed culture medium. At the confluence of 90 - 100% the cells were split. Therefore, the cells were washed once with PBS and incubated for 5 min in 1 ml trypsin/EDTA solution at 37 °C. The trypsin activity was stopped by 9 ml DMEM culture medium. The cells were resuspended in culture media and seeded in respective plates or flasks.

3.3.2 Cryo-conservation and revitalization of MEF

Cells in a T75 cell culture flask were washed once with PBS, trypsinated for 5 min at 37 °C and afterwards resuspended in 1 ml freezing medium (DMEM, 20% FCS, 10% DMSO). The cell suspension was transferred to cryovials and left at -80 °C overnight in a cryogenic freezing container. After 24 h the cells were transferred to liquid nitrogen.

For revitalization, cells were resuspended in 5 ml pre-warmed DMEM culture medium and transferred from the cryovial to a 15 ml tube. Cells were centrifuged at 900 g for 5 min, the supernatant was removed and the cells were suspended in DMEM culture medium and seeded in a T25 culture flask. After 24 h the medium was replaced by fresh DMEM culture medium.

3.3.3 Isolation of bone marrow cells for osteoclasts and osteoblasts cultivation

Bone marrow cells were isolated from tibias and femora of wild-type and *Gnptg^{ko}* mice. Therefore, 10-20 weeks old mice were sacrificed in a CO_2 chamber and the abdomen was sterilized with 70% EtOH. The skin was removed from the middle of the abdomen dawn to the feet. The two legs were removed by a cut between the hips and the femur head. The feet were removed with a chisel and the femur was separated from the tibia with a slight cut in the knee. All the muscles and the fibula were removed. To open the bone marrow space the femur head and the end of the tibia were cut. Afterwards one femur and one tibia were inserted together in a holed PCR tube with the cut side facing the hole. The tube was placed into a 1.5 ml tube and centrifuge at $5,900 \times g$ for 15 sec. The released bone marrow cells were resuspended in 500 µl α-MEM culture medium, passed through a 70 µm cell strainer and transferred to a 50 ml tube.

Cells were plated at a density of 5×10^6 cells/ml in α-MEM culture medium containing 10% FCS and 1% Pen/Strep. Bone marrow cells were grown in α-MEM culture medium that was refreshed every second day. At day 5 after isolation the osteoclast differentiation was induced by 10 nM 1,25-dihydroxyvitamin D3 (in 100% EtOH), 20 ng/ml of M-Csf and 40 ng/ml Rankl and cultured for 10 days. The osteoclast differentiation media was refreshed every second day.

For osteoblast differentiation, 50 µg/ml ascorbic acid and 10 mM β-glycerophosphate was added to bone marrow cells at 90% confluency and cultured for 15 or 25 days. The osteoblast differentiation media was refreshed every second day.

3.3.4 Isolation and culture of calvarial osteoblasts

For the isolation of osteoblast precursor cells, the skull roofs of 3 to 5 days old neonatal wild-type and *Gnptg*^{ko} mice were used. To isolate calvarial osteoblasts the pups were decapitated under sterile condition, the calvaria was cut along the edge and placed in PBS in a 50 ml tube. PBS was aspirated and the calvaria incubated in 10 ml sterile collagenase/dispase solution (1 mg/ml Collagenase I and 2 mg/ml dispase dissolved in α-MEM media) at 37 °C for 10 min in a shaking incubator at 200 rpm. The supernatant was then aspirated and the pellet treated again with 20 ml collagenase/dispase solution for 45 min. The supernatant was transferred through a 70 μm cell strainer into a new 50 ml tube and centrifuged at 1,400 × g for 5 min. The supernatant was discarded and the cell pellet resuspended in 1 ml of pre-warmed α-MEM culture medium containing 10% FCS and 1% Pen/Strep. The cells were seeded at a density of 5×10^3 cells/ml. At 90% confluency of osteoblast precursor cells the differentiation was induced for 25 days using osteoblast differentiation media that was refreshed every second day.

3.3.5 Isolation and culture of ribcage chondrocytes

To isolate chondrocyte progenitor cells, 10-12 days old wild-type and *Gnptg*^{ko} mice were sacrificed by an incubation of 8-10 minutes in a CO_2 chamber followed by removing of the skin. The ribcage containing chondrocytes was then extract and after removing the sternum the ribcage was washed in PBS containing 1% Pen/Strep. To remove the non-cartilage tissue, the ribcages were digested in 25 ml pre-digestion solution containing 0.1% in DMEM/Ham's F-12 for 30 min at 37 °C in a shaking incubator (200 rpm). The supernatant was then aspirated and chondrocytes were separated in 50 ml digestion solution containing 0.2% collagenase in DMEM/Ham's F-12 for 30 min at 37 °C in a shaking incubator (200 rpm). The supernatant was transferred through a 70 μm cell strainer into a new 50 ml tube and centrifuged at 1,400 × g for 8 min. Then the supernatant was discarded and the cell pellet resuspended in 1 ml of prewarmed DMEM/Ham's F-12 containing 1% Pen/Strep and 10% FCS. The cells were plated at a density of 8.75×10^5 cells/ml. At a cell confluence of 80-90%, chondrocyte differentiation was induced by the addition of ascorbic acid (50 μg/ml) and cultured for 10 days. The differentiation media was refreshed every second day.

3.3.6 Alizarin red staining

At day 25 of differentiation, mature osteoblasts isolated from bone marrow were washed three times with PBS. Subsequently, cells were fixed with 1 ml of 90% EtOH for 45 min. After washing twice with H_2O, the cells were stained for 20 min with 1 ml Alizarin red staining solution. Cells were washed five times with H_2O and after stored in PBS. Pictures were acquired using the camera Canon EOS 10D.

3.3.7 Preparation of conditioned media

For media analysis, confluent cells on 6 cm or 6 well cell culture dishes were washed twice with PBS and then incubated 24 h in 2 ml or 1.5 ml Opti-MEM™, respectively.

3.3.8 Stable isotope labelling by amino acids in cell culture (SILAC)

For lysosomal proteome analysis, MEF were cultivated for six passages in SILAC-DMEM supplemented with 10% FCS containing either 87.8 mg/ml L-arginine, 181.2 mg/ml L-lysine for light labelling of *Gnptg^{ko}* cells or L-arginine-$^{13}C_6^{15}N_4$ and L-lysine-$^{13}C_6^{15}N_2$ for heavy labelling of wild-type cells (Thelen *et al*, 2017). MEF were incubated 24 h with magnetite particles followed by a 36 h chase to allow the accumulation of magnetic beads in lysosomes. The SILAC experiment was performed by Dr. M. Thelen (University of Bonn).

For M6P secretome analysis, MEF from three *Gnptg^{ko}* and three wild-type embryos were cultured in 10 cm dishes in duplicates for 24 h in 5 ml SILAC-DMEM supplemented with 10 mM NH_4Cl containing either 87.8 mg/ml L-arginine, 181.2 mg/ml L-lysine for light labelling of *Gnptg^{ko}* cells or L-arginine-$^{13}C_6^{15}N_4$ and L-lysine-$^{13}C_6$ for heavy labelling of wild-type cells. The media, 5 ml for each plate, was collected and further processed (see 3.4.2).

3.3.9 Metabolic $^{35}SO_4$-labeling of MEF and chondrocytes

Confluent MEF and chondrocytes on 6 well cell culture dishes were incubated for 4 days in DMEM culture medium containing 10% FCS, 1% Pen/Strep and 1% GlutaMAX™-100. For glycosaminoglycan (GAG) labelling, MEF and chondrocytes at day 6 of differentiation were incubated for 24 h and 48 h, respectively, in serum-free Opti-MEM™ medium containing 100 µCi/ml $Na^{35}SO_4$ (pulse).

MEF and chondrocytes were then washed twice with PBS and incubated for 24 h and 48 h, respectively, with serum-free Opti-MEM™ medium in the presence or absence of 10 µg/ml human recombinant ARSB. To remove cell surface proteoglycans cells were washed twice with PBS and treated with 0.05% trypsin/EDTA solution for 20 min.

3.4 Biochemical methods

3.4.1 Preparation of cell extracts d culture of mouse embryonic fibroblasts

MEF grown on 6 cm plates were harvested by scraping in 1.5 ml PBS and centrifuged at 900 × g for 10 min at 4 °C. The pellet was resuspended in 200 µl PBS containing 0.5% Triton-X100 and protease inhibitor cocktail (lysis buffer). Osteoclasts and osteoblasts were directly lysed in 200 µl lysis buffer on the 6 well plates. After incubation on ice for 30 min, the samples were centrifuged at 16,000 × g for 10 min at 4°C and the supernatants used for further analysis.

3.4.2 Media preparation

Opti-MEM™ from the cultured cells was centrifuged at 900 × g for 10 min at 4 °C and the supernatants were used for enzyme activity measurements. For western blot analysis media was concentrated 5-fold using Amicon Ultra-0.5 ml centrifugal filters (3 kDa molecular weight cut-off).

3.4.3 Sample preparation for mass spectrometry

For lysosomal proteome analysis, equal amounts of postnuclear supernatants (PNS) from heavy- and light-labelled wild-type and $Gnptg^{ko}$ MEF were combined. Magnetic isolation of lysosomes and mass spectrometry analysis were performed by Dr. M. Thelen (University of Bonn) as previously described (Markmann $et\ al$, 2015; Thelen $et\ al$, 2017). For M6P proteome analysis, 5 ml of NH_4Cl-containing heavy- and light-labelled wild-type and $Gnptg^{ko}$ media, were concentrated 50-fold using Amicon Ultra-0.5 ml centrifugal filters (3 kDa molecular weight cut-off) and equal amounts of concentrated media from both cell lines were combined followed by M6P affinity chromatography.

Therefore, aliquots of 250 µg proteins were adjusted to 500 µl PBS containing 0.2% Triton X-100 and protease inhibitors and incubated with 30 µl scFv M6P-1 antibody immobilized to Amino Link Plus Gel beads (1 mg/ml, kindly provided by Dr. S. Müller-Loennies, Research Center Borstel) at 4 °C for 4 h on a rotating wheel.

After 1 min centrifugation at $1,700 \times g$, the supernatant was removed and the beads were washed three times with PBS containing 0.2% Triton X-100 and three times with PBS. For M6P proteome analysis, proteins bound to M6P beads were trypsinized and analysed by mass spectrometry (Dr. M. Thelen, University of Bonn; Thelen *et al*, 2017).

3.4.4   Preparation of lysosomal-enriched fractions

MEF grown on 10 cm plates were harvested by scraping and centrifuged at $900 \times g$ for 10 min at 4 °C. The cell pellets were resuspended in 20 mM HEPES (pH 7.4) containing 250 mM sucrose and $1\times$ protease inhibitors and incubated for 10 min on ice. Cells were disrupted by 30 times passage through a 24-gauge needle. Nuclei and unbroken cells were removed by centrifugation at $1,000 \times g$ for 2 min at 4 °C. Supernatants were centrifuged at $20,000 \times g$ for 20 min at 4 °C. Pellets representing the lysosome-enriched fraction were resuspended in PBS containing 0.5% Triton X-100 and protease inhibitors and incubated for 30 min on ice. After centrifugation at $16,000 \times g$ for 10 min at 4 °C the supernatant were used for western blot analysis.

3.4.5   Protein quantification

For protein quantification, a standard curve of BSA (0, 2.5, 5, 10, 15 and 20 µg) was prepared. Samples (2 µl) were mixed with H_2O in a total volume of 800 µl. Afterwards 200 µl Biorad Protein Assay Dye Reagent was added and mixed by inversion. After 5 min incubation the standards and the samples were measured by a spectrophotometer at 595 nm.

3.4.6   SDS polyacrylamide gel electrophoresis (SDS-PAGE)

Running and stacking gels were prepared as described in the table 3.1. Samples were solubilized in $1\times$ reducing sample buffer (125 mM Tris/HCl (pH 8.6), 1% SDS, 10% glycerin, Coomassie® Blue R, 10 mM DTT, 0.1 mM β-mercaptoethanol) and incubated at 95 °C for 5 min. The samples and a protein marker were loaded into the pockets of the gel.

Electrophoresis was performed for 3 h at 50 mA for big gels and 1 h at 180 V for mini gels in an electrophoresis chamber filled with anode buffer (192 mM glycine, 25 mM Tris/HCl, pH 8.6) and cathode buffer (0.1% SDS, 192 mM glycine, 25 mM Tris/HCl, pH 8.6).

Table 3.1: Running and stacking gels for SDS-PAGE

Chemicals/Buffers	running gel 10%		running gel 12.5%		stacking gel 4%	
	big	mini	big	mini	big	mini
Acrylamide (30.8 %) (ml)	9.8	1.65	12.1	2.05	1.3	0.325
H_2O (ml)	6.1	2.1	3.2	1.65	6	1.5
1.5 M Tris/HCl pH 8.8 (ml)	7.5	1.25	7.5	1.25	-	-
1.5 M Tris/HCl pH 6.8 (ml)	-	-	-	-	2.5	0.65
10 % SDS (µl)	300	50	300	50	100	25
10 % APS (µl)	250	41.5	250	41.5	100	25
TEMED (µl)	25	4.25	25	4.25	10	2.5

3.4.7 Western blot analysis

After SDS-PAGE, the proteins were transferred to a nitrocellulose membrane. The gel, in direct contact with the membrane, was placed between 2 or 3 blotting papers and 2 fiber pads and fixed in a transfer cassette in the blotting chamber doused with transfer buffer (192 mM glycin, 20% methanol, 25 mM Tris, pH 7.4). The transfers were performed at 900 mA and 4 °C for 3 h or overnight at 150 mA for big gels or for 1 h at 400 mA at room temperature for mini gels.

After blotting, the nitrocellulose membrane was incubated 1 h in blocking buffer containing 5% milk powder or 1% BSA, 0.05% Tween 20 in TBS (10 mM Tris/HCl, 150 mM NaCl, pH 7.4) on a rocking shaker. For protein detection, the membrane was incubated with primary antibody diluted in blocking buffer for 1 h at RT or overnight at 4 °C. After 3 washes of 10 min in TBS with 0.05% Tween 20, the membrane was incubated with the respective HRP-coupled secondary antibody in blocking solution and washed again 3 times. To visualize the protein bands, enhanced chemiluminescence solutions ECL-1 (5 ml 0.1 M Tris/HCl (pH 8.5), 100 µl 250 mM luminol/DMSO, 50 µl 90 mM p-cumaric acid/DMSO) and ECL-2 (5 ml 0.1 M Tris/HCl (pH 8.5), 12 µl 30% H_2O_2) were mixed and placed on the membrane. The chemiluminescence was visualized using the ChemiDoc documentation system.

3.4.8 Enzyme activity measurements

The activities of lysosomal enzymes were measured in cell homogenates, conditioned media and mouse serum using synthetic substrates conjugated to 4-nitrophenol or 4-methylumbelliferone (4-MU).

For photometric assays (β-hexosaminidase and arylsulfatase B activity), the assays were performed in a 96 well half area microplate in a total volume of 170 µl.

For the measurement of β-hexosaminidase activity, nitrophenyl-N-acetyl-β-D-glucosaminide was used as substrate. If required, the samples (4 µg of total protein extract, 15 µl of medium or 2 µl of serum) were diluted to a volume of 15 µl with water. As blank samples, 15 µl of lysis buffer (0.5% Triton-X100 and 1× protease inhibitor cocktail) or Opti-MEM™ were used. The 2 × substrate buffer (15 µl, 10 mM nitrophenyl-N-acetyl-β-D-glucosaminide in 200 mM Na-citrate, pH 4.6, 0.2% TritonX-100 and 0.4% BSA) was added and incubated at 37 °C in a thermoblock. The reaction was stopped after 30 minutes by the addition of 140 µl of stop buffer (0.4 M glycine/NaOH, pH 10.4) and the absorption was measured at 405 nm using a photometer. For the measurement of arylsulfatase B activity, 4-nitrocatechol-sulfate was used as substrate. If required, the samples (4 µg of total protein extract, 15 µl of medium or 2 µl of serum) were diluted to a volume of 15 µl with water. As blank samples, 15 µl of lysis buffer or Opti-MEM™ were used.

The 2 × substrate buffer (10 mM 4-nitrocatechol-sulfate in 200 mM Na-citrate, pH 5.5, 0.2% Triton X-100, 0.4% BSA and 10% NaCl) was added and incubated at 37 °C. The reaction was stopped after 17 h by the addition of 140 µl of stop buffer (0.4 M glycine/NaOH, pH 10.4). The absorption of the liberated 4-nitrocatechol was measured at 515 nm using a photometer.

The activity (A) was calculated according to the following equation:

$$A = \frac{\Delta E/min \times V_M}{\varepsilon \times d \times V_P}$$

A = enzyme activity [U; 1 U = 1 µmol/min]
$\Delta E/min$ = change in absorbance per minutes
ε = extinction or absorbance coefficient
[for 4-nitrophenol 18.45 /µmol*cm; for 4-nitrocatechol 12.6 /µmol*cm]
V_P = sample volume during the reaction [30 µl]
V_M = measured volume [170 µl]
d = layer thickness of the solution [1 cm]

For fluorometric assays (β-galactosidase, α-mannosidase and α-fucosidase activity), the assays were performed in a black 96 well plate.

For the measurement of β-galactosidase, α-fucosidase and α-mannosidase activities, 4-MU-β-D-galactopyranoside, 4-MU-α-L-fucopyranoside or 4-MU-α-D-mannopyranoside, respectively, were used as substrates.

If required, the samples (8 µg of total protein extract, 40 µl of medium or 2 µl of serum) were diluted to a volume of 40 µl with water. As blank samples, 40 µl of lysis buffer or Opti-MEM™ were used. The 2 x substrate buffer (40 µl, 10 mM 4-MU-β-D-galactopyranoside, 2 mM 4-MU-α-L-fucopyranoside or 5 mM 4-MU-α-D-mannopyranoside in 200 mM Na-citrate, pH 4.6, 0.2% TX-100 and 300 mM NaCl) was added and incubated at 37 °C. The reaction was stopped after 60 min by the addition of 120 µl of stop buffer (0.4 M glycine/NaOH, pH 10.4). The release of 4-MU was measured at 355 nm excitation and 460 nm emission using a fluorometer. The determination of enzymatic activity of N-acetylgalactosamine-6-sulfatase was performed according to the manufacturer´s instruction. To determine the amount of liberated 4-MU during the enzyme reaction, a standard concentration series of 0.03, 0.06, 0.125, 0.25, 0.5, 1 and 2 nM 4-methylumbelliferon in reaction buffer (100 mM Na-citrate pH 4.6, 0.1% TX-100 and 150 mM NaCl) were measured to create a calibration curve.

GlcNAc-1-phosphotransferase activity was measured by Dr. R. Voltolini Velho (Velho *et al*, 2015).

3.4.9 Purification of GAGs by anion exchange chromatography

After metabolic labelling of MEF and chondrocytes (3.3.9), cells were lysed in 200 µl or 400 µl 0.1 M NaOH, respectively. The protein concentration of the lysates was determined and subsequently diluted to 1 ml wash buffer (50 mM sodium acetate, pH 6.0, 0.2 M NaCl). For protein digestion the lysates were incubated overnight with 100 µg/ml pronase at 37 °C. The lysate was filtered through a 0.2 µm pore size filter and the GAGs were purified using diethylaminoethylcellulose (DEAE)-sepharose anion exchange chromatography. A volume of 500 µl DEAE-sepharose was placed into the column and washed with 10 ml pre-wash buffer (0.5% Triton X-100 in wash buffer). The lysate was diluted to 5 ml with wash buffer and placed into the column. The strongly negatively charged GAGs bind to the positively charged DEAE-sepharose. After washing the column with 1 ml wash buffer, GAGs were eluted with 2.5 ml elution buffer (50 mM sodium acetate, pH 6.0, 1 M NaCl). Afterwards the radioactive GAG amount was measured in a scintillation counter using an aliquot of 100 µl eluate.

To determine the relative amounts of chondroitin/dermatan sulfate and heparansulfate the purified GAGs were first desalted by a sephadex PD-10 column.

Therefore, the column was equilibrated with 25 ml H_2O and the sample loaded into the column and eluted with 3.5 ml H_2O. The eluate containing the purified GAGs was split into two equal aliquots and digested with chondroitinase ABC or heparinase I, II and III. For chondroitinase ABC digestion, 1.75 ml of purified and desalted GAGs were diluted to a final volume of 1.970 ml chondroitinase buffer (50 mM Tris (pH 7.9), 50 mM NaCl) supplemented with 0.2 mU/µl chondroitinase ABC.

For heparinase digestion, 1.75 ml of purified and desalted GAGs were diluted to a final volume of 1.980 ml heparinase buffer (50 mM sodium acetate, pH 7.0, 50 mM calcium acetate) supplemented with 0.02 mU/µl of each heparinase I, II and II.

For both reactions, the samples were incubated overnight at 37 °C in a shaking thermoblock. The undigested material was purified using DEAE chromatography as described above. After elution with 2.5 ml elution buffer, the amounts of radioactive chondroitin/dermatan sulfate and heparin sulfate were measured in a scintillation counter.

3.5 Histochemical methods

3.5.1 Examinations of *Gnptg* expression by Lacz staining

Fresh tissue from P0, P3 and 12 weeks old $Gnptg^{lacZ}$ mice was quickly dissected, embedded and frozen in Tissue-Tek® O.C.T.™. Sections of 16-20 µm thickness were prepared with a Leica 9000 sliding microtome. The sections were permeabilized in PBS containing 0.1% sodium deoxycholate, 0.2% Nonidet P-40 and fixed in 1% paraformaldehyde and 0.2% glutardialdehyde for 5 to 10 min. After washing with PBS the sections were incubated overnight in PBS containing substrate solution: 0.02% Nonidet NP-40, 0.1% sodium deoxycholate, 5 mM $K_3Fe(CN)_6$, 5 mM $K_4Fe(CN)_6$, 10 mM $MgCl_2$ and 1 mg/ml of the β-galactosidase substrate 5-bromo-4-chloro-indolyl-β-D-galactopyranoside (X-gal) at RT. Pictures were taken with a Zeiss Axiophot equipped with a digital camera and software from Kappa Optronics.

3.5.2 Histological examinations on tissue sections by electron microscopy

To analyse bone tissue by electron microscopy, 40 weeks old mice were perfused and fixed with a mixture of 4% paraformaldehyde and 1% glutaraldehyde in PBS (pH 7.2). Electron microscopy was performed by Dr. M. Schweizer (ZMNH, University Medical Center Hamburg-Eppendorf).

3.5.3 Histomorphometric analysis and µCT of bone tissue

The skeletal analysis was kindly performed by Dr. T. Yorgan (Department of Osteology and Biomechanics, University Medical Center Hamburg-Eppendorf). Therefore, vertebrae and tibiae from 4 and 25 weeks old wild-type and $Gnptg^{ko}$ mice were prepared and stained by von Kossa/Van Gieson to visualize the mineralized and non-mineralized bone. The histomorphometric analysis allow the quantification of specific parameters, such as bone volume per tissue volume (BV/TV), trabecular thickness (Tb.Th), trabecular number (Tb.N) and trabecular space (Tb.Sp). Moreover, by cellular histomorphometry the number of osteoblasts and osteoclasts per bone perimeter (N.Ob/B.Pm and N.Oc/B.Pm), the number of osteocytes per bone area (N.Ot/B.Ar) and the osteoid volume per bone volume (OV/BV) were quantified as previously described (Schinke *et al*, 2009; Kollmann *et al*, 2013). Histomorphometric analysis permitted also the quantification of the growth plate (GP) width, proliferation and hypertrophic zones.

Femurs sections from 25 weeks old mice were prepared and analysed by micro-computed tomography (µCT) which allowed the three-dimensional reconstruction of the femur and further quantification of specific parameters including BV/TV, Tb.Th, Tb.N, and Tb.Sp (Bouxsein *et al*, 2010). Tibia sections from 40 weeks old mice were analysed by touloidine blue to visualize cartilage in purple and nuclei in blue.

3.6 Statistical analysis

Microsoft Excel was used to perform the statistical analysis of the data. The arithmetic mean and the standard deviation were calculated. Statistical analysis was performed using unpaired two-tailed Student's t tests. Asterisks indicate statistically significant differences (* P-value < 0.05; ** P-value < 0.01; *** P-value < 0.001).

4. Results

4.1 Expression analysis of GlcNAc-1-phosphotransferase

The expression and tissue distribution of the GlcNAc-1-phosphotransferase is largely unknown. Similar transcript levels of *GNPTG*, encoding the human γ-subunit, were found in heart, brain, placenta, lung, liver, skeletal muscle, kidney and pancreas based on Northern blot analysis (Raas-Rothschild *et al*, 2000). The expression levels of *GNPTAB*, encoding the α- and β-subunits, in different organs were not described yet.

To analyse the *in-vivo* expression of GlcNAc-1-phosphotransferase, the mRNA levels of *Gnptg* and *Gnptab* were measured in 23 different tissues of 12 weeks old wild-type mice by quantitative real-time PCR (qPCR). Both genes were ubiquitously expressed in all analysed tissues (Fig. 4.1). Interestingly, the expression of *Gnptg* was found to be considerably higher than *Gnptab* mainly in brain, eye, liver, kidney, thyroid gland and lung. The lowest *Gnptg* expression value was found in the femur (0.7) and high transcript level in the lung (17.7), in eyes (10.1), spleen (9.8), subcutaneous fat (9.0) and kidney (8.5) in comparison with bone marrow (Fig. 4.1).
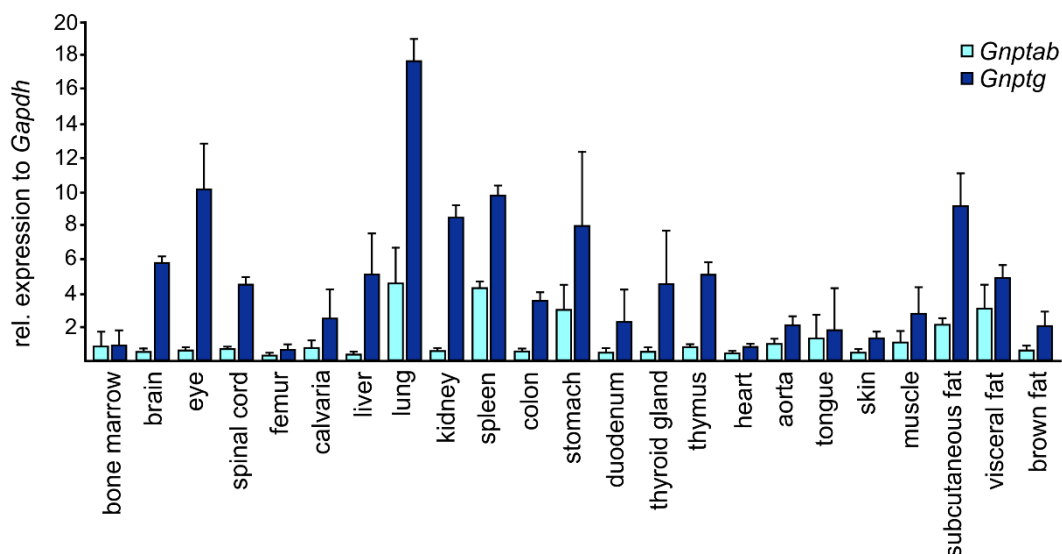
Figure 4.1. **Expression of GlcNAc-1-phosphotransferase subunits**. The relative *Gnptg* and *Gnptab* mRNA levels were measured by qPCR in different tissues of 12 weeks old wild-type mice. The data were normalized to *Gapdh*. The *Gnptg* expression in bone marrow was set as 1. Data are mean ± SD, n = 3.

Although *GNPTAB* and *GNPTG* mRNAs were found to be higher expressed in human primary macrophages in comparison to Hela cells (Pohl *et al*, 2010b), no expression data in other cell types are available so far, in particular in bone and cartilage cells mainly affected in MLIII patients.

Therefore chondrocytes were isolated from the ribcage of 10 days old wild-type mice and cultured for 10 days. In addition, bone marrow cells were isolated from 12 weeks old wild-type mice and differentiated for 10 days to osteoblasts or osteoclasts. The differentiation of the three cell types was confirmed by qPCR using cell type-specific markers. The proteoglycan aggrecan (*Acan*) mRNA encoding a prominent component of the extracellular matrix in cartilage (Kozhemyakina *et al*, 2015) was expressed in chondrocytes but not in osteoblasts and osteoclasts (Fig. 4.2 A). *Bglap* encoding osteocalcin, a marker for bone formation (Zoch *et al*, 2016), was specifically detectable in osteoblasts. The calcitonin receptor (*Calcr*) regulates osteoclast-mediated bone resorption (Zaidi *et al*, 2004). *Calcr* was highly expressed in osteoclasts but not in chondrocytes and osteoblast (Fig. 4.2). Next, the *Gnptg* and *Gnptab* mRNA expression level were analysed, which were detectable in all three primary cell types (Fig. 4.2 B). In chondrocytes and osteoblasts similar expression levels of *Gnptg* and *Gnptab* were found, whereas in osteoclasts the *Gnptab* mRNA expression was more than 2-fold increased compared to the *Gnptg* expression (Fig 4.2 B).
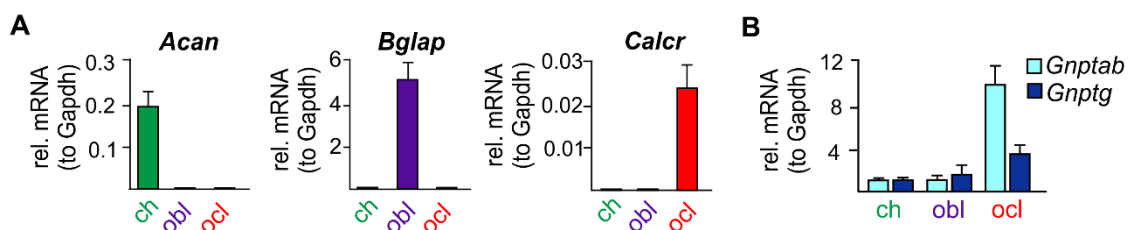
**Figure 4.2. Relative *Gnptg* and *Gnptab* expression in primary cultured bone and cartilage cells
A)** Relative mRNA level cell type-specific marker genes in chondrocytes (green, ch), osteoblasts (violet, obl) and osteoclasts (red, ocl) of wild-type mice (mean ± SD, n = 4). *Acan*, aggrecan; *Bglap*, osteocalcin; *Calcr*, calcitonin receptor. **B)** *Gnptab* and *Gnptg* mRNA expression in chondrocytes (ch), osteoblasts (obl) and osteoclasts (ocl) of wild-type mice. The transcript level of *Gnptab* and *Gnptg* in chondrocytes was assigned as 1 (mean ± SD, n = 3).

In a second approach, the *in-vivo* expression of *Gnptg* was analysed using *Gnptg^{lacZ}* reporter mice. In this mouse model the *lacZ* gene expression, encoding for the bacterial β-galactosidase, is driven by the *Gnptg* promotor and was detected using the artificial X-gal substrate that turns blue upon β-galactosidase hydrolysis. In P0 mice unspecific *lacZ* expression was observed in the gastro-intestinal tract of both wild-type and *Gnptg^{lacZ}* mice due to the presence of β-galactosidase expressing bacteria in the mucosa of the intestine (Fig. 4.3 A, c).

Specific *Gnptg* expression was detected in dorsal root ganglia and central nervous system (CNS) (a, b) of *Gnptg^lacZ* mice. Likewise, *Gnptg^lacZ* P3 mice showed strong *Gnptg* expression in the CNS (Fig. 4.3 B, a) but also in the olfactory epithelium (b), the maxilla and mandible (c, d), the trigeminal ganglion (e), the first cervical vertebra and ganglion (f) and cervical vertebra and ganglion (g). In addition to the brain (Fig. 4.3 C), *Gnptg* expression was detected in the renal pelvis of the kidney, the femur, the vertebra, in the inner segments of photoreceptors and ganglia cells of the retina, and in the sebaceous gland of hair roots (Fig. 4.3 D).
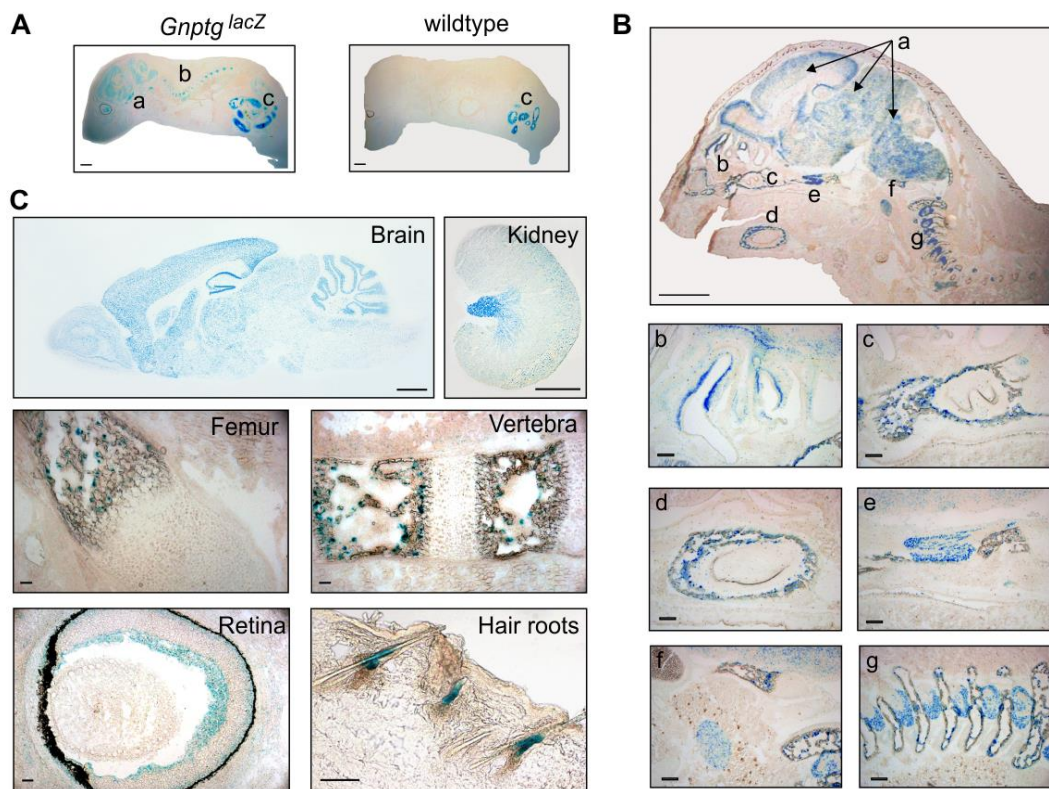
Figure 4.3. *In-vivo* expression of *Gnptg*. A) *LacZ* staining in P0 wild-type and *Gnptg^lacZ* mice in a) dorsal root ganglia, b) central nervous system, c) intestine. Scale bar: 1 mm. **B**) *LacZ* staining in P3 *Gnptg^lacZ* mice. (a) brain regions, (b) olfactory epithelium, (c) maxilla and (d) mandible, (e) trigeminal ganglion, (f) first cervical vertebra and ganglia, (g) cervical vertebra and ganglia. Scale bar left panel: 1 mm, magnified right panel b-g: 200 µm. **C)** *LacZ* staining in 12 weeks old *Gnptg^lacZ* brain (scale bar: 1 mm), kidney, vertebra, femur, retina and hair roots (scale bar: 100 µm)

Taken together, these data demonstrates ubiquitous expression pattern of the γ-subunits suggesting a crucial role of GlcNAc-1-phosphotransferase for lysosomal homeostasis and cellular functionality in several tissues and cell-types.

4.2 Role of the γ-subunits for M6P formation on lysosomal enzymes

The function of γ-subunits of the GlcNAc-1-phosphotransferase complex is unknown. In the second part, *Gnptg^{ko}* mice were used to decipher the role of γ-subunits for GlcNAc-1-phosphotransferase activity and M6P formation on lysosomal enzymes.

4.2.1 Molecular and biochemical analysis of *Gnptg^{ko}* mice

In *Gnptg^{ko}* mice the exons 4 to 11 of the murine *Gnptg* gene were deleted leading to a truncated protein of 59 amino acids (Fig. 4.4 A). Since the N-glycosylated soluble γ-subunits were found to be secreted (Encarnação *et al*, 2011), serum from wild-type, *Gnptg^{ko}* and *Gnptab^{ki}* were analysed by western blotting using an antibody against murine γ-subunit (Pohl *et al*, 2010b). Serum samples were incubated with Concanavalin A-Sepharose, which binds specifically α-D-mannose and α-D-glucose residues on glycoproteins (Surolia *et al*, 1975) and enable the enrichment of glycoproteins. In serum from wild-type and *Gnptab^{ki}* mice a 36 kDa immunoreactive protein was found, whereas no polypeptides were detectable in the serum of *Gnptg^{ko}* mice (Fig. 4.4 B). Defective γ-subunits in MLIII patients result in missorting of lysosomal enzymes to serum and urine, which is used for the biochemical diagnosis of affected patients (Raas-Rothschild *et al*, 2012).
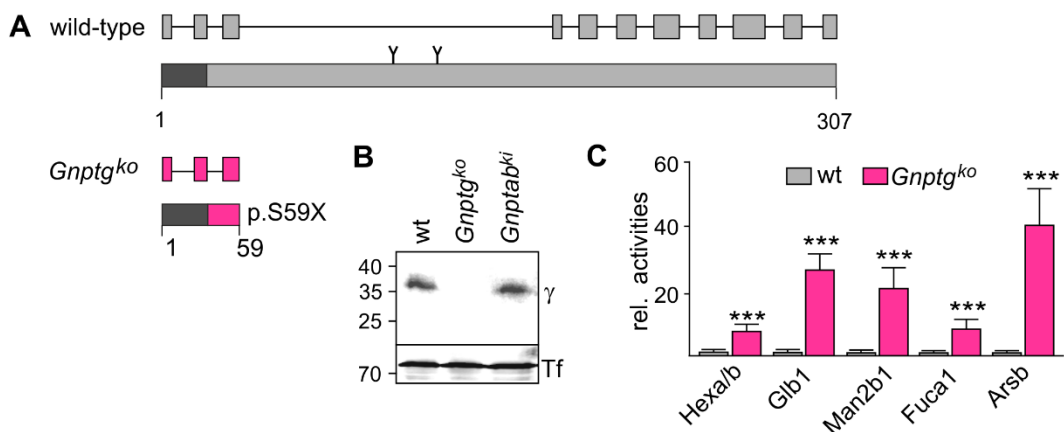
Figure 4.4. Analysis of serum from *Gnptg^{ko}* mice. A) The wild-type murine *Gnptg* gene is composed by 11 exons and translated into a protein of 307 amino acids. In the *Gnptg^{ko}* mouse exon 4 to 11 were deleted leading to a truncated protein of 59 amino acids (p.S59X). **B)** Concanavalin A-Sepharose-enriched proteins from serum of 12 weeks old wild-type (wt) and *Gnptg^{ko}* mice were separated by SDS-PAGE followed by western blot analysis using a polyclonal antibody against murine γ-subunits. Transferrin was used as loading control. **C)** The relative activities of β-hexosaminidase (Hexa/b), β-galactosidase (Glb1), α-mannosidase (Man2b1), α-fucosidase (Fuca1) and arylsulfatase B (Arsb) were measured in the serum from 12 weeks old wild-type (wt, assigned as 1) and *Gnptg^{ko}* mice (mean ± SD, ***$P \leq 0.001$, n = 3).

In the serum of *Gnptg^ko* mice, the activities of β-hexosaminidase, β-galactosidase, α-mannosidase, l-α-fucosidase and arylsulfatase B were 8- to 42-fold increased compared to serum activities of wild-type mice (Fig. 4.5 C).

To confirm the absence of γ-subunits intracellularly, mouse embryonic fibroblasts (MEF) were prepared from *Gnptg^ko* and wild-type littermates. The mRNA expression of *Gnptg* and *Gnptab* were measured by qPCR and revealed that the *Gnptg* gene expression was reduced to 4% in *Gnptg^ko* compared to wild-type MEF (Fig. 4.5 A) most likely due to nonsense-mediated decay of the mutant RNA. Moreover, the *Gnptab* mRNA expression in *Gnptg^ko* was not affected by the loss of *Gnptg* (Fig. 4.5 A). In cell extracts from *Gnptg^ko* MEF no γ-subunits were detectable whereas three immunoreactive polypeptides of approximately 35 kDa, corresponding to different glycosylated forms of γ-subunits, were found in wild-type cells (Fig. 4.5 B).
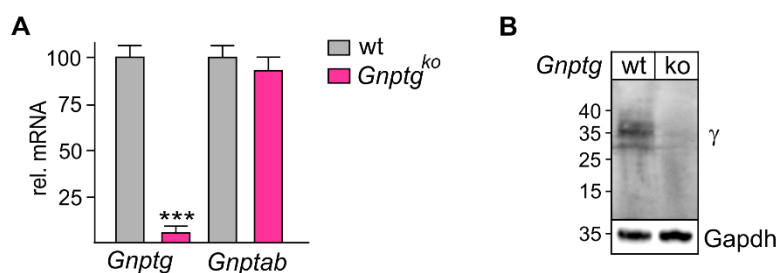
Figure 4.5. Analysis of MEF from *Gnptg^ko* mice. A) Relative *Gnptg* and *Gnptab* mRNA expression levels were measured by qPCR in wild-type (wt, 100%) and *Gnptg^ko* MEF, and normalized to *Gapdh* (mean ± SD, ***$P \leq 0.001$, n = 5). **B)** Cell extracts from wt and *Gnptg^ko* MEF were separated by SDS-PAGE and analysed by γ-subunit western blotting. Glyceraldehyde-3-phosphate dehydrogenase (Gapdh) was used as loading control.

4.2.2 Role of the γ-subunits for GlcNAc-1-phosphotransferase activity

To analyse the impact of the γ-subunits in the formation of M6P residues, the enzymatic activity of GlcNAc-1-phosphotransferase was measured using [³H]UDP-GlcNAc and α-methylmannoside as artificial phosphate donor and acceptor, respectively (Velho *et al*, 2015). In *Gnptg^ko* MEF the GlcNAc-1-phosphotransferase activity was reduced to 60% compared to wild-type cells (Fig. 4.6 A). This result indicates that the γ-subunits are required for maximum activity of the GlcNAc-1-phosphotransferase. Next, the effect of decreased GlcNAc-1-phosphotransferase activity on the formation of M6P residues was analysed. Cell extracts, corresponding media and lysosome-enriched fractions (LF) obtained by differential centrifugation from wild-type and *Gnptg^ko* MEF were analysed by western blotting using an anti-M6P antibody (Müller-Loennies *et al*, 2010).

M6P-containing proteins between 15 kDa and 100 kDa were detected in wild-type cell extracts (Fig. 4.6 A, lane 1). Significant less immunoreactive signals were found in *Gnptg^{ko}* MEF (lane 2). In lysosome-enriched fractions of wild-type MEF, elevated concentration and numbers of M6P-containing proteins were detectable compared to non-fractionated cell extracts (lane 3). Cytosolic glyceraldehyde-3-phosphate dehydrogenase (Gapdh) was used as loading control of cell extracts and not present in lysosomal fractions demonstrating the successful enrichment of lysosomal proteins. More importantly, LF of *Gnptg^{ko}* MEF showed lower amounts of M6P-containing proteins compared to wild-type controls (lane 4). Furthermore, the intracellular activities of selected lysosomal enzymes were measured in *Gnptg^{ko}* in relation to wild-type cells. The activities of arylsulfatase B, β-hexosaminidase, β-galactosidase, α-mannosidase and L-α-fucosidase were reduced to 18 - 47% compared to wild-type cells, whereas the activity of N-acetylgalactosamine-6-sulfatase was unaffected in *Gnptg^{ko}* MEF (Fig.4.6 B).
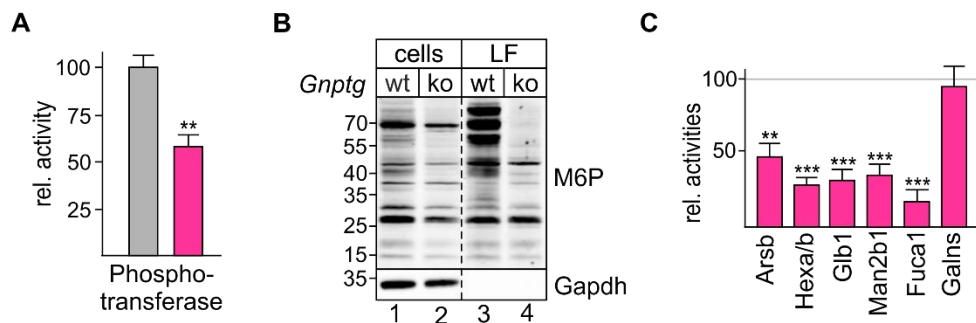
Figure 4.6. Role of the γ-subunits for GlcNAc-1-phosphotransferase activity. A) Relative GlcNAc-1-phosphotransferase activity was determined in cell extracts of wt (100%) and *Gnptg^{ko}* MEF (mean ± SD, **$P \leq 0.01$, n = 3). **B)** Cell extracts (100 µg) and lysosome-enriched fractions (LF, 75 µg) from wt and *Gnptg^{ko}* MEFs were separated by SDS-PAGE followed by western blotting using a single-chain anti-M6P antibody fragment. Gapdh was used as loading control. **C)** Relative enzyme activities of arylsulfatase B (Arsab), β-hexosaminidase (Hexa/b), β-galactosidase (Glb1), α-mannosidase (Man2b1), L-α-fucosidase (Fuca1) and N-acetylgalactosamine-6-sulfatase (Galns) in cell extracts of wt (100%) and *Gnptg^{ko}* MEFs (mean ± SD, **$P \leq 0.01$, ***$P \leq 0.001$, n = 5).

These data show that the absence of γ-subunits in *Gnptg^{ko}* mice leads to decreased GlcNAc-1-phosphotransferase activity, impaired M6P formation on lysosomal enzymes and consequently to missorting of specific lysosomal enzymes, the characteristic biochemical phenotype observed in MLIII patients.

4.2.3 Lysosomal proteome of Gnptg^{ko} MEF

To determine the relative amounts of lysosomal proteins in lysosomes at steady-state, SILAC-based comparative mass spectrometry (MS) was performed. Therefore, MEF were cultivated for six passages in SILAC-DMEM containing either L-arginine and L-lysine for light labeling of *Gnptg^{ko}* cells or L-arginine-$^{13}C_6^{15}N_4$ and L-lysine-$^{13}C_6^{15}N_2$ for heavy labeling of wild-type cells. MEF were incubated for 24 h with magnetite particles followed by a 36 h chase to allow the accumulation of magnetic beads in lysosomes (Thelen *et al*, 2017). Equal amounts of postnuclear supernatants (PNS) from both cell lines were combined, followed by magnetic isolation of lysosomes and MS analysis (Fig. 4.7 A). Among 51 identified soluble lysosomal proteins 29 proteins show statistically significant alterations in their concentration in lysosomes of *Gnptg^{ko}* compared to wild-type cells ($p \leq 0.005$, Table 4.1).

Table 4.1. Lysosomal soluble proteins identified in lysosomal fractions of wt and *Gnptg^{ko}* cells in three replicates.

Gene	Protein	ko/wt ratio		
		mean	SD	P-value
Plbd2	putative phospholipase B-like 2	0.10	0.02	0.001
Ppt2	palmitoyl-protein thioesterase 2	0.11	0.01	0.002
Pla2g15	phospholipase A2, group XV	0.13	0.01	0.001
Arsa	arylsulfatase A	0.13	0.03	0.001
Siae	sialate O-acetylesterase	0.15	0.03	0.001
Arsb	arylsulfatase B	0.16	0.01	0.001
Manba	β-mannosidase	0.16	0.05	0.001
Aga	aspartylglucosaminidase	0.17	0.01	0.001
Dpp7	dipeptidyl-peptidase 7	0.17	0.05	0.001
Ctsc	cathepsin C	0.22	0.02	0.011
Hexa	β-hexosaminidase α-subunit	0.23	0.06	0.002
Man2b2	α-mannosidase, class 2B member 2	0.23	0.08	0.002
Glb1	β-galactosidase	0.23	0.03	0.002
Tpp1	tripeptidyl peptidase I	0.25	0.06	0.002
Ctbs	di-N-acetylchitobiase	0.27	0.08	0.010
Ctsz	cathepsin Z	0.27	0.06	0.004
Creg1	Creg1 protein	0.28	0.11	0.003
Hexb	β-hexosaminidase β-subunit	0.29	0.08	0.004
Ggh	γ-glutamyl hydrolase	0.29	0.10	0.010
Ctss	cathepsin S	0.32	0.15	0.005
Prcp	prolylcarboxypeptidase	0.35	0.10	0.005

Gns	N-acetylglucosamine-6-sulfatase	0.38	0.16	0.009
Galc	galactocerebrosidase	0.39	0.29	0.011
Cpq	carboxypeptidase Q	0.40	0.18	0.043
Asah1	acid ceramidase	0.45	0.16	0.016
Neu1	sialidase 1	0.46	0.09	0.044
Lipa	lysosomal acid lipase	0.46	0.17	0.015
Cln5	ceroid-lipofuscinosis neuronal protein 5	0.47	0.07	0.050
Lgmn	legumain	0.54	0.29	0.053
Scpep1	serine carboxypeptidase 1	0.55	0.17	0.044
Ctsa	cathepsin A	0.57	0.11	0.037
Man2b1	α-mannosidase, class 2B member 1	0.61	0.33	0.168
Rnaset2	ribonuclease T2	0.63	0.28	0.171
Naaa	N-acylethanolamine acid amidase	0.64	0.05	0.138
Galns	N-acetylgalactosamine-6-sulfatase	0.66	0.19	0.092
Ctsd	cathepsin D	0.68	0.30	0.267
Epdr1	mammalian ependymin-related protein 1	0.69	0.16	0.137
Ctsh	cathepsin H	0.70	0.08	0.096
Gaa	α-glucosidase	0.73	0.30	0.319
Ctsb	cathepsin B	0.74	0.28	0.352
Gm2a	ganglioside GM2 activator	0.76	0.27	0.267
Gla	α-galactosidase	0.77	0.25	0.301
Dnase2	Deoxyribonuclease II	0.78	0.36	0.420
Acp2	lysosomal acid phosphatase	0.86	0.17	0.367
Gusb	β-glucuronidase	0.91	0.40	0.545
Naga	α-N-acetylgalactosaminidase	0.92	0.34	0.526
Ppt1	palmitoyl-protein thioesterase 1	0.98	0.44	0.533
Psap	prosaposin	1.06	0.30	0.614
Npc2	Niemann-Pick disease type C2 protein	1.12	0.06	0.480
Ctsl	cathepsin L	1.47	0.57	0.545
Gba	β-glucocerebrosidase	1.78	0.15	0.030

The relative quantities of individual proteins were presented as *Gnptg*[ko]/wild-type (light/heavy) ratio (Fig. 4.7B). The threshold line (set as 1.0) reflects no alteration of lysosomal protein levels in the *Gnptg*[ko] compared to wild-type cells. The concentrations of 19 lysosomal enzymes were decreased to ≤ 50% and of 9 proteins to ≤ 20% in *Gnptg*[ko] lysosomal fractions compared to wild-type MEF (Fig. 4.7B, blue circles). The least abundant enzyme was found to be the putative phospholipase B-like 2 (Plbd2) accounting 10% of in *Gnptg*[ko] lysosomal compared to wild-type controls.

Others enzymes present below 20% of control were palmitoyl-protein thioesterase 2 (Ppt2) and group XV phospholipase A2 (Pla2g15) involved in lipid degradation, arylsulfatases A and B (Arsa and Arsb), sialate O-acetylesterase (Siae), β-mannosidase (Manba) and aspartylglucosaminidase (Aga) required for glycan degradation, and dipeptidyl-peptidase 7 (Dpp7) for peptide degradation. In contrast, 22 lysosomal proteins were slightly or not altered in *Gnptg^{ko}* lysosomal fractions compared to wild-type MEF (Fig. 4.7B, black circles), suggesting that they are transported to lysosomes with comparable efficiency as in wild-type cells. These results further suggest that α- and β-subunits are sufficient for the correct M6P-phosphorylation and/or transport of those enzymes to lysosomes. The amount of β-glucocerebrosidase (Gba), a lysosomal enzyme targeted independent of M6P residues (Reczek *et al*, 2007), was 1.8-fold increased in lysosomal fractions of *Gnptg^{ko}* compared to wild-type MEF (Fig. 4.7B, red circle). In addition, the concentration of cathepsin L (Ctsl) was 1.5- fold elevated in *Gnptg^{ko}* lysosomes compared to the control cells.
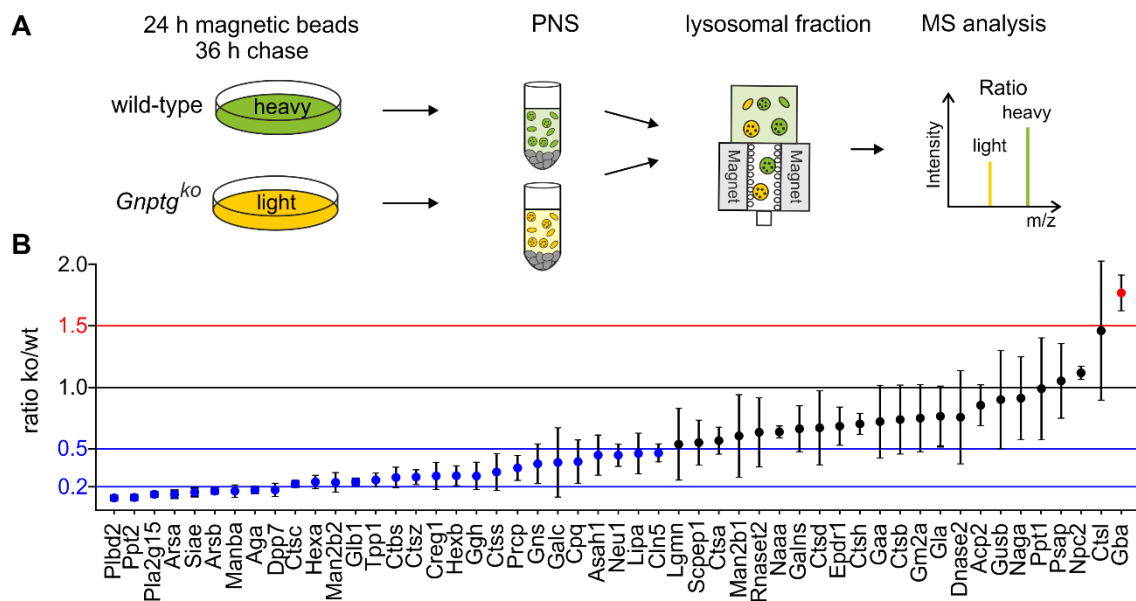
Figure 4.7. SILAC-based quantitative lysosomal proteome analysis of *Gnptg^{ko}* MEF. A) MEF were grown in light (*Gnptg^{ko}*) and heavy-isotope (wild-type) labelled medium, incubated with magnetite particles followed by a 36 h chase to allow magnetic beads accumulation in lysosomes. Equal amounts of postnuclear supernatants (PNS) proteins from both cell lines were combined, followed by magnetic isolation of lysosomes and MS analysis. **B)** Proteomic data of soluble lysosomal enzymes are plotted against *Gnptg^{ko}*/wild-type (ko/wt) ratio (mean ± SD, n = 3). The threshold lines of 0.2 and 0.5 (blue), 1.0 (black) as well as 1.5 (red) are marked.

To analyse whether the altered lysosomal proteome might be caused by changes of mRNA expression levels, qPCR was performed measuring the transcript levels of 42 selected lysosomal enzymes in wild-type and *Gnptg^{ko}* MEF. The gene expression level of most lysosomal enzymes in *Gnptg^{ko}* MEF was comparable to wild-type cells (Fig. 4.8) with the exception of *Ctss* that was reduced to 50% in *Gnptg^{ko}* MEF. The transcript levels of 8 enzymes (*Manba*, *Aga*, *Dpp7*, *Neu1*, *Cln5*, *Epdr1*, *Gba,* and *Arsk*) were moderately increased, whereas the of *Npc2* mRNA was 2.8-fold up-regulated in *Gnptg^{ko}* MEF (Fig. 4.8). These data showed that the *Gnptg* deficiency affects the correct targeting of subsets of enzymes to lysosomes rather than their transcriptional regulation.
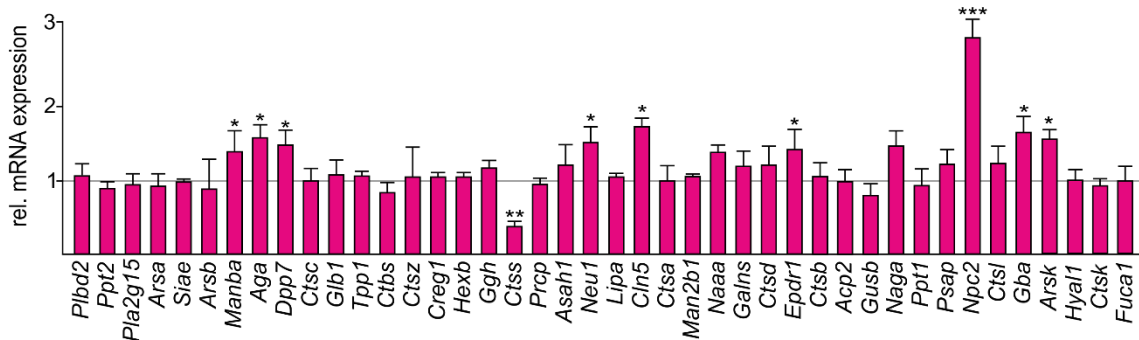
Figure 4.8. mRNA expression of lysosomal matrix proteins in *Gnptg^{ko}* MEF. Relative mRNA expression levels of indicated genes were measured by qPCR encoding soluble lysosomal enzymes and proteins in wild-type (wt, 1) and *Gnptg^{ko}* MEF (mean ± SD, $*P \leq 0.05$, $**P \leq 0.01$, $***P \leq 0.001$, n = 3). The data were normalized to the transcript level of *Actb*.

4.2.4 Validation of the lysosomal proteome analysis

To verify the proteomic data, the distribution of selected lysosomal enzymes, based on the availability of commercial antibodies, was analysed by western blotting. For this purpose, aliquots of cell extracts, corresponding media conditioned for 24 h and lysosome-enriched fractions were used. Many lysosomal enzymes are synthesized as precursor forms of higher molecular mass in the ER, posttranslationally modified in the Golgi apparatus, and eventually proteolytically processed to mature forms in lysosomes. For example, the precursor and mature forms of cathepsin C (Ctsc) were detected at 55 kDa and 25 kDa, respectively, in wild-type cell extract (Fig. 4.9 A, lane 1), whereas decreased Ctsc mature forms were observed in *Gnptg^{ko}* cell extracts (lane 2). In the media of *Gnptg^{ko}* cells, elevated amounts of Ctsc precursors were observed compared to media of wild-type cells (Fig. 4.9 A, lane 3 and 4). In lysosome-enriched fractions a strong reduction of mature lysosomal Ctsc was detected in the absence of γ-subunits compared to controls (lane 5 and 6).

Likewise, the amounts of mature Ctsz and Ctss forms were decreased in lysosome-enriched fractions from *Gnptg^ko* MEF (Fig 4.9 A, lane 5 and 6), accompanied by elevated secreted precursor forms into the media of *Gnptg^ko* cells (lane 4). The intracellular protein levels of precursor and mature forms of Ctsb and Ctsd were slightly increased in *Gnptg^ko* cells associated with elevated secretion of the precursors into the extracellular space of *Gnptg^ko* MEF (Fig. 4.9 B).
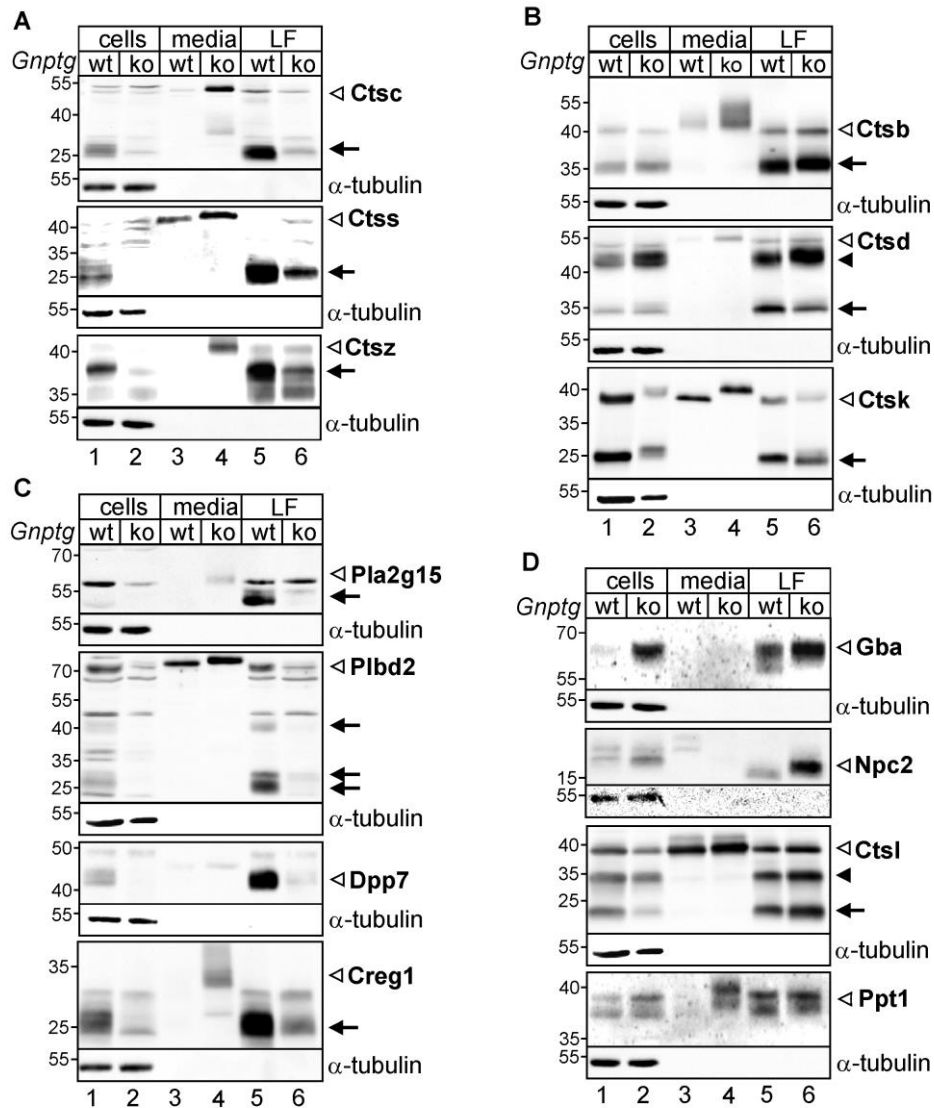
Figure 4.9. Distribution of selected soluble lysosomal proteins in *Gnptg^ko* MEF and media. A-D) Cell extracts (100 µg proteins), corresponding, conditioned media (20%) and lysosome-enriched fractions (LF, 75 µg proteins) from wild-type (wt) and *Gnptg^ko* (ko) MEF were separated by SDS-PAGE and analysed by western blotting using antibodies against soluble lysosomal enzymes. Cellular α-tubulin was used as loading control. The mature forms of lysosomal enzymes are marked with black arrows, intermediate and precursor forms with black and non-filled arrowheads, respectively.

Although Ctsk was not identified by mass spectrometry, Ctsk precursor and mature form were detected by western blotting, which demonstrates that Ctsk was delivered to lysosomes of both *Gnptg^{ko}* and wild-type cells (Fig. 4.9 B, lane 5 and 6). In addition, the steady-state levels of Pla2g15, Plbd2, Dpp7 and Creg1 were found to be strongly reduced in lysosome-enriched fractions of *Gnptg^{ko}* MEF associated with hypersecretion of the respective precursor forms (Fig 4.9 C). The loss of Dpp7 both in lysosome-enriched fractions and media suggested rapid degradation in *Gnptg^{ko}* cells (Fig 4.9 C, lane 2, 4 and 6). Gba is delivered to lysosomes in an M6P-independent manner via binding to the lysosomal integral membrane protein (Limp2) (Reczek *et al*, 2007). In agreement with the proteomic data and mRNA expression, the concentration of Gba protein levels were increased in *Gnptg^{ko}* cell extracts (Fig. 4.9 D, lane 2) and lysosome-enriched fractions compared to wild-type (lane 6), supporting the concept of the M6P-independent transport of Gba to lysosomes. Likewise, the Npc2 protein level was elevated in *Gnptg^{ko}* lysosomal-enriched fractions (lane 6), whereas, the amounts of Ctsl and Ppt1 were comparable to wild-type cells. Why Ppt1 was in addition hypersecreted into the media of *Gnptg^{ko}* cells (lane 5 and 6) is unclear.

These western blot analyses confirmed that Ctsc, Ctss, Ctsz, Pla2g15, Plbd2, Dpp7 and Creg1 were partially missorted to the media and less present in the lysosomes of *Gnptg^{ko}* MEF compared to wild-type cells, which is in accordance with the proteomic data. Furthermore, the altered delivery of certain lysosomal enzymes to the lysosomes affects the processing of Ctsb and Ctsd which accumulate in *Gnptg^{ko}* lysosomes. Finally, the absence of γ-subunits impaired the electrophoretic mobility of some secreted precursor forms of certain lysosomal enzymes such as Ctsc, Ctss, Ctsz, Pla2g15, Plbd2, Dpp7, Creg1, Ctsk and Ppt1 indicating conversions of their high mannose-type disaccharides to complex sugar chain.

4.2.5 M6P proteome of *Gnptg^{ko}* MEF

The lysosomal proteome analysis revealed the dependency of several lysosomal proteins of γ-subunits of GlcNAc-1-phosphotransferase for lysosomal trafficking. However, the γ-subunits-dependent missorting of lysosomal enzymes and the analysis of these enzymes in defective lysosomes can be misleading because subpopulation of lysosomal enzymes can be targeted also in the absence of M6P via alternative processes via secreted-recapture mechanism (Hickman & Neufeld, 1972; Markmann *et al*, 2015).

To examine the direct role of γ-subunits for M6P generation on soluble lysosomal enzymes, the lysosomal proteome of MEF cells was determined. For this purpose, MEF were grown for 24 h in light- (*Gnptg^{ko}*) and heavy-isotope (wild-type) labelled medium containing 10 mM NH$_4$Cl (Fig. 4.10 A) which increases the pH of acidic compartments such as the TGN, endosomes and lysosomes (Braulke *et al*, 1987). This leads to elevated pH values preventing the dissociation of newly synthesized lysosomal enzymes from M6P receptors, which subsequently caused a deficiency of binding-active M6P-receptors in the TGN and increased secretion of lysosomal enzymes. Secreted M6P-containing proteins from both wild-type and *Gnptg^{ko}* culture media were isolated by M6P affinity chromatography using a single-chain anti-M6P antibody fragment coupled to agarose beads. Proteins bound to M6P beads were analysed by mass spectrometry and the *Gnptg^{ko}*/wild-type (light/heavy) ratios of the identified 33 soluble lysosomal proteins were plotted. Among those, 12 lysosomal enzymes were significantly reduced to ≤ 50% in the M6P bound fraction of *Gnptg^{ko}* media, i.e. Tpp1, Prcp, Plbd2, Hexa/b, Ctsk, Glb1, Man2b2, Creg1, Arsb, Ctss and Asah1 (Fig. 4.10 B).
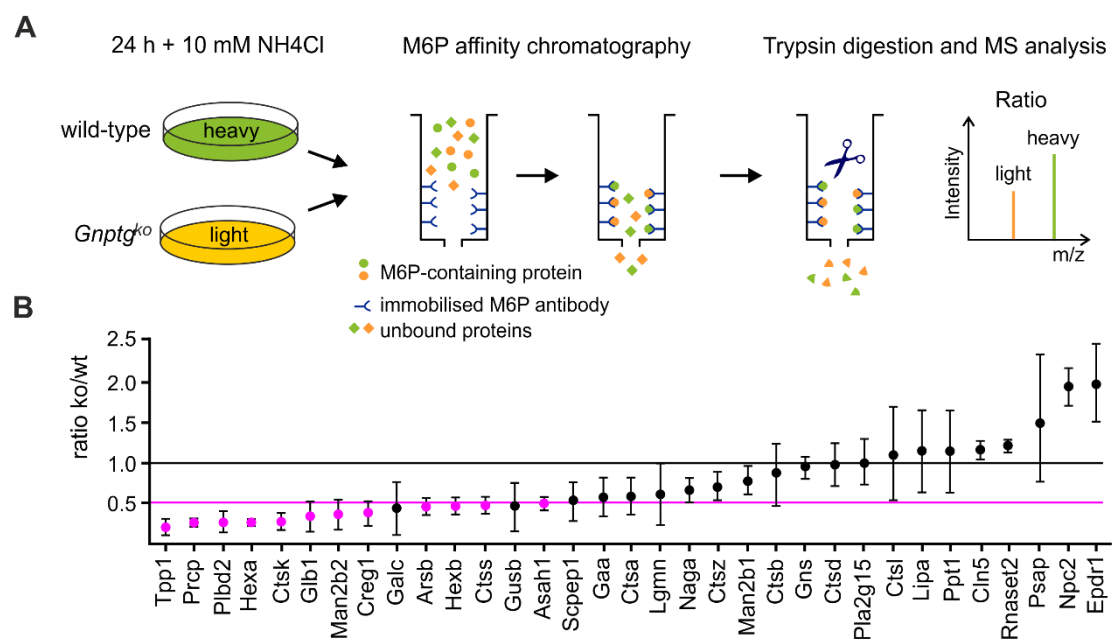
Figure 4.10. Selective M6P formation on lysosomal enzymes in *Gnptg^{ko}* MEF. A) MEF were grown in light (*Gnptg^{ko}*) and heavy-isotope (wild-type, wt) labelled medium containing 10 mM NH$_4$Cl for 24 h. Equal amounts of concentrated media from both cell lines were combined, followed by M6P affinity chromatography, trypsin digestion of bound proteins and MS analysis. **B)** M6P affinity chromatography of NH$_4$Cl-supplemented media were analysed by MS and the soluble lysosomal proteins were plotted against *Gnptg^{ko}*/wild-type (ko/wt) ratio (mean ± SD, n = 3). Significantly reduced lysosomal enzymes are indicated in magenta. Ratios of ≤ 0.5 and 1.0 are marked as magenta and black lines, respectively.

In contrast, double amounts of M6P-modified Npc2 and Epdr1 were secreted by *Gnptg*[^ko]

in comparison to wild-type cells.The residual 19 lysosomal enzymes in *Gnptg*[^ko] were

comparable to wild-type cells. These data demonstrate that γ-subunits are essential for

selective M6P formation on specific lysosomal enzymes.

4.2.6   Loss of Arsb causes accumulation of GAGs in *Gnptg*[^ko] MEF

The comparative lysosomal proteome and M6P secretome analyses of MEF demonstrated

a lower M6P formation on selected lysosomal enzymes leading to their altered delivery

to lysosomes in *Gnptg*[^ko] cells. Among them, the sorting of lysosomal arylsulfatase B

(Arsb) was found to be highly dependent on the γ-subunit (Fig. 4.4, 4.6, 4.7 and 4.10).

Arsb (N-acetylgalactosamine-4 sulfatase) is involved in the degradation of

glycosaminoglycans (GAGs) by removing the C4 sulfate group from chondroitin sulfates

and dermatan sulfates (Fig. 4.11 A). For GAG analysis, wild-type and *Gnptg*[^ko] MEF were

labelled with $^{35}SO_4$ for 24 h (pulse) to mark all sulfate groups on newly synthesized GAG.

During a chase period in non-radioactive media for 24 h radioactively labelled GAG

reached the lysosomal compartment for degradation. In *Gnptg*[^ko] MEF the $^{35}SO_4$-labelled

molecules were 6-fold elevated compared to wild-type cells (Fig. 4.11 B). By anion-

exchange chromatography, GAGs were purified and the $^{35}SO_4$-labelled GAGs were

measured by liquid scintillation spectrometry (LSS) revealing 6.2-fold elevated total

GAGs in *Gnptg*[^ko] compared to wild-type cells (Fig. 4.11 C).

For specific analysis, equal amounts of purified GAGs were treated with chondroitinase

ABC (cleaving e.g. chondroitin 4-sulfates, chondroitin 6-sulfates and dermatan sulfates,

CS/DS) or heparinase I, II and III (cleaving heparansulfate, HS) and the respective

resistant GAGs purified by anion exchange chromatography followed by LSS. In *Gnptg*[^ko]

MEF a 5.5- and 10-fold accumulation of HS and CS/DS was observed compared to wild-

type MEF (Fig. 4.11 D).
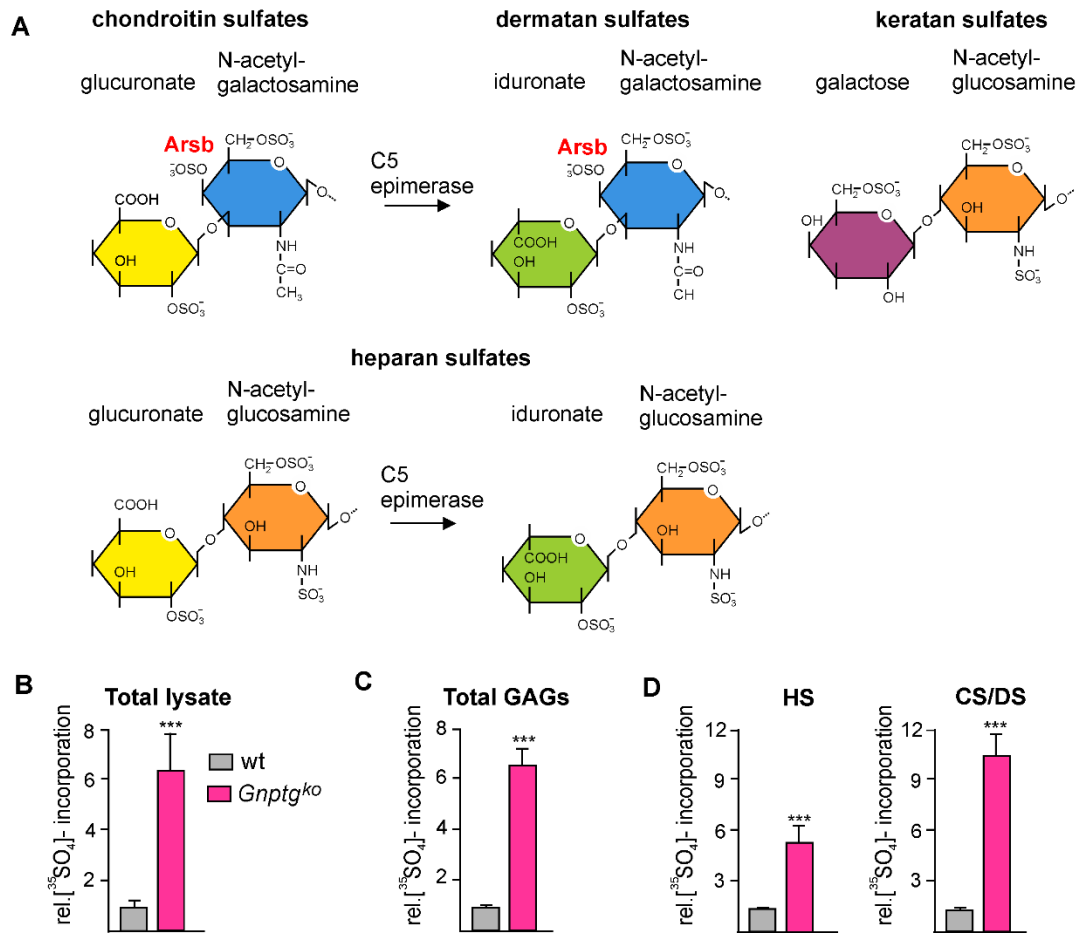
Figure 4.11. Accumulation of sulfated GAGs in *Gnptg^{ko}* MEF. A) Schematic presentation of disaccharide units of chondroitin sulfates, dermatan sulfates, heparan sulfates and keratan sulfates. Chondroitin sulfates consist of N-acetylgalactosamine and glucuronate that can epimerize to iduronate resulting in dermatan sulfates. Heparan sulfates are composed by N-acetylglucosamine and glucuronate that can epimerize to iduronate. Keratan sulfates consist of galactose and N-acetylglucosamine. Arsb, cleaving the C4 sulfate group from chondroitin sulfates and dermatan sulfates, is marked in red. **B**) Relative [^{35}SO$_4$]-content in wild-type (wt) and *Gnptg^{ko}* MEF after 24 h pulse and 24 h chase measured in the total lysate (wt was set as 1; n=2). **C**) Quantification of purified ^{35}SO$_4$-labelled GAGs (wt was assign as 1; ***$P \leq 0.001$, n = 2). **D**) Quantification of purified ^{35}SO$_4$-labelled HS and CS/DS after digestion with chondroitinase ABC or heparinase I, II and III, respectively (wt was set as 1) (***$P \leq 0.001$, n = 2).

To investigate whether the CS/DS accumulation in *Gnptg^{ko}* MEF was caused by the loss of Arsb, the cells were incubated with recombinant human ARSB (75 nM) during the chase period. The uptake and lysosomal delivery of recombinant ARSB in wild-type MEF was documented by western blot analysis using an antibody against human ARSB. The recombinant ARSB was detected as 68 kDa precursor protein in the input and as mature 40 kDa lysosomal form in cell extracts of wild-type MEF incubated for 4 h with ARSB (Fig. 4.12 A).

By the measurement of the intracellular ARSB activity, an approximately 5-fold increase was observed in wild-type and *Gnptg^{ko}* cells compared to non-treated cells (Fig. 4.12 B).
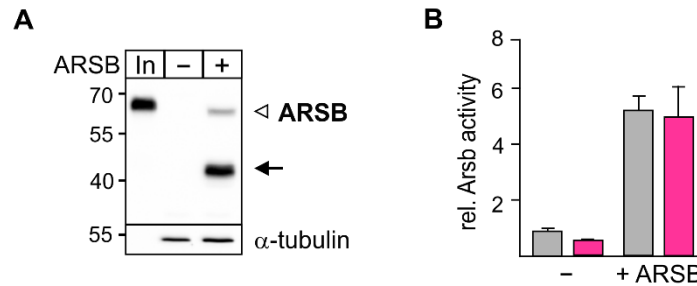
Figure 4.12. ARSB uptake in wild-type and *Gnptg^{ko}* MEF. A) Aliquots containing 50 ng of recombinant ARSB (input, IN) and cell extracts (25 µg proteins) from wild-type MEF incubated in the absence (-) or presence (+) of ARSB were separated by SDS-PAGE and analysed by western blotting. Cellular α-tubulin was used as loading control. The mature form of ARSB is marked by a black arrow and the precursor by a non-filled arrowhead. **B)** Relative ARSB activities in wild-type (wt) and *Gnptg^{ko}* MEFs in the absence (-) or presence (+) of ARSB (non-treated wt was set as 1; mean ± SD; n = 2).

In ARSB-treated *Gnptg^{ko}* cells a decrease in GAG accumulation was observed compared to non-treated *Gnptg^{ko}* cells (Fig. 4.13 A). Equal amounts of purified GAG were treated with chondroitinase ABC or heparinase I, II and III and HS and CS/DS were quantified by LSS. Strikingly, the treatment with recombinant ARSB reduced the CS/DS accumulation in *Gnptg^{ko}* by 40%, whereas the HS content was comparable to non-treated cells (Fig. 4.13 B).
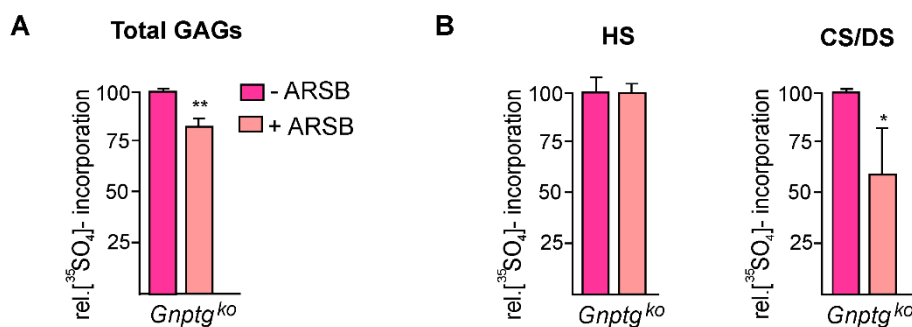
Figure 4.13. ARSB partially abolishes the accumulation of sulfated GAGs in *Gnptg^{ko}* MEF. A) Quantification of purified $^{35}SO_4$-labelled GAGs in *Gnptg^{ko}* MEF after 24 h pulse and 24 h chase in the absence (-) or presence (+) of human recombinant ARSB (non-treated *Gnptg^{ko}* was assign as 100%) (**$P \leq 0.01$, n = 2). **B)** Quantification of purified $^{35}SO_4$-labelled HS and CS/DS after digestion with chondroitinase ABC or heparinase I, II and III, respectively (non-treated *Gnptg^{ko}* was set as 100%) (*$P \leq 0.05$, n = 2).

To prove whether the partial ARSB-mediated reduction in CD/DS content was due to limiting amounts of endocytosed ARSB, the same experiment was performed in wild-type and $Arsb^{ko}$ MEF (kindly provided by Dr. T. Schinke, UKE). In $Arsb^{ko}$ cells the total GAG fraction was 6.9-fold increased compared to wild-type MEF (Fig. 4.14 A).
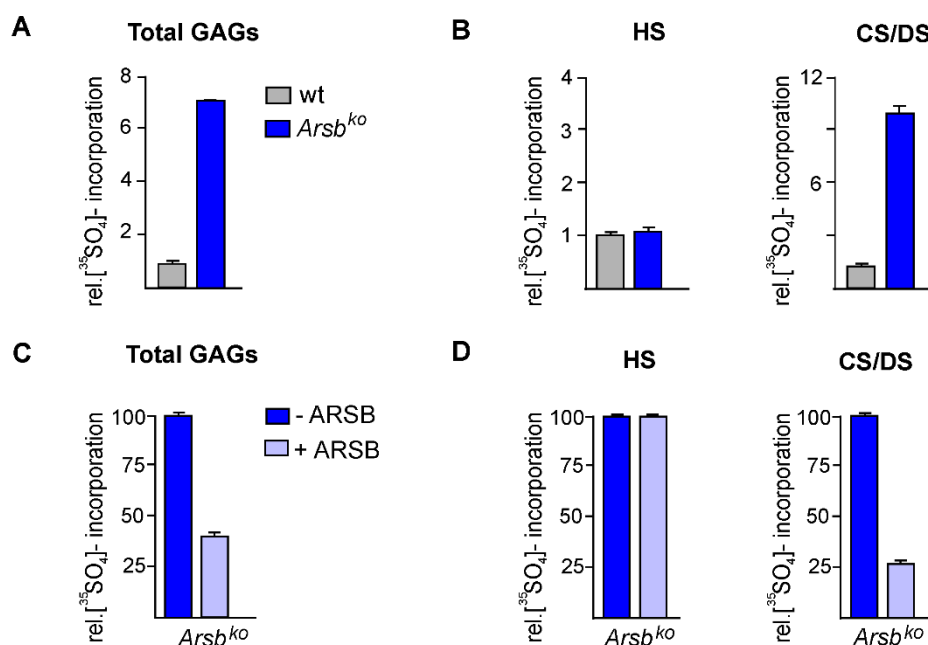
Figure 4.14. [^{35}SO$_4$] content in $Arsb^{ko}$ MEF. A) Quantification of purified ^{35}SO$_4$-labelled GAGs in wild-type (wt) and $Arsb^{ko}$ MEF after 24 h pulse and 24 h chase (wt was set as 1) (mean ± SD, n = 2). **B)** Quantification of purified ^{35}SO$_4$-labelled HS and CS/DS after digestion with chondroitinase ABC or heparinase I, II and III, respectively (wt was set as 1) (n = 2). **C)** Quantification of purified ^{35}SO$_4$-labelled GAGs in $Arsb^{ko}$ MEF after 24 h pulse and 24 h chase in the absence (-) or presence (+) of human recombinant ARSB (non-treated $Arsb^{ko}$ cells were assigned as 100%) (n = 2). **D)** Quantification of purified ^{35}SO$_4$-labelled HS and CS/DS after digestion with chondroitinase ABC or heparinase I, II and III, respectively (non-treated $Arsb^{ko}$ cells were set as 100%) (n = 2).

As expected for $Arsb$-deficient cells, exclusively CS/DS levels were 10.6-fold increased compared to wild-type cells (Fig. 4.14 B). Upon ARSB treatment of wild-type and $Arsb^{ko}$ MEF, the ^{35}SO$_4$-labelled GAG accumulation was reduced to 34% and the storage of ^{35}SO$_4$-labelled CS/DS was completely rescued (Fig. 4.14 C and D). These results demonstrated that the $Arsb$-deficiency can be fully corrected using human recombinant ARSB. These data indicate that the partial rescue of the CS/DS accumulation observed in $Gnptg^{ko}$ MEF is due to the missorting of additional lysosomal enzymes rather than insufficient ARSB treatment.

In summary, the absence of the γ-subunits of GlcNAc-1-phosphotransferase reduces the efficiency of M6P formation on lysosomal enzymes. The low M6P content of Arsb in particular leads to its missorting and consequently to accumulation of sulfated CS/DS levels in lysosomes of *Gnptg*^*ko* cells. The treatment of *Gnptg*^*ko* cells with recombinant ARSB reduces lysosomal GAGs accumulation.

4.3 Role γ-subunits for bone and cartilage homeostasis

Since skeletal abnormalities are the most prominent disabling features in MLIII patients, the effects of the loss γ-subunits on bone and cartilage were analysed in *Gnptg*^*ko* mice.

4.3.1 Bone architecture of *Gnptg*^*ko* mice

Non-decalcified skeletal sections from 4 weeks old mice were analysed by von Kossa/Van Gieson staining, which stain mineralized bone (black colour) and non-mineralized matrix (pale pink). No visible mineralization abnormalities were observed in vertebral bodies and tibiae of *Gnptg*^*ko* mice compared to wild-type littermates (Fig. 4.15 A, B). In addition, quantitative histomorphometric analysis of structural parameters of vertebral bodies and tibia revealed no quantitative differences in bone volume, trabecular thickness, trabecular number and trabecular spacing in *Gnptg*^*ko* mice compared to wild-type controls. (Fig. 4.15 C, D). Furthermore, based on the quantification of cellular parameters no significant differences in the number of osteoblasts, osteoclasts and osteocytes were observed in the tibia of *Gnptg*^*ko* mice compared to wild-type littermates (Fig. 4.15 E). Accordingly, the mineralization of the bone matrix was unaffected demonstrated by unchanged osteoid content per bone volume in *Gnptg*^*ko* in comparison to wild-type mice (Fig. 4.15 F).
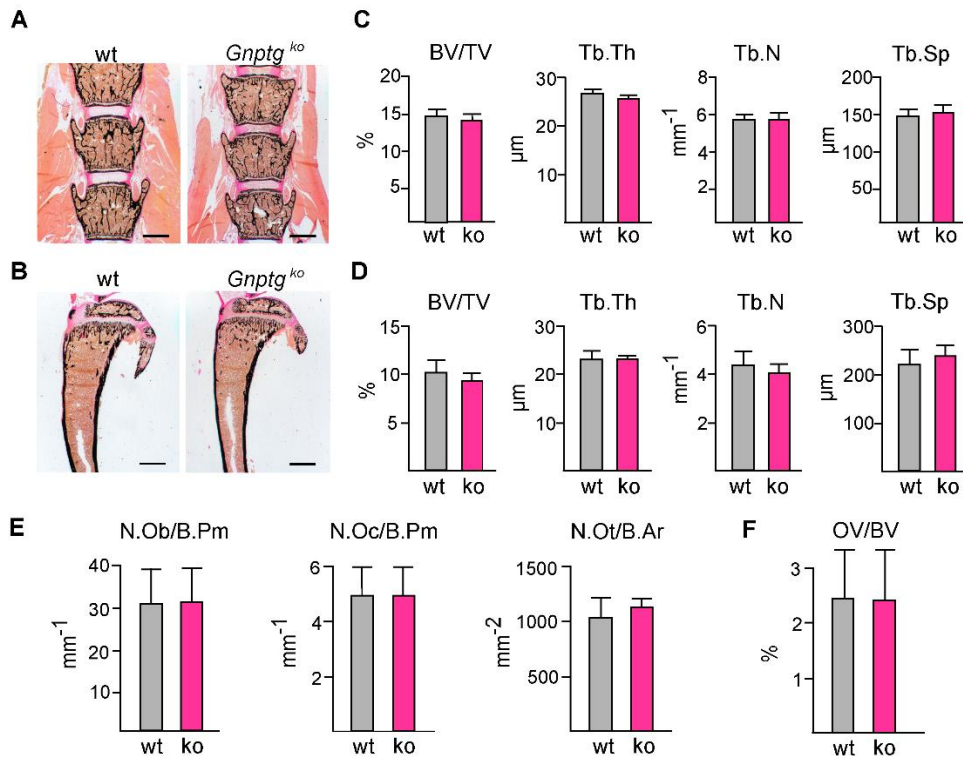
Figure 4.15 Histomorphometric analyses of 4 weeks old *Gnptg^{ko}* mice. A and **B)** Representative non-decalcified sections of vertebral bodies **(A)** and tibia **(B)** from female wild-type (wt) and *Gnptg^{ko}* (ko) mice stained after von Kossa/Van Gieson (scale bar: 1 mm). **C** and **D)** Quantification of structural parameters of vertebral bodies **(C)** and tibia **(D)** of the same mice: bone volume per tissue volume (BV/TV), trabecular thickness (Tb.Th), trabecular number (Tb.N) and trabecular spacing (Tb.Sp). **E)** Quantification of cellular parameters in the trabecular area of the tibia of female wild-type (wt) and *Gnptg^{ko}* (ko) mice: number of osteoblasts per bone perimeter (N.Ob/B.Pm), number of osteoclasts per bone perimeter (N.Oc/B.Pm), number of osteocytes per bone area (N.Ot/B.Ar). **F)** Quantification of the bone osteoid volume per bone volume (OV/BV) in the same mice. (n = 4, mean ± SD).

MLIII patients are clinically characterized by short stature. Since skeletal growth primarily depends on the coordinated differentiation of growth plate chondrocytes, the width of the growth plates from tibiae was examined. The thickness of the growth plates in 4 weeks old *Gnptg^{ko}* mice, both the proliferation and the hypertrophic zone, was comparable to wild-type littermates (Fig. 4.16).
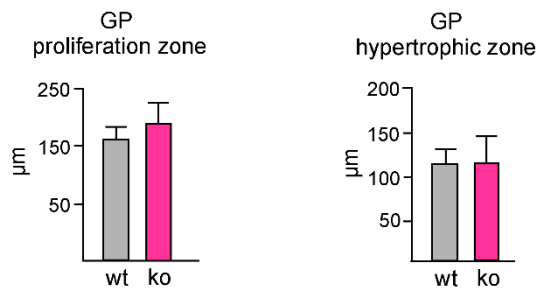
Figure 4.16 Histomorphometric analyses of growth plate chondrocytes in 4 weeks old *Gnptg^{ko}* mice. Quantification of the growth plate (GP) width, proliferation and hypertrophic zones, in 4 weeks old wild-type (wt) and *Gnptg^{ko}* (ko) mice (n = 4, mean ± SD)

Next, structural and cellular bone parameters of the skeletons of 25 weeks old mice were analysed, since the skeletal symptoms appear in juvenile MLIII patients. However, the vertebral bodies revealed no differences between the genotypes (Fig. 4.17 A, C), whereas the tibia of *Gnptg*[ko] mice showed a slight but not significant increase in trabecular bone mass (Fig. 4.17 B, D). This increase was based on an elevated trabecular number supported by reduced trabecular spacing. However, the increased bone volume in the tibia of *Gnptg*[ko] mice was not caused by an elevated number of bone-forming osteoblasts or decreased number of bone-resorbing osteoclasts (Fig. 4. A). As a consequence, the non-mineralized tissue represented by the osteoid content was not altered in *Gnptg*[ko] animals compared to wild-type littermates (Fig. 4.17 B). Furthermore, the width of the growth plate revealed proper differentiation of both proliferating and hypertrophic chondrocytes in the tibia of 25 weeks old *Gnptg*[ko] mice and wild-type animals.
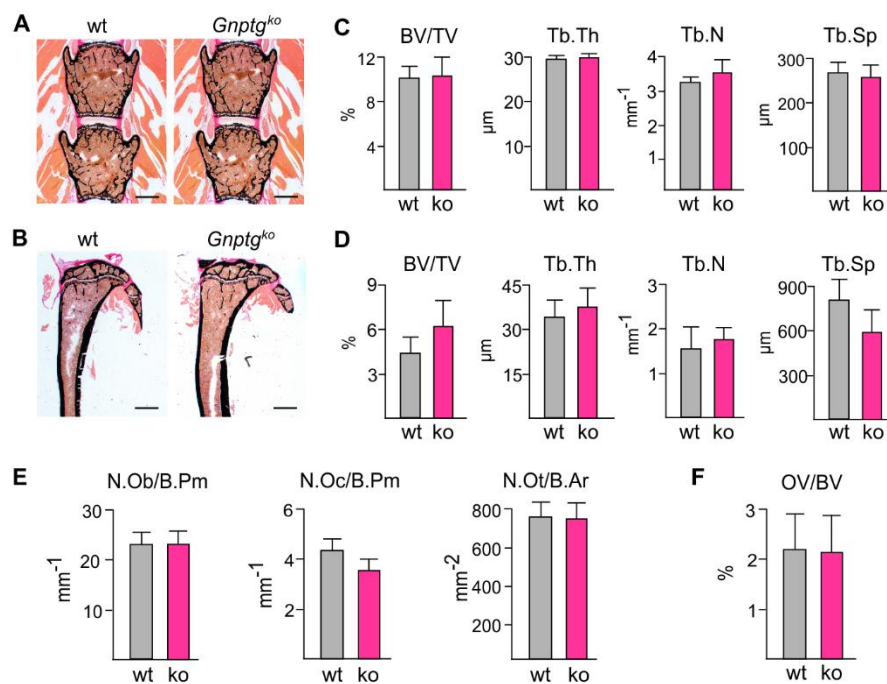
Figure 4.17 Histomorphometric analyses of 25 weeks old *Gnptg*[ko] mice. A and **B)** Representative non-decalcified sections of vertebral bodies (**A**) and tibiae (**B**) from female wild-type (wt) and *Gnptg*[ko] (ko) mice stained by von Kossa/Van Gieson (scale bar: 1 mm). **C** and **D)** Quantification of structural parameters of vertebral bodies (**C**) and tibiae (**D**) in the same mice: bone volume per tissue volume (BV/TV), trabecular thickness (Tb.Th), trabecular number (Tb.N) and trabecular spacing (Tb.Sp). **E)** Quantification of cellular parameters in the trabecular area of the tibia of female wild-type (wt) and *Gnptg*[ko] (ko) mice: number of osteoblasts per bone perimeter (N.Ob/B.Pm), number of osteoclasts per bone perimeter (N.Oc/B.Pm), number of osteocytes per bone area (N.Ot/B.Ar). **F)** Quantification of the osteoid volume per bone volume (OV/BV) in the same mice. (n = 4, mean ± SD)

Finally, the bone architecture of femurs was examined by micro-computed tomography (μCT), which allows the three-dimensional (3D) reconstruction of the scanned samples and the automatic analysis of bone parameters in 3D space (Fig. 4.18 A). Similar to the histomorphometric analysis of the tibia, a statistically significant increase of bone mass was observed in *Gnptg*^{ko} mice compared to wild-type littermates (Fig. 4.18 B). This increase was based on the elevated number of trabeculae and increased trabecular separation in *Gnptg*^{ko} animals (Fig. 4.18 B).
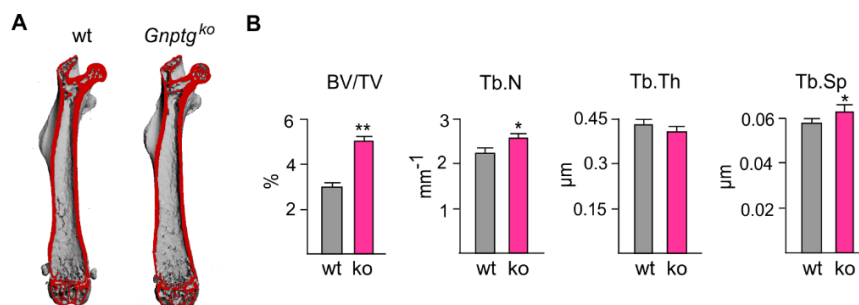
Figure 4.18 Micro-computed tomography (μCT) analyses of femurs from 25 weeks old *Gnptg*^{ko} mice. A) Representative μCT images of femur from female wild-type (wt) and *Gnptg*^{ko} (ko) mice. The virtual cut edges are coloured red. **B)** Quantification of trabecular structural parameters of the distal femoral metaphysis in the same mice: bone volume per tissue volume (BV/TV), trabecular thickness (Tb.Th), trabecular number (Tb.N) and trabecular separation (Tb.Sp). (n = 4, mean ± SD, *$P \leq 0.05$, **$P \leq 0.01$).

4.3.2 Analysis of storage material in bone and cartilage in *Gnptg*^{ko} mice

Since the histomorphometric skeleton analysis revealed no significant changes, cellular structure analyses of bone from 25-30 weeks old *Gnptg*^{ko} and wild-type mice were performed by transmission electron microscopy. Few vesicular structures filled with electron-lucent storage material were found in *Gnptg*^{ko} bone-forming osteoblasts attached to the bone surface and surrounded by bone marrow cells (Fig. 4.19 A). The number of these lysosomal storage vacuoles was found to be increased in osteocytes representing terminally differentiated osteoblasts within the mineralized bone matrix (Fig. 4.19 B). These results demonstrate a crucial role of γ-subunits of GlcNAc-1-phosphotransferase for efficient macromolecule degradation in bone cells.
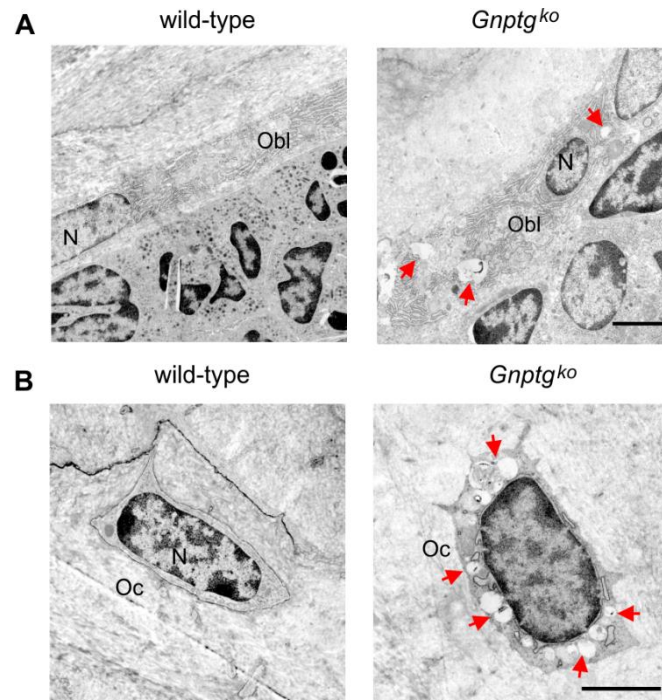
Figure 4.19 Ultrastructural analysis of tibia from *Gnptg^{ko}* mice. Ultra-thin cryosections of decalcified tibia from 25-30 weeks old *Gnptg^{ko}* and wild-type mice were used for electron microscopy to analyse accumulation of storage material in (**A**) osteoblasts (Obl) and (**B**) osteocytes (Oc). N, nucleus; red arrows, storage lysosomes. (scale bars: 2.5 µm).

4.3.3 Differentiation and mineralization of *Gnptg^{ko}* osteoblasts

To investigate whether the accumulation of lysosomal storage material in osteoblasts and osteocytes influences the proper function of these cell types, the parameter of osteoblast differentiation were analysed. Primary cultured osteoblasts were analysed at day 5 (d5) and day 15 (d15) by qPCR. *Col1a1* encodes the α-chain of collagen type 1, the most abundant protein in the bone extracellular matrix, and was found to be 3.4-fold increased at d15 in comparison to d5 in wild-type and *Gnptg^{ko}* cells (Fig. 4.20 A). The mRNA level of *Sp7,* encoding an essential transcription factor during bone formation (Karsenty, 2008), was 2- to 3-fold increased at d15 in osteoblasts from wild-type and *Gnptg^{ko}* mice. Sclerostin, encoded by *Sost* and mainly expressed in osteocytes as a negative regulator of bone formation (van Bezooijen *et al*, 2005), was 2.5-fold elevated during differentiation of wild-type and *Gnptg^{ko}* cells. In addition, Alizarin red staining of calcium-containing cells was performed to determine the proper mineralization of osteocytes at day 25 of differentiation. No changes in the mineralization capacity were observed in *Gnptg^{ko}* compared to wild-type osteocytes (Fig. 4.20 B).

The data indicate that the differentiation and function of cultured osteoblasts and osteocytes from *Gnptg^(ko)* mice is not negatively affected.
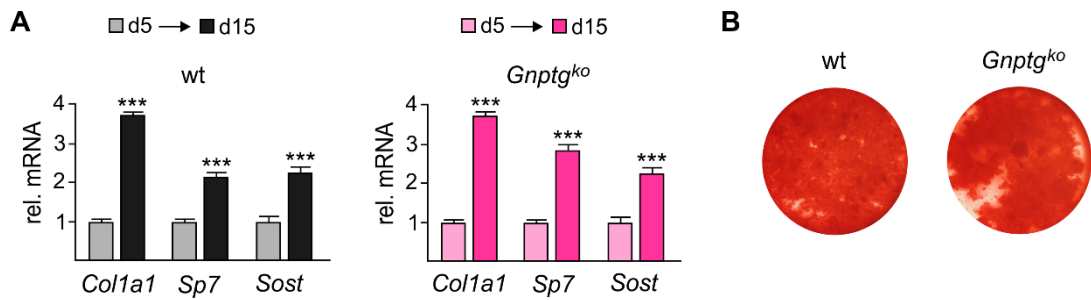
Figure 4.20 Differentiation analyses of *ex-vivo Gnptg^(ko)* osteoblasts and osteocytes. **A)** Relative mRNA expression levels of *Col1a1*, *Sp7* and *Sost* normalized to *Gapdh* measured by qPCR in wild-type (wt) and *Gnptg^(ko)* osteoblasts at day 5 (d5, set as 1) and day 15 (d15) of differentiation. **B)** Alizarin red staining of wt and *Gnptg^(ko)* osteocytes at day 25 of differentiation.

4.3.4 Trafficking of lysosomal enzymes in osteoblasts and osteocytes

In lysosomes of osteoblasts and osteocytes of *Gnptg^(ko)* mice, the accumulation of non-degraded storage material was observed (Fig. 4.19). Therefore, the sorting of selected soluble lysosomal enzymes in 15 days differentiated *Gnptg^(ko)* osteoblasts was analysed by western blotting. At steady-state the levels of intracellular mature Plbd2 and Creg1 forms were strongly reduced in *Gnptg^(ko)* cell extracts compared to wild-type controls (Fig. 4.21 A, lane 1 and 2).
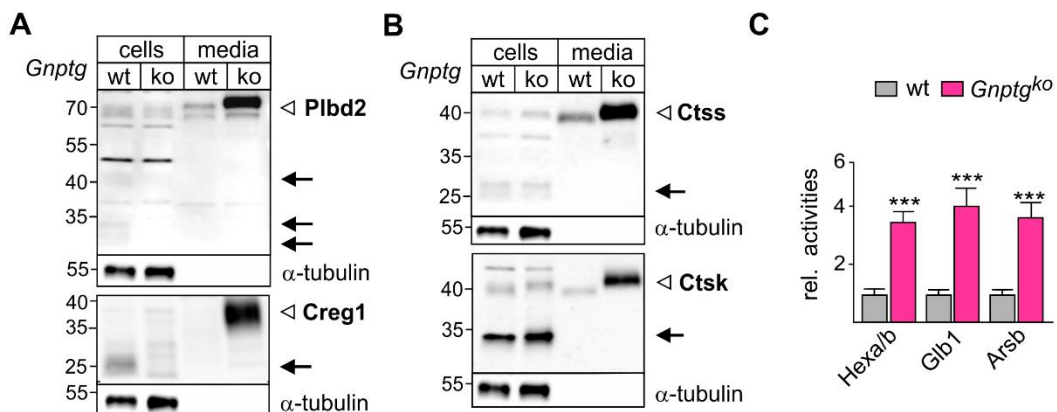
Figure 4.21 Missorting of soluble lysosomal enzymes in *Gnptg^(ko)* osteoblasts and osteocytes. A) and **B)** Cell extracts (25 µg proteins) and corresponding, conditioned media (10%) from wild-type (wt) and *Gnptg^(ko)* (ko) osteoblasts at day 15 of differentiation were separated by SDS-PAGE and analysed by western blotting using antibodies against indicated soluble lysosomal enzymes. Cellular α-tubulin was used as loading control. The mature forms of lysosomal enzymes are marked with black arrows and precursors with non-filled arrowheads. **C)** Relative activities of β-hexosaminidase (Hexa/b), β-galactosidase (Glb1) and arylsulfatase B (Arsb) in wt and *Gnptg^(ko)* osteocytes media (wt was set as 1, n = 3, mean ± SD, ***$P \leq$ 0.001).

In contrast, the intracellular amounts of mature Ctss and Ctsk forms in *Gnptg^ko* osteoblasts were not affected (Fig. 4.21 B, lane 1 and 2). However, the amounts of secreted Plbd2, Creg1, Ctss and Ctsk precursors were increased in *Gnptg^ko* compared to wild-type media (Fig. 4.21 A, B, lane 3 and 4). The targeting of lysosomal enzymes was also analysed by enzyme activity measurements using wild-type and *Gnptg^ko* media from 25 days differentiated osteocytes. The assays revealed a 3.5- to 4-fold increased secretion of β-hexosaminidase (Hexa/b), β-galactosidase (Glb1) and arylsulfatases B (Arsb) in *Gnptg^ko* compared to wild-type media (Fig. 4.21 C). These data showed that in the absence of γ-subunits several lysosomal enzymes are missorted into the media of *ex-vivo* cultured osteoblasts and osteocytes.

4.3.5 Analysis of storage material in cartilage in *Gnptg^ko* mice

Since the histomorphometric analysis revealed no significant changes in the growth plate chondrocytes width, cellular structural analyses of cartilage from 25-30 weeks old *Gnptg^ko* and wild-type mice were performed. A remarkable elevation in the number of storage-containing lysosomes was observed in the *Gnptg^ko* hypertrophic chondrocytes residing in the cartilaginous matrix (Fig 4.22).
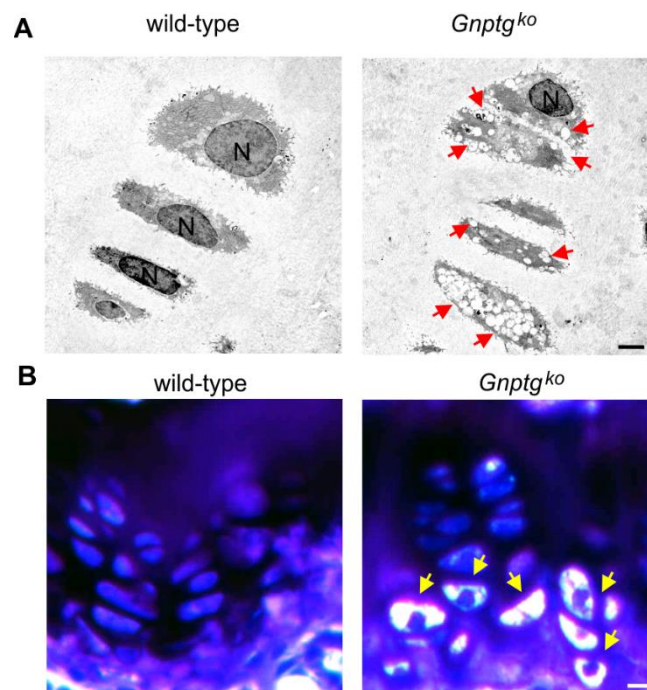
Figure 4.22 Analysis of chondrocytes from the tibia of *Gnptg^ko* mice. A) Ultra-thin cryosections of decalcified tibia from 25-30 weeks old *Gnptg^ko* and wild-type mice were used for electron microscopy to analyse accumulation of storage material in chondrocytes. N, nucleus; red arrows, storage vacuoles (scale bars: 2.5 µm). **B)** Representative non-decalcified sections of tibiae from 40 weeks old female wild-type and *Gnptg^ko* mice stained by toluidine blue. Yellow arrows indicate storage lysosomes (scale bar: 10 µm)

In addition, toluidine blue staining of non-decalcified tibia sections revealed accumulation of storage material in the hypertrophic chondrocytes of the $Gnptg^{ko}$ growth plate (Fig 4.22). These results demonstrate a crucial role of γ-subunits of GlcNAc-1-phosphotransferase for proper substrates degradation in cartilage cells.

4.3.6 Loss of Arsb causes accumulation of GAGs in $Gnptg^{ko}$ chondrocytes

In $Gnptg^{ko}$ MEF and osteoblasts/osteocytes the sorting of arylsulfatase B (Arsb) was found to be highly dependent on the γ-subunits (Fig. 4.4, 4.6, 4.7, 4.10 and 4.21). The intra- and extracellular amounts of Arsb was analysed in in cell extracts and corresponding media of cultured primary chondrocytes from wild-type and $Gnptg^{ko}$ mice by Arsb enzyme activity measurement. A drastic reduction of intracellular Arsb levels to 8% was observed in $Gnptg^{ko}$ cells compared to controls, accompanied by a 3-fold increased Arsb secretion to the $Gnptg^{ko}$ media (Fig. 4.23 A) demonstrating the missorting of Arsb in $Gnptg^{ko}$ chondrocytes.

Since $Gnptg^{ko}$ MEF displayed proteoglycans accumulation partially due to the missorting of Arsb (Fig. 4.11 and 4.13), the storage material observed in the growth plate of $Gnptg^{ko}$ mice (Fig. 4.22) might be composed of proteoglycans as well. Therefore, the lysosomal GAG degradation was analysed in cultured chondrocytes. Wild-type and $Gnptg^{ko}$ chondrocytes were incubated with $^{35}SO_4$-containing media for 48 h (pulse) followed by 48 h incubation in non-radioactive media which allow the radioactively labelled GAG to reach the lysosomes for degradation. GAGs were purified by anion-exchange chromatography and the $^{35}SO_4$-content was measured by LSS. A 4.3-fold accumulation of $^{35}SO_4$-labelled GAGs was observed in $Gnptg^{ko}$ chondrocytes compared to wild-type cells (Fig. 4.23 B). Chondrocytes mainly contain chondroitin sulfates (CS), dermatan sulfates (DS) and keratan sulfates (KS) proteoglycans (Vynios, 2014, Fig. 4.11 A). To determine the amounts of these proteoglycans in wild-type and $Gnptg^{ko}$ chondrocytes, purified GAGs were treated with heparinase I, II and III followed by the respective resistant GAGs purification by anion exchange chromatography and quantification by LSS. In $Gnptg^{ko}$ chondrocytes a 5-fold accumulation of CS/DS and KS was observed compared to wild-type cells (Fig. 4.23 B). Although KS is highly abundant in chondrocytes, Arsb is not involved in KS degradation (Fig. 4.11 A).

To determine whether the CS/DS accumulation was caused by the loss of Arsb as observed in MEF (Fig. 4.13), chondrocytes were incubated with recombinant human ARSB (75 nM) during the chase period. By measurement of the intracellular ARSB activity, a 3- and 2-fold increase was observed in wild-type and $Gnptg^{ko}$ cells, respectively, compared to non-treated cells demonstrating the proper uptake of recombinant ARSB (Fig. 4.23 C). Due to ARSB treatment the GAG accumulation in $Gnptg^{ko}$ chondrocytes decreased to 50%, in particular, a 70% reduction of CS/DS storage was observed in $Gnptg^{ko}$ chondrocytes (Fig. 4.23 D).
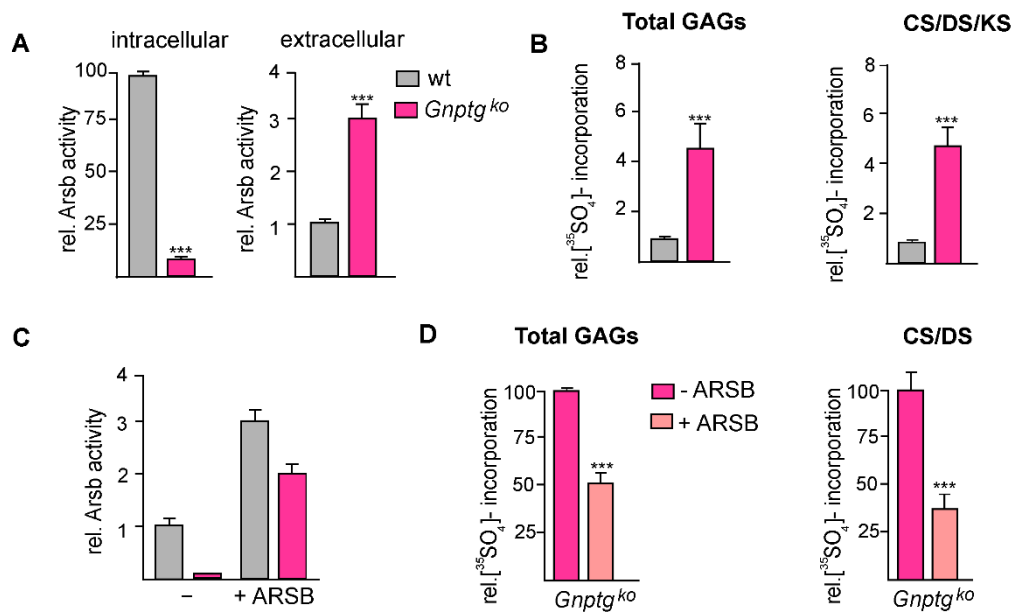
Figure 4.23 ARSB partially abolishes the accumulation of sulfated GAGs in $Gnptg^{ko}$ chondrocytes
A) Relative enzyme activities of Arsb in cell extracts and media of wt (set as 100% and 1, respectively) and $Gnptg^{ko}$ chondrocytes after 48 chase period (mean $\pm$ SD, ***$P \leq 0.001$, n = 2). **B)** Quantification of purified $^{35}SO_4$-labelled GAGs in wild-type (wt) and $Gnptg^{ko}$ chondrocytes after 48 h pulse and 48 h chase. Quantification of purified $^{35}SO_4$-labelled CS/DS and KS after digestion with heparinase I, II and III (wt was assign as 1; ***$P \leq 0.001$, n = 2). **C)** Relative ARSB activities in wt and $Gnptg^{ko}$ chondrocytes in the absence (-) or presence (+) of ARSB (non-treated wt was set as 1; mean $\pm$ SD; n = 2).**D)** Quantification of purified $^{35}SO_4$-labelled GAGs in $Gnptg^{ko}$ chondrocytes after 48 h pulse and 48 h chase in the absence (-) or presence (+) of human recombinant ARSB (non-treated $Gnptg^{ko}$ was assign as 100%). Quantification of purified $^{35}SO_4$-labelled CS/DS and KS after digestion with heparinase I, II and III (non-treated $Gnptg^{ko}$ was set as 100%) (mean $\pm$ SD, ***$P \leq 0.001$, n = 2).

These results demonstrated that the absence of the γ-subunits of GlcNAc-1-phosphotransferase leads to missorting of Arsb in cultured chondrocytes as shown in MEF and osteoblasts from $Gnptg^{ko}$ as well, indicating that the missorting of Arsb is cell type-independent. As a consequence sulfated CS/DS proteoglycans accumulate in $Gnptg^{ko}$ chondrocytes. Importantly, the treatment of $Gnptg^{ko}$ chondrocytes with recombinant ARSB reduces lysosomal CS/DS accumulation.

5. Discussion

The Golgi-resident GlcNAc-1-phosphotransferase complex is the key enzyme for the formation of M6P recognition marker on newly synthesized lysosomal enzymes, required for their efficient receptor-mediated transport to lysosomes. Loss of γ-subunits of the GlcNAc-1-phosphotransferase cause the lysosomal storage disorder MLIII that is mainly characterized by abnormalities of the skeleton and cartilage. This thesis provides a number of new insights into the role of the γ-subunits for 1) the activity and substrate specificity of the hexameric GlcNAc-1-phosphotransferase complex, 2) for lysosome function in general, in particular in bone and cartilage homeostasis and 3) for substrate degradation by specific lysosomal enzymes.

5.1 Reduced GlcNAc-1-phosphotransferase activity in the absence of γ-subunits

The membrane-bound α- and β-subunits exhibit the catalytic activity of the GlcNAc-1-phosphotransferase and it was suggested that the soluble γ-subunits are required for recognition and binding of lysosomal enzymes. In contrast, γ-subunit affinity chromatography and plasmon resonance spectrometry failed to show direct interactions of γ-subunits with lysosomal enzymes (Tiede *et al*, 2005; Pohl *et al*, 2009b). Other data led to the suggestion that the γ-subunits enhance the recognition and binding of a subpopulation of lysosomal enzymes by the α- and β-subunits (Qian *et al*, 2010).

To examine the role of γ-subunits for GlcNAc-1-phosphotransferase activity, MEF from *Gnptg*^{ko} mice were used in this thesis. In the absence of γ-subunits the GlcNAc-1-phosphotransferase activity was reduced to 60% compared to wild-type MEF (Fig. 4.5). This result is supported by a recent study showing a reduction of GlcNAc-1-phosphotransferase activity to 50% of controls in CRISPR/Cas9-mediated knock-out of *GNPTG* in human haploid HAP1 (ΔGNPTG) cells (De Pace *et al*, 2015). Furthermore, it was shown that also the deletion of the γ-subunit-binding domain in the α-subunits resulted in a reduction of the GlcNAc-1-phosphotransferase activity to 70% (De Pace *et al*, 2015). These activity measurements, however, used methyl mannoside as phosphate acceptor, which is not directly comparable to higher molecular mass lysosomal enzymes. Together these results underlined the crucial role of γ-subunits to maximize the GlcNAc-1-phosphotransferase activity for all soluble lysosomal proteins.

The reduction of the GlcNAc-1-phosphotransferase activity results in impaired M6P formation on lysosomal enzymes as has been shown in cell extracts and lysosome-enriched fractions of MEF from *Gnptg^ko* using a single chain antibody against M6P residues (Fig. 4.5). Less M6P-containing proteins were also found in extracts from MLIII patient fibroblasts (Pohl *et al*, 2010a; Pohl *et al*, 2012) and in ΔGNPTG HAP1 cells (Dr. S. Pohl, unpublished) demonstrating the useful application of the M6P antibody for biochemical diagnosis of MLIII patients as well as for basic research (Müller-Loennies *et al*, 2010). Previous studies by Kornfeld and colleagues using MPR300 affinity chromatography of *Gnptg^-/-* mouse brain homogenates have shown that in the absence of the γ-subunits the extent of M6P formation of two third of all analysed lysosomal enzymes was decreased (Fig 5.1) (Qian *et al*, 2010). These results implicate the reduced binding capacity of newly synthesized lysosomal enzymes to M6P receptors that leads to their subsequent intracellular missorting. This is the rationale behind the determination of increased lysosomal enzyme activities in the serum of MLII and MLIII patients for biochemical diagnosis of these diseases (Raas-Rothschild *et al*, 2012; Braulke *et al*, 2013). Accordingly, the hypersecretion of lysosomal enzymes into the serum of *Gnptg^ko* mice was accompanied by a reduced intracellular amount of lysosomal enzymes in *Gnptg^ko* MEF (Fig. 4.4 and 4.6). These data demonstrate that *Gnptg^ko* mice represent a proper model of the human MLIII disease.

To identify the lysosomal enzymes which require the γ-subunits for correct delivery into lysosomes, comparative SILAC-based M6P secretome and lysosomal proteome analyses were performed. The results demonstrated that the M6P formation of 11 identified soluble lysosomal enzymes is strongly dependent on γ-subunits and those enzymes were found in a very low concentration in lysosomes of *Gnptg^ko* cells: Tripeptidylpeptidase I (Tpp1), prolylcarboxypeptidase (Prcp), putative phospholipase B-like 2 (Plbd2), β-hexosaminidase (Hexa/b), cathepsin K (Ctsk), β-galactosidase (Glb1), α-mannosidase (Man2b2), Creg1 protein, arylsulfatase B (Arsb), cathepsin S (Ctss) and acid ceramidase (Asah1) (Fig. 5.1). Among these proteins, 9 lysosomal enzymes have been also identified with the lowest abundance using the MPR affinity chromatography approach of brain homogenates from *Gnptg^-/-* mice (Fig. 5.1; Qian *et al*, 2010). Of note, the approach used by the Kornfeld group does not provide information on the cellular origin or intracellular localization of the lysosomal enzymes.

These data sets suggest that the γ-subunit-dependent M6P formation is specific and cell type-independent for a subset of lysosomal proteins.
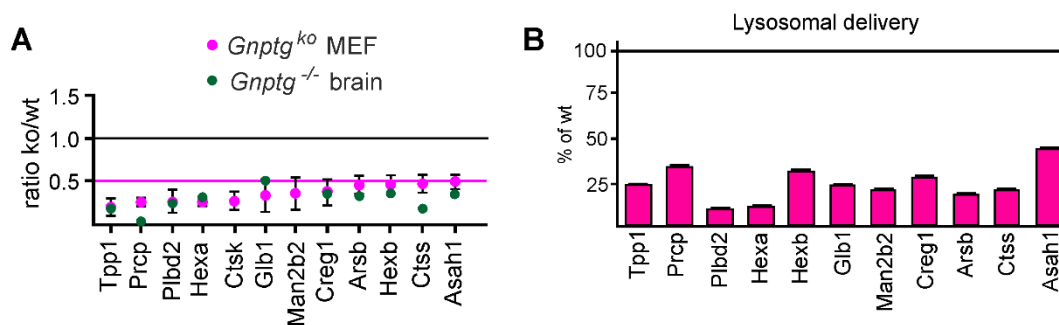
Figure 5.1. Comparison of M6P secretome of *Gnptg^ko* MEF with M6P proteome of *Gnptg^-/-* brain homogenates. **A**) Significantly reduced lysosomal enzymes of the M6P secretome in *Gnptg^ko* MEF are indicated in magenta. Ratios of ≤ 0.5 and 1.0 are marked as magenta and black lines, respectively. Lysosomal enzymes from *Gnptg^-/-* brain homogenates that bind weakly to the MPR affinity matrix (Qian *et al*, 2010) are marked in green. **B**) Percentage of delivery of lysosomal enzymes to lysosomes in *Gnptg^ko* MEF compared to the wild-type (wt) cells.

However, the present study could not confirm the effects of missing γ-subunits on the selective M6P formation of glycosidases versus cathepsins as reported in *gnptg^-/-* zebrafish (Flanagan-Steet *et al*, 2016). The enzymes that depend on their M6P formation by the γ-subunits in mouse cells belong to different classes involved in the degradation of lipids, proteins and glycans suggesting rather a species-dependent M6P formation on some lysosomal enzymes. Furthermore, sequence alignments suggested no structural similarities between those 11 murine enzymes using the Multiple Sequence Alignment Tool "Clustal Omega" offered by the European Bioinformatics Institute (EMBL-EBI, https://www.ebi.ac.uk/Tools/msa/clustalo/).

In the absence of α- and β-subunits which cause the complete loss of the GlcNAc-1-phosphotranserase activity, the trafficking of many lysosomal enzymes to the lysosomes was affected in the *Gnptab^ki* MEF (Markmann *et al*, 2015). The comparison of the data sets obtained from *Gnptab^ki* and *Gnptg^ko* lysosomal proteome analyses allow a closer view on the specificity of α-, β- and γ-subunits of the GlcNAc-1-phosphotransferase for recognition and binding of lysosomal enzymes. The concentration of Plbd2, Arsb and Glb1 in *Gnptab^ki* and *Gnptg^ko* was found to be ≤ 25% compared to wild-type lysosomes (Fig 5.2). These data suggested that the M6P modification and the proper transport of these enzymes are highly dependent on the γ-subunits.

In contrast, the lysosomal concentrations of Dnase2, Npc2 and Gusb were strongly reduced in *Gnptab^{ki}* cells but more than 60% of these enzymes reach the lysosomes in the absence of γ-subunits (Fig. 4.7). These results indicate that α- and β-subunits are sufficient for the proper M6P modification and delivery of these three proteins to lysosomes. The analyses also revealed that a subgroup of enzymes were only partially missorted or correctly delivered to lysosomes such as the cathepsins D, B and L (Fig. 5.2), suggesting the presence of M6P-independent transport routes to lysosomes. Thus, the type I membrane glycoprotein sortilin was found to bind non-phosphorylated Ctsd and Ctsh *in vitro* (Canuel *et al*, 2008) and was thought as alternative M6P-independent cargo receptor for these proteins. However, the analysis of MEF derived from *Gnptab^{ki}*/sortilin^{ko} mice clearly showed that both cathepsines D and B reach the lysosomes independent on M6P and sortilin (Markmann *et al*, 2015). In addition to intracellular transport mechanisms, secreted lysosomal enzymes can also be recaptured via non-M6P receptors at the plasma membrane, re-internalized and transported to the lysosomes (Hickman & Neufeld, 1972). Recently it was demonstrated that the internalization of non-phosphorylated Ctsb and Ctsd were mediated by LDL (low-density lipoprotein) receptor and Lrp1 (low-density lipoprotein receptor-related protein 1) in MEF (Markmann *et al*, 2015).
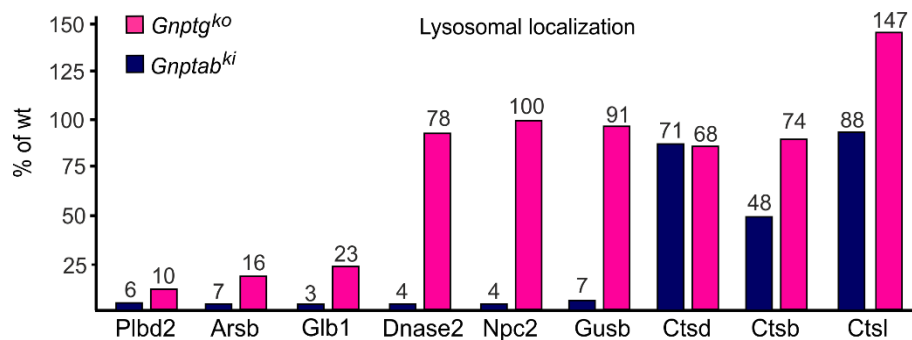
Figure 5.2. Comparison of the lysosomal localization of selected lysosomal enzymes in *Gnptg^{ko}* and *Gnptab^{ki}* MEF. Percentage of lysosomal delivery of lysosomal enzymes in *Gnptg^{ko}* and *Gnptab^{ki}* MEF compared to the wild-type (wt).

With the exception of Ctss, the altered amounts of certain lysosomal enzymes in lysosomes of *Gnptg^{ko}* MEF were not due to transcriptional regulation as shown by qPCR (Fig. 4.7). Also in MEF and brain tissue of *Gnptab^{ki}* mice the mRNA expression of numerous lysosomal enzymes was not affected (Kollmann *et al*, 2012).

Surprisingly, the mRNA levels of *Npc2* encoding the Niemann-Pick type C2 protein that is involved in the egress of cholesterol from lysosomes (Wang *et al*, 2010) was 2.8-fold upregulated in *Gnptg*^{ko} cells (Fig. 4.8) but not in *Gnptab*^{ki} cells (Kollmann *et al*, 2012). Increased concentration of immunoreactive Npc2 was also present in lysosomal fractions of *Gnptg*^{ko} MEF (Fig. 4.9). Of note, double amounts of newly synthesized M6P-modified Npc2 were detected in the medium of *Gnptg*^{ko} MEF (Fig. 4.10). The elevated levels of M6P-containing Npc2 in brain extracts of *Gnptg*$^{-/-}$ mice (Qian *et al*, 2010) is probably also due to transcriptional activation. It has been reported that the inhibition of histone deacetylase 1/2 (HDAC1/2) by administration of specific inhibitors or sphingosine 1-phosphate enhances the expression of Npc1 and Npc2 (Hait *et al*, 2009; Newton *et al*, 2017). The signalling mechanism, most likely initiated by dysfunctional lysosomes, to control the selective transcriptional regulation of Npc2 in *Gnptg*^{ko} MEF, and presumably brain cells, is needed to be examined.

5.2 The role of γ-subunits for bone and cartilage homeostasis

MLIII patients are characterized by skeletal alterations summarized as *dysostosis multiplex* leading to progressive decline of mobility, stiffness and chronic joint pain which strongly reduce the quality of life. To better understand the skeletal pathomechanisms in the MLIII disease, the sorting of lysosomal enzymes in the absence of the γ-subunits was analysed in cultured bone cells of *Gnptg*^{ko} mice. By enzyme activity measurements and western blot analyses of cell extracts and media, missorting of the lysosomal enzymes Plbd2, Creg1, Ctss, Ctsk, Hexa/b, Glb1 and Arsb was found in *ex-vivo* cultured primary *Gnptg*^{ko} osteoblasts (Fig. 4.21). These data indicate a γ-subunit-dependent sorting of these lysosomal enzymes in bone-forming cells. To find out, which lysosomal enzymes are directly affected by impaired M6P formation in the absence of the γ-subunits rather than by compensatory sorting via M6P-independent transport routes, currently the M6P proteome of *Gnptg*^{ko} osteoblasts is analysed. These experiments can further provide information on cell type-specific M6P formation and trafficking of lysosomal enzymes in wild-type and *Gnptg*^{ko} cells by comparing data sets obtained from MEF (Fig. 4.10) and osteoblasts.

The absence of the α- and β-subunits of the GlcNAc-1-phosphotransferase leads to the complete loss of M6P residues on lysosomal enzymes. It was shown that Ctsz, Hexa/b and Glb1 are missorted in osteoblasts of *Gnptab^{ki}* mice and lysosomal storage accumulation was observed in *Gnptab^{ki}* osteoblasts and terminally differentiated osteocytes (Kollmann *et al*, 2013). The functional deficits of *Gnptab^{ki}* osteoblasts have been shown by Alizarin red-positive mineralization defects and strongly decreased mRNA expression of osteoblast mineralisation marker proteins (Kollmann *et al*, 2013) (Fig. 1.5). In the present study, electron microscopy of tibia from *Gnptg^{ko}* mice also revealed accumulation of non-degraded material in enlarged lysosomes in osteoblasts, which was more pronounced in osteocytes (Fig. 4.19). Of note, since it is presently not clear whether the same subpopulation of lysosomal enzymes are affected in their M6P content and targeting in osteoblasts and osteocytes, it is not possible to speculate on the nature of the storage material. In contrast to *Gnptab^{ki}* osteoblasts, the differentiation and mineralization was not affected in *Gnptg^{ko}* osteoblasts (Fig. 4.20). These data suggest that the missorting of lysosomal enzymes and the subsequent accumulation of lysosomal storage material in dysfunctional lysosomes is not in general directly linked to cellular dysfunction, at least in cultured bone cells.

Functional lysosomes are essential for bone resorption by osteoclasts (Teitelbaum, 2000) and it was suggested that missorting of lysosomal enzymes to the extracellular resorption lacuna is responsible for increased bone resorption activity of *Gnptab^{-/-}* osteoclasts (van Meel *et al*, 2011). Therefore, it was a surprising finding that the resorption activity of osteoclasts from *Gnptab^{ki}* mice was not affected, and the osteoporotic phenotype was rather caused by a strongly elevated number of osteoclasts accompanied by dysfunctional bone forming osteoblasts (Kollmann *et al*, 2013) (Fig. 1.5). Similar to *Gnptab^{ki}* mice, the function of *Gnptg^{ko}* osteoclasts was not impaired (data not shown). In contrast, however, compared to *Gnptab^{ki}* mice also the osteoclast number of *Gnptg^{ko}* mice was not affected (Fig. 4.17).

The *in-vitro* cellular analysis revealed no functional impairment of *Gnptg^{ko}* osteoblasts and osteoclasts required for balanced skeletal remodelling. In agreement with these results, no skeletal abnormalities were observed in 4 and 25 weeks old *Gnptg^{ko}* mice (Fig. 4.15 and 4.17), which has been also reported in *Gnptg^{-/-}* mice (Vogel *et al*, 2009).

However, a slight increase of the trabecular bone mass was detected in the femur and tibia of 25 weeks old *Gnptg^(ko)* mice, whereas the vertebral bodies were unaffected (Fig. 4.17 and 4.18). The increased bone volume in the tibia of *Gnptg^(ko)* mice was not caused by an elevated number of osteoblasts or decreased number of osteoclasts (Fig. 4.17). Unlike the µCT, histomorphometry is based on the analysis of a single plane section, suggesting that the non-significant increase of the trabecular parameters in the tibia is most likely due to the high variability and low sensitivity of the technique. To better understand the increase in bone mass of the appendicular skeleton, further investigation of the *in-vivo* cellular functionality are required, such as the measurement of alkaline phosphatase activity in the *Gnptg^(ko)* mouse serum which is a marker for bone mineralization (Millan, 2013).

MLIII patients are clinically characterized by short stature, and skeletal growth primarily depends on the coordinated functionality of growth plate chondrocyte. The analysis of the width of the growth plates from tibiae revealed that both the proliferation and the hypertrophic zone, showed no differences between *Gnptg^(ko)* and wild-type mice (Fig. 4.16).

Taken together, the characteristic skeletal abnormalities and retarded growth of MLIII patients were not observed in *Gnptg^(ko)* mice. This is in contrast to the skeletal phenotype of *Gnptab^(ki)* mice that was found to be highly similar to MLII patients (Kollmann *et al*, 2013). It is likely that the absence of growth defects in *Gnptg^(ko)* mice are due to the different sizes of growth plates in mice and humans. It is also possible that both the genetic background of the mouse models, C57BL/6J in *Gnptg^(ko)* mice and the 50:50 mixed C57Bl/6-129/SvJ background in *Gnptab^(ki)* mice contributes to the discrepancy in clinical phenotype between MLIII patients and *Gnptg^(ko)* mice as well as MLII patients and *Gnptab^(ki)* mice, respectively (Gelfman *et al*, 2007; Kollmann *et al*, 2012).

Stiffness of fingers, shoulders, hip and ankle are additional prominent clinical features of MLIII patients, but are also present in MLII patients (Raas-Rothschild *et al*, 2012). The bone and cartilage interface (joints) consist of articular cartilage which is composed of chondrocytes and extracellular matrix. Furthermore, chondrocytes are involved in endochondral ossification required for skeletal development and growth (Fig. 1.3) (Kozhemyakina *et al*, 2015). In *Gnptab^(-/-)* and *Gnptab^(ki)* mice chondrocytes were enlarged and filled with lysosomal storage material leading to a significant growth defect compared to wild-type mice (Vogel *et al*, 2009; Marschner *et al*, 2011; Kollmann *et al*, 2013).

In contrast, chondrocytes in $Gnptg^{-/-}$ mice were completely normal and no storage material accumulation was detected, even in aged $Gnptg^{-/-}$ mice (Vogel $et\ al$, 2009). In agreement, these mice do not display any growth defects. Interestingly, the present study showed accumulation of many vesicles full of non-degraded material in the $Gnptg^{ko}$ hypertrophic chondrocytes of the tibia visualized by ultra-structural analysis and toluidine blue staining (Fig. 4.22) even though the growth of $Gnptg^{ko}$ mice was not impaired. Since the growth rate is only moderately slowed in MLIII patients, affected growth in $Gnptg^{ko}$ mice is probably not detectable. However, the characteristic joint stiffness of MLIII patients is most likely caused by articular cartilage defects. Preliminary toluidine blue staining showed accumulation of storage material also in the chondrocytes comprising the articular cartilage of the tibia from 40 weeks old $Gnptg^{ko}$ mice (not shown). Surprisingly however, the articular cartilage in the acetabulum of 40 weeks old $Gnptg^{ko}$ mice was not affected (not shown), indicating that the storage material do not alter the articular cartilage morphology and function. Of note, histological analysis is not adequate to identify disruption of the articular cartilage especially in small animals. To visualize specific articular cartilage defects in mice, the induction of osteoarthritis is often necessary (Echtermeyer $et\ al$, 2009). The direct effects of the deficiency of γ-subunits on the cartilage are so far unclear. Currently the Achilles tendons of $Gnptg^{ko}$ and $Gnptab^{ki}$ are analysed using atomic force microscopy which allows the quantification of the distribution, diameter and elastic properties of collagen fibres in the cartilage.

Of note, similar discrepancies between the human and mouse phenotype were observed in mouse models for mucopolysaccharidoses (MPS). For example, $Galns$-deficient mice lack abnormalities of bone and cartilage typical for MPS-IVA patients. This was explained by the differences in the amount of synthesis and distribution of keratan sulfate between murine and human tissue (Venn & Mason, 1985; Tomatsu $et\ al$, 2003). In contrast to the human MPS-I disease characterized by several skeletal defects and short stature (Wraith & Jones, 2014), $Idua$-deficient mice showed altered bone remodelling but no growth retardation (Kühn $et\ al$, 2015). Whereas bone and cartilage are the most affected tissue in MPS-IVB patients characterized by keratan sulfates accumulation (Kubaski $et\ al$, 2016), the respective mouse model do not show significant abnormalities in the bone, most likely due to the absence of keratan sulfates accumulation (Itoh $et\ al$, 2001).

5.3 Enzyme replacement for reduction of GAG accumulation in *Gnptg^{ko}* cells

Most lysosomal storage disorders are caused by the inherited deficiency of a single lysosomal enzyme that results in the accumulation of specific non-degradable macromolecules. In contrast, impaired GlcNAc-1-phosphotransferase leads to deficiencies of multiple lysosomal enzymes and subsequently to storage accumulation of different kind of macromolecules. The MLIII-associated storage material accumulating in γ-subunit-defective patients and animal models has not been identified so far. Electron microscopy analysis revealed electron-lucent storage material in lysosomes of *Gnptg^{ko}* cells (Fig. 4.19 and 4.22) suggesting that non-degraded sugar-containing macromolecules were present but washed out during the fixation procedure. The most abundant polysaccharides in animal cells are sulfated GAGs that are mainly present at the cell surface and in the extracellular matrix. GAGs are covalently attached to proteoglycans and are composed of linear repetitive disaccharides consisting of an amino sugar (N-acetylglucosamine or N-acetylgalactosamine) and an uronic acid (glucuronate or iduronate) or galactose (Fig. 5.3; Lindahl *et al*, 2015).
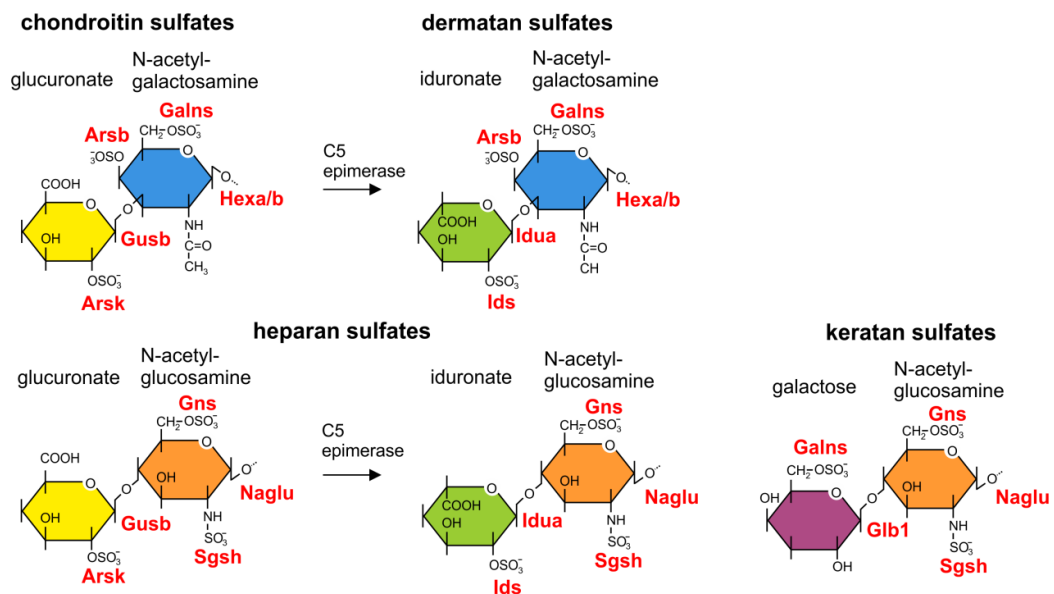
Figure 5.3: Schematic presentation of disaccharide units GAGs. Chondroitin sulfates consist of N-acetylgalactosamine and glucuronate that can epimerize to iduronate resulting in dermatan sulfates. Heparan sulfates are composed by sulfated N-acetylglucosamine and glucoronate residues that can epimerize to iduronate. Sulfated keratan sulfates consist of sulfated galactose and N-acetylglucosamine disaccharides. Marked in red are the glycosidases (Gusb, Idua, Hexa/b, Naglu, Glb1) and sulfatases (Arsb, Galns, Arsk, Ids, Gns, Sgsh) involved in the degradation of these GAGs.

Based on the different disaccharide units, GAGs can be classified into four main groups: chondroitin sulfates, dermatan sulfates, heparan sulfates and keratan sulfates (Fig. 5.3). GAG sulfation at the C2, C4 or C6 position leads to their high negative charge required for the binding to a variety of molecules such as water, ions, collagen, cell adhesion proteins and growth factors (Kjellen & Lindahl, 1991). The abundance and turn-over of GAGs are regulated in lysosomes by sequential degradation catalysed by different lysosomal enzymes starting from the non-reducing end (Esko, 1991).

In the present work the intracellular levels of GAG-degrading Arsb, Glb1, Hexa/b and Gns (Fig. 4.6 and 4.7) as well as Idua and Ids (not shown) were found to be decreased in *Gnptg*^{ko} MEF, whereas the sorting of Galns and Gusb was not affected in *Gnptg*^{ko} mice (Fig. 4.6 and 4.7). As expected, the partial missorting of GAG-degrading enzymes resulted in a 6- to 10-fold increased intracellular accumulation of heparan sulfates, chondroitin sulfates, dermatan sulfates and keratan sulfates in *Gnptg*^{ko} MEF compared to wild-type cells (Fig. 4.11; Fig. 5.3). These results are supported by an increased concentration of non-degraded GAGs found in the urine and blood from MLIII and MLII patients (Langereis *et al*, 2015; Kubaski *et al*, 2017). Proteoglycans are highly secreted by osteoblasts/osteocytes and chondrocytes to generate the extracellular matrix in bone and cartilage tissues, respectively. They are not only important for tissue structuring but also regulate bone cells homeostasis by promoting osteogenesis and suppressing osteoclast differentiation and resorption (Salbach-Hirsch *et al*, 2014). Furthermore, hydration of the most abundant cartilage proteoglycan aggrecan prevents swelling pressure to the cartilage, that allows to withstand compressional forces occuring during normal joint motion (Kiani *et al*, 2002; Lindahl *et al*, 2015). As shown in *Gnptg*^{ko} MEF, also the intracellular levels of the GAG-degrading enzymes Arsb, Glb1, Idua and Hexa/b were found to be decreased in primary cultured *Gnptg*^{ko} osteoblasts/osteocytes (Fig. 4.21) and chondrocytes (not shown). Proteoglycans expressed and secreted by chondrocytes mainly contain chondroitin sulfates and keratan sulfates. Indeed, in *Gnptg*^{ko} chondrocytes 4.3-fold elevated intracellular amounts of these sulfated GAGs were detected compared to wild-type cells (Fig. 4.23). In summary, these experiments identified for the first time sulfated GAGs as non-degraded substrates accumulating in lysosomes of *Gnptg*^{ko} fibroblasts, bone and cartilage cells. However, the lysosomal storage observed in MLIII osteoblasts (Fig. 4.21) did neither impair osteoblast differentiation nor function (Fig. 4.20).

Whether the accumulation of non-degraded material in lysosomes impairs the function of *Gnptg^(ko)* chondrocytes is not known so far. The correct differentiation of chondrocytes can be determined by mRNA expression analysis of chondrocyte-specific marker genes such as collagen type II (*Col2a1*) and aggrecan (*Acan*) (Kozhemyakina *et al*, 2015). In addition, defective, hypertrophic or de-differentiated chondrocytes express cartilage-untypical collagen transcripts (*Col1a1, Col1a2, Col9a1* and *Col10a1*) and synthesize less aggrecan mRNA (*Acan*) but more biglycan mRNA (*Bgn*) (Martin & Buckwalter, 2001; Cs-Szabo *et al*, 2002), which can be also measured by qPCR in *Gnptg^(ko)* chondrocytes. Non-degraded GAGs also accumulate in cells from patients with MPS caused by the deficiency of single GAG-degrading enzymes (Lawrence *et al*, 2012). Similar to MLII and MLIII patients common clinical features of the MPS subtypes are skeletal abnormalities summarized as *dysostosis multiplex* (Wraith & Jones, 2014). In particular, MPS-I, -II, -IVA, -VI and -VII patients are characterized by severe skeletal problems, coarse facial features, short stature and joint stiffness (Tylki-Szymanska, 2014; Wraith & Jones, 2014; Vairo *et al*, 2015). These clinical symptoms are associated with lysosomal accumulation of dermatan and heparan sulfates, chondroitin and heparan sulfates or chondroitin and dermatan sulfates. The storage of dermatan, chondroitin and keratin sulfates in MPS-IVA is associated with severe skeletal abnormalities (Table 5.1).

Table 5.1: Storage of sulfated GAGs and skeletal phenotype of MPS. Modified from Coutinho *et al*, 2011

Disease	Lysosomal enzyme	GAG storage	Skeletal phenotype
MPS-I	*IDUA*	DS + HS	moderate to severe
MPS-II	*IDS*	DS + HS	moderate to severe
MPS-IIIA	*SGSH*	HS + KS	mild
MPS-IIIB	*NAGLU*	HS + KS	mild
MPS-IIID	*GNS*	HS + KS	mild
MPS-IVA	*GALNS*	CS + DS + KS	severe
MPS-IVB	*GLB1*	KS	moderate
MPS-VI	*ARSB*	CS + DS	moderate to severe
MPS-VII	*GUSB*	CS + HS	moderate to severe

CS: chondroitin sulfates, DS: dermatan sulfates, HS: heparan sulfates, KS: keratan sulfates

In contrast, the accumulation of keratan sulfates alone or in combination with heparan sulfates is associated with a milder or moderate skeletal phenotype such as coarse face and reduced bone density in MPS-IIIA, -IIIB, and IVB patients (Andrade *et al*, 2015; Kubaski *et al*, 2016). One of the leading treatment options for lysosomal storage disorders is enzyme replacement therapy (ERT), which is also available for MPS-I, -II, -IVA, -VI and -VII (Muenzer, 2014; Tomatsu *et al*, 2014). ERT is based on the weekly intra-venous injection of the respective recombinant enzyme that is missing in the respective desease and which is modified with M6P residues to allow MPR-mediated cellular uptake and lysosomal delivery (Lachmann, 2011; Giugliani *et al*, 2016). Of note, ERT has been proven to attenuate disease progression although the treatment success depends on the age of patients at the start of the therapy and the level of recombinant enzymes that are able to reach the cells of affected tissues. Therefore both the low expression of MPR300 and low M6P content of the recombinant protein limit the cellular uptake. In addition, ERT seems to have limited therapeutic efficacy on the skeletal and joint abnormalities (Muenzer, 2014; Parenti *et al*, 2015). Recent data, however demonstrated that ERT given for 12 weeks to MPS-VI mouse model, lacking Arsb, corrected the trabecular bone pathologies (Angermann *et al*, 2018). However, cartilaginous tissues such as the growth plates and articular cartilage are poorly vascularized, and therefore poorly accessible to applied recombinant enzymes. In general, the earliest, pre-symptomatic start of ERT is thought to be most beneficial prior to formation of irreversible bone lesion (Tomatsu *et al*, 2015).

It was suspected that the GAG accumulation in *Gnptg*^{ko} cells, caused by missorting of the GAG-degrading and MPS-related enzymes Arsb, Glb1, Gns, Idua and Ids, can be decreased by *in-vitro* treatment with the respective recombinant enzymes (Table 5.2). Since among these enzymes the targeting of Arsb was most affected in *Gnptg*^{ko} cells, recombinant human ARSB was supplemented to the medium of primary cultured *Gnptg*^{ko} MEF and chondrocytes. In both cell-types the uptake of the recombinant enzyme was documented by increased intracellular ARSB activity compared to the endogenous activity level (Fig. 4.12 and Fig. 4.23). By western blotting the lysosomal delivery of endocytosed ARSB was shown by the presence of the proteolytically processed mature ARSB form (Fig. 4.12). Importantly, the ARSB treatment led to a reduction of 40% and 70% of chondroitin and dermatan sulfates accumulating in *Gnptg*^{ko} MEF and chondrocytes, respectively (Fig. 4.13 and Fig. 4.23).

These data clearly demonstrate that ARSB treatment can reduce *in-vitro* the lysosomal accumulation of sulfated GAGs in *Gnptg^{ko}* cells.

Since ARSB treatment completely rescued the 10-fold increased amount of GAGs in *Arsb^{ko}* MEF used as control (Fig. 4.14), the partial ARSB-mediated GAG reduction in *Gnptg^{ko}* cells is most likely due to the missorting of other GAG-degrading enzymes. Indeed, preliminary data showed that the *in-vitro* treatment of *Gnptg^{ko}* chondrocytes with human recombinant IDUA resulted in 60% reduction of sulfated GAGs (not shown). Although *Gnptg^{ko}* mice do not show evident skeletal abnormalities, these data opened a notable expectation for the treatment of MLIII patients with recombinant lysosomal enzymes to reduce lysosomal GAG accumulation wich will hopefully prevent or reduce bone and cartilage defects. In particular, since Arsb, Idua and Ids were found to be missorted in *Gnptg^{ko}* cells, the combinatorial treatment with Naglazyme®, Aldurazyme® and Elaprase® could be a potential therapeutic strategy for MLIII patients (Table 5.2).

Table 5.2: Availability of ERT for potential treatment of *Gnptg^{ko}* cells to restore GAG accumulation.

Enzyme	Missorting in *Gnptg^{ko}* cells	Expected GAG storage in *Gnptg^{ko}* cells	ERT
Arsb	yes	CS + DS	yes (Naglazyme®)
Arsk	n.a.	CS + HS	no
Galns	no	-	yes (Elosulfase® alfa)
Glb1	yes	KS	no
Gns	yes	KS + HS	no
Gusb	no*	CS + HS	yes (Vestronidase® alfa)
Idua	yes	DS + HS	yes (Aldurazyme®)
Ids	yes	DS + HS	yes (Elaprase®)
Naglu	n.a.	HS + KS	no
Sgsh	n.a.	HS + KS	no

CS: chondroitin sulfates, DS: dermatan sulfates, HS: heparan sulfates, KS: keratan sulfates; n.a.: not analysed in this study; *missorting of GUSB was shown in fibroblasts and/or serum from MLIII patients (Tiede *et al.* 2004; Pohl *et al.* 2009b; Velho *et al.* 2016b)

Although the amount of Gusb in lysosomes of *Gnptg*[ko] MEF was comparable to wild-type cells (Fig. 4.7), missorting of Gusb was shown in MLIII patients (Tiede *et al*, 2004; Pohl *et al*, 2009b; Velho *et al*, 2016b). Whether Vestronidase® alfa might represents an additional beneficial candidate for MLIII patients remains to be studied.

The efficient uptake of different recombinant lysosomal enzymes in combination has to be tested *in-vitro* and *in-vivo*. Furthermore it has to be tested whether and how the simultaneous uptake of different enzymes impair their uptake efficency. Since skeletal abnormalities were not detected in *Gnptg*[ko] mice, the efficiency of individual and combinatorial ERT cannot be tested in these mice. However, for proof-of-principle ERT studies in primary bone and cartilage cells isolated from *Gnptg*[ko] mice are suitable and helpful as demonstrated in this work.

6. Summary

Lysosomes contain about 70 soluble enzymes which have to be modified with mannose 6-phosphate (M6P) residues for efficient targeting to lysosomes. The key enzyme in the formation of M6P residues is the Golgi-resident hexameric GlcNAc-1-phosphotransferase complex ($\alpha_2\beta_2\gamma_2$). The α- and β-subunits exhibit catalytic activity, whereas the function of the γ-subunits encoded by the *GNPTG* gene is unknown. Mutations in the *GNPTG* gene cause the lysosomal storage disorder mucolipidosis type III (MLIII) that is mainly characterized by tissue-specific missorting of lysosomal enzymes and abnormalities of bone and cartilage.

The experiments performed in this thesis revealed novel insights into the role of γ-subunits of the GlcNAc-1-phosphotransferase in the pathogenesis of the MLIII disease:

1. Analysis of *Gnptg*^{lacZ} reporter mice demonstrated tissue and cell-specific expression, e.g. in bone and cartilage cells (osteoblasts, osteoclasts and chondrocytes), the major functionally impaired cell types in MLIII disease.

2. In fibroblasts of *Gnptg*^{ko} mice the loss of γ-subunits led to reduction of GlcNAc-1-phosphotransferase activity by 40%. SILAC-based M6P secretome and lysosomal proteome analyses in *Gnptg*^{ko} fibroblasts revealed that the M6P formation of 11 lysosomal enzymes is dependent on γ-subunits that impairs their intracellular targeting efficiency to lysosomes. Among these enzymes arylsulfatase B (Arsb), involved in the degradation of glycosaminoglycans (GAGs), was found to be missorted in primary cultured fibroblasts, osteoblasts and chondrocytes of *Gnptg*^{ko} mice accompanied by the accumulation of non-degraded GAGs in lysosomes.

3. The accumulation of storage material, a typical feature of MLIII patients, was surprisingly not associated with functional impairment of *Gnptg*^{ko} bone and cartilage cells. Therefore no skeletal abnormalities were detected in *Gnptg*^{ko} mice.

4. Incubation of chondroitin/dermatan sulfates-accumulating *Gnptg*^{ko} fibroblasts and chondrocytes with the human recombinant M6P-containing ARSB (Naglazyme®) partially rescued the lysosomal GAG storage, thereby identifying Arsb as a critical player in lysosome homeostasis in *Gnptg*^{ko} cells, and most likely in the MLIII disease. This result is a proof-of-principle that the approved Naglazyme® replacement therapy significantly reduces non-degraded GAGs in cultured *Gnptg*^{ko} cells. Further studies are needed to evaluate the efficiency of Naglazyme® in patients with MLIII.

7. References

Andrade F, Aldamiz-Echevarria L, Llarena M & Couce ML (2015) Sanfilippo syndrome: Overall review. *Pediatr Int* 57: 331-338

Angermann A, Pohl S, Jeschke A, Yorgan T, Makrypidi-Fraune G, Hendrickx G, Steigert A, Kühn S, Rolvien T, Schweizer M, Köhne T, Neven M, Winter O, Albers J, Streichert T, Pestka J, Baldauf C, Breyer S, Stuecker R, Muschol N, Cox T, Saftig P, Paganini C, Rossi A, Amling M, Braulke T & Schinke T (2018) The lysosomal protein arylsulfatase B is a key enzyme involved in skeletal turnover. *J Bone Miner Res* under review:

Bao M, Booth JL, Elmendorf BJ & Canfield WM (1996) Bovine UDP-N-acetylglucosamine:lysosomal-enzyme N-acetylglucosamine-1-phosphotransferase. I. Purification and subunit structure. *J Biol Chem* 271: 31437-31445

Barea JJ, van Meel E, Kornfeld S & Bird LM (2015) Tuberous sclerosis, polycystic kidney disease and mucolipidosis III gamma caused by a microdeletion unmasking a recessive mutation. *Am J Med Genet A* 167A: 2844-2846

Bouxsein ML, Boyd SK, Christiansen BA, Guldberg RE, Jepsen KJ & Muller R (2010) Guidelines for assessment of bone microstructure in rodents using micro-computed tomography. *J Bone Miner Res* 25: 1468-1486

Braulke T, Geuze HJ, Slot JW, Hasilik A & von Figura K (1987) On the effects of weak bases and monensin on sorting and processing of lysosomal enzymes in human cells. *Eur J Cell Biol* 43: 316-321

Braulke T & Bonifacino JS (2009) Sorting of lysosomal proteins. *Biochim Biophys Acta* 1793: 605-614

Braulke T, Raas-Rothschild A & Kornfeld S. 2013. I-cell disease and pseudo-Hurler polydystrophy: Disorders of lysosomal enzyme phosphorylation and localization. In The online metabolic and molecular basis of inherited diseases. Valle D BA, Vogelstein B, Kinzler KW, Antonarakis SE, Ballabio A, Scriver CR, Sly WS, Bunz F, Gibson KM, Mitchell G, editor

Cagle S (2017) A case report of a Hispanic male with mucolipidosis III gamma with mild disease in the presence of a homozygous nonsense mutation. *Mol Genet Metab* 120: S34

Canuel M, Korkidakis A, Konnyu K & Morales CR (2008) Sortilin mediates the lysosomal targeting of cathepsins D and H. *Biochem Biophys Res Commun* 373: 292-297

Cappariello A, Maurizi A, Veeriah V & Teti A (2014) The Great Beauty of the osteoclast. *Arch Biochem Biophys* 558: 70-78

Cathey SS, Kudo M, Tiede S, Raas-Rothschild A, Braulke T, Beck M, Taylor HA, Canfield WM, Leroy JG, Neufeld EF & McKusick VA (2008) Molecular order in mucolipidosis II and III nomenclature. *Am J Med Genet A* 146A: 512-513

Cathey SS, Leroy JG, Wood T, Eaves K, Simensen RJ, Kudo M, Stevenson RE & Friez MJ (2010) Phenotype and genotype in mucolipidoses II and III alpha/beta: a study of 61 probands. *J Med Genet* 47: 38-48

References

Clarke LA & Hollak CE (2015) The clinical spectrum and pathophysiology of skeletal complications in lysosomal storage disorders. *Best Pract Res Clin Endocrinol Metab* 29: 219-235

Cohen MM, Jr. (2000) Merging the old skeletal biology with the new. I. Intramembranous ossification, endochondral ossification, ectopic bone, secondary cartilage, and pathologic considerations. *J Craniofac Genet Dev Biol* 20: 84-93

Coutinho MF, Lacerda L and Alves S (2011). Glycosaminoglycan Storage Disorders: A Review. *Biochem Res Int* 2012: 471325

Costa AG, Cusano NE, Silva BC, Cremers S & Bilezikian JP (2011) Cathepsin K: its skeletal actions and role as a therapeutic target in osteoporosis. *Nat Rev Rheumatol* 7: 447-456

Cs-Szabo G, Ragasa-San Juan D, Turumella V, Masuda K, Thonar EJ & An HS (2002) Changes in mRNA and protein levels of proteoglycans of the anulus fibrosus and nucleus pulposus during intervertebral disc degeneration. *Spine* 27: 2212-2219

Dallas SL, Prideaux M & Bonewald LF (2013) The osteocyte: an endocrine cell ... and more. *Endocr Rev* 34: 658-690

De Duve C, Pressman BC, Gianetto R, Wattiaux R & Appelmans F (1955) Tissue fractionation studies. 6. Intracellular distribution patterns of enzymes in rat-liver tissue. *Biochem J* 60: 604-617

De Pace R, Velho RV, Encarnacao M, Marschner K, Braulke T & Pohl S (2015) Subunit interactions of the disease-related hexameric GlcNAc-1-phosphotransferase complex. *Hum Mol Genet* 24: 6826-6835

Deuschl F, Kollmann K, von Figura K & Lubke T (2006) Molecular characterization of the hypothetical 66.3-kDa protein in mouse: lysosomal targeting, glycosylation, processing and tissue distribution. *FEBS Lett* 580: 5747-5752

Echtermeyer F, Bertrand J, Dreier R, Meinecke I, Neugebauer K, Fuerst M, Lee YJ, Song YW, Herzog C, Theilmeier G & Pap T (2009) Syndecan-4 regulates ADAMTS-5 activation and cartilage breakdown in osteoarthritis. *Nat Med* 15: 1072-1076

Encarnação M, Lacerda L, R. C, Prata MJ, Coutinho MF, Ribeiro H, Lopes L, Pineda M, Ignatius J, Galvez H, Mustonen A, Lima MR & Alves S (2009) Molecular analysis of the GNPTAB and GNPTG genes in 13 patients with mucolipidosis type II or type III - identification of eight novel mutations. *Clin Genet* 76: 76-84

Encarnação M, Kollmann K, Trusch M, Braulke T & Pohl S (2011) Post-translational modifications of the gamma-subunit affect intracellular trafficking and complex assembly of GlcNAc-1-phosphotransferase. *J Biol Chem* 286: 5311-5318

Esko JD (1991) Genetic analysis of proteoglycan structure, function and metabolism. *Curr Opin Cell Biol* 3: 805-816

References

Flanagan-Steet H, Matheny C, Petrey A, Parker J & Steet R (2016) Enzyme-specific differences in mannose phosphorylation between GlcNAc-1-phosphotransferase alphabeta and gamma subunit deficient zebrafish support cathepsin proteases as early mediators of mucolipidosis pathology. *Biochim Biophys Acta* 1860: 1845-1853

Franke M, Braulke T & Storch S (2013) Transport of the GlcNAc-1-phosphotransferase alpha/beta-subunit precursor protein to the Golgi apparatus requires a combinatorial sorting motif. *J Biol Chem* 288: 1238-1249

Gao Y, Yang K, Xu S, Wang C, Liu J, Zhang Z, Yuan M, Luo X, Liu M, Wang QK & Liu JY (2011) Identification of compound heterozygous mutations in GNPTG in three siblings of a Chinese family with mucolipidosis type III gamma. *Mol Genet Metab* 102: 107-109

Gelfman CM, Vogel P, Issa TM, Turner CA, Lee WS, Kornfeld S & Rice DS (2007) Mice lacking alpha/beta subunits of GlcNAc-1-phosphotransferase exhibit growth retardation, retinal degeneration, and secretory cell lesions. *Invest Ophthalmol Vis Sci* 48: 5221-5228

Gentili C & Cancedda R (2009) Cartilage and bone extracellular matrix. *Curr Pharm Des* 15: 1334-1348

Giugliani R, Federhen A, Vairo F, Vanzella C, Pasqualim G, da Silva LM, Giugliani L, de Boer AP, de Souza CF, Matte U & Baldo G (2016) Emerging drugs for the treatment of mucopolysaccharidoses. *Expert Opin Emerg Drugs* 21: 9-26

Hait NC, Allegood J, Maceyka M, Strub GM, Harikumar KB, Singh SK, Luo C, Marmorstein R, Kordula T, Milstien S & Spiegel S (2009) Regulation of histone acetylation in the nucleus by sphingosine-1-phosphate. *Science* 325: 1254-1257

Helenius A & Aebi M (2001) Intracellular functions of N-linked glycans. *Science* 291: 2364-2369

Hickman S & Neufeld EF (1972) A hypothesis for I-cell disease: defective hydrolases that do not enter lysosomes. *Biochem Biophys Res Commun* 49: 992-999

Idol RA, Wozniak DF, Fujiwara H, Yuede CM, Ory DS, Kornfeld S & Vogel P (2014) Neurologic abnormalities in mouse models of the lysosomal storage disorders mucolipidosis II and mucolipidosis III gamma. *PLoS One* 9: e109768

Itoh M, Matsuda J, Suzuki O, Ogura A, Oshima A, Tai T, Suzuki Y & Takashima S (2001) Development of lysosomal storage in mice with targeted disruption of the beta-galactosidase gene: a model of human G(M1)-gangliosidosis. *Brain Dev* 23: 379-384

James RA, Singh-Grewal D, Lee SJ, McGill J & Adib N (2016) Lysosomal storage disorders: A review of the musculoskeletal features. *J Paediatr Child Health* 52: 262-271

Karsenty G (2008) Transcriptional control of skeletogenesis. *Annu Rev Genomics Hum Genet* 9: 183-196

Karsenty G, Kronenberg HM & Settembre C (2009) Genetic control of bone formation. *Annu Rev Cell Dev Biol* 25: 629-648

Kiani C, Chen L, Wu YJ, Yee AJ & Yang BB (2002) Structure and function of aggrecan. *Cell Res* 12: 19-32

Kjellen L & Lindahl U (1991) Proteoglycans: structures and interactions. *Annu Rev Biochem* 60: 443-475

Köhne T, Markmann S, Schweizer M, Muschol N, Friedrich RE, Hagel C, Glatzel M, Kahl-Nieke B, Amling M, Schinke T & Braulke T (2016) Mannose 6-phosphate-dependent targeting of lysosomal enzymes is required for normal craniofacial and dental development. *Biochim Biophys Acta* 1862: 1570-1580

Kollmann K, Pohl S, Marschner K, Encarnação M, Sakwa I, Tiede S, Poorthuis BJ, Lübke T, Müller-Loennies S, Storch S & Braulke T (2010) Mannose phosphorylation in health and disease. *Eur J Cell Biol* 89: 117-123

Kollmann K, Damme M, Markmann S, Morelle W, Schweizer M, Hermans-Borgmeyer I, Röchert AK, Pohl S, Lübke T, Michalski JC, Kakela R, Walkley SU & Braulke T (2012) Lysosomal dysfunction causes neurodegeneration in mucolipidosis II 'knock-in' mice. *Brain* 135: 2661-2675

Kollmann K, Pestka JM, Kühn SC, Schöne E, Schweizer M, Karkmann K, Otomo T, Catala-Lehnen P, Failla AV, Marshall RP, Krause M, Santer R, Amling M, Braulke T & Schinke T (2013) Decreased bone formation and increased osteoclastogenesis cause bone loss in mucolipidosis II. *EMBO Mol Med* 5: 1871-1886

Kozhemyakina E, Lassar AB & Zelzer E (2015) A pathway to bone: signaling molecules and transcription factors involved in chondrocyte development and maturation. *Development* 142: 817-831

Kubaski F, Kecskemethy HH, Harcke HT & Tomatsu S (2016) Bone mineral density in mucopolysaccharidosis IVB. *Mol Genet Metab Rep* 8: 80-84

Kubaski F, Suzuki Y, Orii K, Giugliani R, Church HJ, Mason RW, Dung VC, Ngoc CT, Yamaguchi S, Kobayashi H, Girisha KM, Fukao T, Orii T & Tomatsu S (2017) Glycosaminoglycan levels in dried blood spots of patients with mucopolysaccharidoses and mucolipidoses. *Mol Genet Metab* 120: 247-254

Kühn SC, Köhne T, Cornils K, Markmann S, Riedel C, Pestka JM, Schweizer M, Baldauf C, Yorgan TA, Krause M, Keller J, Neven M, Breyer S, Stuecker R, Muschol N, Busse B, Braulke T, Fehse B, Amling M & Schinke T (2015) Impaired bone remodeling and its correction by combination therapy in a mouse model of mucopolysaccharidosis-I. *Hum Mol Genet* 24: 7075-7086

Lachmann RH (2011) Enzyme replacement therapy for lysosomal storage diseases. *Curr Opin Pediatr* 23: 588-593

Lacombe J, Karsenty G & Ferron M (2013) Regulation of lysosome biogenesis and functions in osteoclasts. *Cell Cycle* 12: 2744-2752

Langereis EJ, Wagemans T, Kulik W, Lefeber DJ, van Lenthe H, Oussoren E, van der Ploeg AT, Ruijter GJ, Wevers RA, Wijburg FA & van Vlies N (2015) A Multiplex Assay for the Diagnosis of Mucopolysaccharidoses and Mucolipidoses. *PLoS One* 10: e0138622

References

Lawrence R, Brown JR, Al-Mafraji K, Lamanna WC, Beitel JR, Boons GJ, Esko JD & Crawford BE (2012) Disease-specific non-reducing end carbohydrate biomarkers for mucopolysaccharidoses. *Nat Chem Biol* 8: 197-204

Lee WS, Payne BJ, Gelfman CM, Vogel P & Kornfeld S (2007) Murine UDP-GlcNAc:lysosomal enzyme N-acetylglucosamine-1-phosphotransferase lacking the gamma-subunit retains substantial activity toward acid hydrolases. *J Biol Chem* 282: 27198-27203

Lindahl U, Couchman J, Kimata K & Esko JD (2015) Proteoglycans and sulfated glycosaminoglycans. 207-221

Liu S, Zhang W, Shi H, Meng Y & Qiu Z (2014) Three novel homozygous mutations in the GNPTG gene that cause mucolipidosis type III gamma. *Gene* 535: 294-298

Long F & Ornitz DM (2013) Development of the endochondral skeleton. *Cold Spring Harb Perspect Biol* 5: a008334

Makrypidi G, Damme M, Müller-Loennies S, Trusch M, Schmidt B, Schlüter H, Heeren J, Lübke T, Saftig P & Braulke T (2012) Mannose 6 dephosphorylation of lysosomal proteins mediated by acid phosphatases Acp2 and Acp5. *Mol Cell Biol* 32: 774-782

Markmann S, Thelen M, Cornils K, Schweizer M, Brocke-Ahmadinejad N, Willnow T, Heeren J, Gieselmann V, Braulke T & Kollmann K (2015) Lrp1/LDL receptor play critical roles in mannose 6-phosphate-independent lysosomal enzyme targeting. *Traffic* 16: 743-759

Marschner K, Kollmann K, Schweizer M, Braulke T & Pohl S (2011) A key enzyme in the biogenesis of lysosomes is a protease that regulates cholesterol metabolism. *Science* 333: 87-90

Martin JA & Buckwalter JA (2001) Roles of articular cartilage aging and chondrocyte senescence in the pathogenesis of osteoarthritis. *Iowa Orthop J* 21: 1-7

Millan JL (2013) The role of phosphatases in the initiation of skeletal mineralization. *Calcif Tissue Int* 93: 299-306

Mistri M, Dalal A, Nath P, Nampoothiri S, Mehta S, Singh S, Sheth F & Sheth J (2018) Identification of novel and known mutation in 19 patients with mucolipidosis type II and III from India and validation of novel method of screening for mucolipidosis-II and III screening. *Mol Genet Metab* 123: S96

Muenzer J (2014) Early initiation of enzyme replacement therapy for the mucopolysaccharidoses. *Mol Genet Metab* 111: 63-72

Müller-Loennies S, Galliciotti G, Kollmann K, Glatzel M & Braulke T (2010) A novel single chain antibody fragment for detection of mannose 6-phosphate-containing proteins: Application in mucolipidosis type II patients and mice. *Am J Pathol* 177: 240-247

Newton J, Hait NC, Maceyka M, Colaco A, Maczis M, Wassif CA, Cougnoux A, Porter FD, Milstien S, Platt N, Platt FM & Spiegel S (2017) FTY720/fingolimod increases NPC1

and NPC2 expression and reduces cholesterol and sphingolipid accumulation in Niemann-Pick type C mutant fibroblasts. *FASEB J* 31: 1719-1730

Otomo T, Schweizer M, Kollmann K, Schumacher V, Muschol N, Tolosa E, Mittrucker HW & Braulke T (2015) Mannose 6 phosphorylation of lysosomal enzymes controls B cell functions. *J Cell Biol* 208: 171-180

Parenti G, Andria G & Ballabio A (2015) Lysosomal storage diseases: from pathophysiology to therapy. *Annu Rev Med* 66: 471-486

Persichetti E, Chuzhanova NA, Dardis A, Tappino B, Pohl S, Thomas NS, Rosano C, Balducci C, Paciotti S, Dominissini S, Montalvo AL, Sibilio M, Parini R, Rigoldi M, Di Rocco M, Parenti G, Orlacchio A, Bembi B, Cooper DN, Filocamo M & Beccari T (2009) Identification and molecular characterization of six novel mutations in the UDP-N-acetylglucosamine-1-phosphotransferase gamma subunit (GNPTG) gene in patients with mucolipidosis III gamma. *Hum Mutat* 30: 978-984

Pohl S, Marschner K, Storch S & Braulke T (2009a) Glycosylation- and phosphorylation-dependent intracellular transport of lysosomal hydrolases. *Biol Chem* 390: 521-527

Pohl S, Tiede S, Castrichini M, Cantz M, Gieselmann V & Braulke T (2009b) Compensatory expression of human N-Acetylglucosaminyl-1-phosphotransferase subunits in mucolipidosis type III gamma. *Biochim Biophys Acta* 1792: 221-225

Pohl S, Encarnação M, Castrichini M, Müller-Loennies S, Muschol N & Braulke T (2010a) Loss of N-Acetylglucosamine-1-phosphotransferase gamma-subunit due to intronic mutation in GNPTG causes mucolipidosis type III gamma: Implications for molecular and cellular diagnostics. *Am J Med Genet A* 152A: 124–132

Pohl S, Tiede S, Marschner K, Encarnação M, Castrichini M, Kollmann K, Muschol N, Ullrich K, Müller-Loennies S & Braulke T (2010b) Proteolytic processing of the gamma-subunit is associated with the failure to form GlcNAc-1-phosphotransferase complexes and mannose 6-phosphate residues on lysosomal enzymes in human macrophages *J Biol Chem* 285: 23936-23944

Pohl S, Braulke T & Müller-Loennies S. (2012) A novel mannose 6-phosphate specific antibody fragment for diagnosis of mucolipidosis II and III. In: Anticarbohydrate antibodies - From molecular basis to clinical application. Kosma P & Müller-Loennies S (editors). Springer, Wien

Qian Y, Lee I, Lee W, Qian M, Kudo M, Canfield W, Lobel P & Kornfeld S (2010) Functions of the alpha, beta, and gamma subunits of UDP-GlcNAc:lysosomal enzyme N-acetylglucosamine-1-phosphotransferase. *J Biol Chem.* 285: 3360-3370

Raas-Rothschild A, Cormier-Daire V, Bao M, Genin E, Salomon R, Brewer K, Zeigler M, Mandel H, Toth S, Roe B, Munnich A & Canfield WM (2000) Molecular basis of variant pseudo-hurler polydystrophy (mucolipidosis IIIC). *J Clin Invest* 105: 673-681

Raas-Rothschild A, Bargal R, Goldman O, Ben-Asher E, Groener JE, Toutain A, Stemmer E, Ben-Neriah Z, Flusser H, Beemer FA, Penttinen M, Olender T, Rein AJ, Bach G & Zeigler M (2004) Genomic organisation of the UDP-N-acetylglucosamine-1-

phosphotransferase gamma subunit (GNPTAG) and its mutations in mucolipidosis III. *J Med Genet* 41: e52

Raas-Rothschild A, Pohl S & Braulke T (2012) Multiple enzyme deficiencies - Defects in transport: Mucolipidosis II alpha/beta; mucolipidosis III alpha/beta and mucolipidosis III gamma. In: Lysosomal storage diseases: A practical guide. Mehta AB & Winchester B (editors). Wiley-Blackwell, Oxford

Reczek D, Schwake M, Schröder J, Hughes H, Blanz J, Jin X, Brondyk W, Van Patten S, Edmunds T & Saftig P (2007) LIMP-2 is a receptor for lysosomal mannose-6-phosphate-independent targeting of beta-glucocerebrosidase. *Cell* 131: 770-783

Ruddock LW & Molinari M (2006) N-glycan processing in ER quality control. *J Cell Sci* 119: 4373-4380

Russell RG (2011) Bisphosphonates: the first 40 years. *Bone* 49: 2-19

Salbach-Hirsch J, Ziegler N, Thiele S, Moeller S, Schnabelrauch M, Hintze V, Scharnweber D, Rauner M & Hofbauer LC (2014) Sulfated glycosaminoglycans support osteoblast functions and concurrently suppress osteoclasts. *J Cell Biochem* 115: 1101-1111

Saraogi I & Shan SO (2011) Molecular mechanism of co-translational protein targeting by the signal recognition particle. *Traffic* 12: 535-542

Schinke T, Schilling AF, Baranowsky A, Seitz S, Marshall RP, Linn T, Blaeker M, Huebner AK, Schulz A, Simon R, Gebauer M, Priemel M, Kornak U, Perkovic S, Barvencik F, Beil FT, Del Fattore A, Frattini A, Streichert T, Püschel K, Villa A, Debatin KM, Rueger JM, Teti A, Zustin J, Sauter G & Amling M (2009) Impaired gastric acidification negatively affects calcium homeostasis and bone mass. *Nat Med* 15: 674-681

Schmittgen TD & Livak KJ (2008) Analyzing real-time PCR data by the comparative C(T) method. *Nat Protoc* 3: 1101-1108

Schrader KA, Heravi-Moussavi A, Waters PJ, Senz J, Whelan J, Ha G, Eydoux P, Nielsen T, Gallagher B, Oloumi A, Boyd N, Fernandez BA, Young TL, Jones SJ, Hirst M, Shah SP, Marra MA, Green J & Huntsman DG (2011) Using next-generation sequencing for the diagnosis of rare disorders: a family with retinitis pigmentosa and skeletal abnormalities. *J Pathol* 225: 12-18

Smuts I, Potgieter D & van der Westhuizen FH (2009) Combined tarsal and carpal tunnel syndrome in mucolipidosis type III. A case study and review. *Ann N Y Acad Sci* 1151: 77-84

Surolia A, Bishayee S, Ahmad A, Balasubramanian KA, Thambi-Dorai D, Podder SK & Bachhawat BK (1975) Studies on the interaction of concanavalin A with glycoproteins. *Adv Exp Med Biol* 55: 95-115

Teitelbaum SL (2000) Bone resorption by osteoclasts. *Science* 289: 1504-1508

Thelen M, Winter D, Braulke T & Gieselmann V (2017) SILAC-based comparative proteomic analysis of lysosomes from mammalian cells using LC-MS/MS. *Methods Mol Biol* 1594: 1-18

Tiede S, Cantz M, Raas-Rothschild A, Muschol N, Bürger F, Ullrich K & Braulke T (2004) A novel mutation in UDP-N-acetylglucosamine-1-phosphotransferase gamma subunit (GNPTAG) in two siblings with mucolipidosis type III alters a used glycosylation site. *Hum Mutat* 24: 535

Tiede S, Storch S, Lübke T, Henrissat B, Bargal R, Raas-Rothschild A & Braulke T (2005) Mucolipidosis II is caused by mutations in GNPTA encoding the alpha/beta GlcNAc-1-phosphotransferase. *Nat Med* 11: 1109-1112

Tomatsu S, Orii KO, Vogler C, Grubb JH, Snella EM, Gutierrez M, Dieter T, Holden CC, Sukegawa K, Orii T, Kondo N & Sly WS (2003) Production of MPS VII mouse (Gus(tm(hE540A x mE536A)Sly)) doubly tolerant to human and mouse beta-glucuronidase. *Hum Mol Genet* 12: 961-973

Tomatsu S, Yasuda E, Patel P, Ruhnke K, Shimada T, Mackenzie WG, Mason R, Thacker MM, Theroux M, Montano AM, Almeciga-Diaz CJ, Barrera LA, Chinen Y, Sly WS, Rowan D, Suzuki Y & Orii T (2014) Morquio A syndrome: diagnosis and current and future therapies. *Pediatr Endocrinol Rev* 12 Suppl 1: 141-151

Tomatsu S, Almeciga-Diaz CJ, Montano AM, Yabe H, Tanaka A, Dung VC, Giugliani R, Kubaski F, Mason RW, Yasuda E, Sawamoto K, Mackenzie W, Suzuki Y, Orii KE, Barrera LA, Sly WS & Orii T (2015) Therapies for the bone in mucopolysaccharidoses. *Mol Genet Metab* 114: 94-109

Tüysüz B, Kasapcopur O, Alkaya DU, Sahin S, Sozeri B & Yesil G (2018) Mucolipidosis type III gamma: Three novel mutation and genotype-phenotype study in eleven patients. *Gene* 642: 398-407

Tylki-Szymanska A, Czartoryska B, Groener JE & Lugowska A (2002) Clinical variability in mucolipidosis III (pseudo-Hurler polydystrophy). *Am J Med Genet* 108: 214-218

Tylki-Szymanska A (2014) Mucopolysaccharidosis type II, Hunter's syndrome. *Pediatr Endocrinol Rev* 12 Suppl 1: 107-113

Vairo F, Federhen A, Baldo G, Riegel M, Burin M, Leistner-Segal S & Giugliani R (2015) Diagnostic and treatment strategies in mucopolysaccharidosis VI. *Appl Clin Genet* 8: 245-255

van Bezooijen RL, ten Dijke P, Papapoulos SE & Lowik CW (2005) SOST/sclerostin, an osteocyte-derived negative regulator of bone formation. *Cytokine Growth Factor Rev* 16: 319-327

van Meel E, Boonen M, Zhao H, Oorschot V, Ross FP, Kornfeld S & Klumperman J (2011) Disruption of the Man-6-P targeting pathway in mice impairs osteoclast secretory lysosome biogenesis. *Traffic* 12: 912-924

References

Velho RV, Alegra T, Sperb F, Ludwig NF, Saraiva-Pereira ML, Matte U & Schwartz IV (2014) A de novo or germline mutation in a family with Mucolipidosis III gamma: Implications for molecular diagnosis and genetic counseling. *Mol Genet Metab Rep* 1: 98-102

Velho RV, De Pace R, Klünder S, Sperb-Ludwig F, Lourenco CM, Schwartz IV, Braulke T & Pohl S (2015) Analyses of disease-related GNPTAB mutations define a novel GlcNAc-1-phosphotransferase interaction domain and an alternative site-1 protease cleavage site. *Hum Mol Genet* 24: 3497-3505

Velho RV, De Pace R, Tidow H, Braulke T & Pohl S (2016a) Identification of the interaction domains between alpha- and gamma-subunits of GlcNAc-1-phosphotransferase. *FEBS Lett* 590: 4287-4295

Velho RV, Ludwig NF, Alegra T, Sperb-Ludwig F, Guarany NR, Matte U & Schwartz IV (2016b) Enigmatic in vivo GlcNAc-1-phosphotransferase (GNPTG) transcript correction to wild type in two mucolipidosis III gamma siblings homozygous for nonsense mutations. *J Hum Genet* 61: 555-560

Venn G & Mason RM (1985) Absence of keratan sulphate from skeletal tissues of mouse and rat. *Biochem J* 228: 443-450

Vynios DH (2014) Metabolism of cartilage proteoglycans in health and disease. *Biomed Res Int* 2014: 452315

Vogel P, Payne BJ, Read R, Lee WS, Gelfman CM & Kornfeld S (2009) Comparative Pathology of Murine Mucolipidosis Types II and IIIC. *Vet Pathol* 46: 313-324

Wang ML, Motamed M, Infante RE, Abi-Mosleh L, Kwon HJ, Brown MS & Goldstein JL (2010) Identification of surface residues on Niemann-Pick C2 essential for hydrophobic handoff of cholesterol to NPC1 in lysosomes. *Cell Metab* 12: 166-173

Wraith JE & Jones S (2014) Mucopolysaccharidosis type I. *Pediatr Endocrinol Rev* 12 Suppl 1: 102-106

Zaidi M, Moonga BS & Huang CL (2004) Calcium sensing and cell signaling processes in the local regulation of osteoclastic bone resorption. *Biol Rev Camb Philos Soc* 79: 79-100

Zaidi M (2007) Skeletal remodeling in health and disease. *Nat Med* 13: 791-801

Zarghooni M & Dittakavi SS (2009) Molecular analysis of cell lines from patients with mucolipidosis II and mucolipidosis III. *Am J Med Genet A* 149A: 2753-2761

Zoch ML, Clemens TL & Riddle RC (2016) New insights into the biology of osteocalcin. *Bone* 82: 42-49

Zrhidri A, Amasdl S, Lyahyai J, Elouardi H, Chkirate B, Raymond L, Egea G, Taoudi M, El Mouatassim S & Sefiani A (2017) Next Generation Sequencing identifies mutations in GNPTG gene as a cause of familial form of scleroderma-like disease. *Pediatr Rheumatol Online J* 15: 72

8. Publications, conference contributions and awards

8.1 Publications

Abstracts

- **Di Lorenzo G**, De Pace R, Schweizer M, Braulke T, Pohl S (2016) In vivo expression of the γ-subunit of MLIII-related GlcNAc-1-phosphotransferase. *J Inborn Errors Metab Screen 4: 71*

- Westermann L, **Di Lorenzo G**, Schweizer M, Schinke T, Rose-John S, Braulke T, Pohl S (2018) Targeting of pro-osteoclastogenic interleukin-6 in mucolipidosis type II as potential corrective approach. *Monatsschr Kinderheilkd* 4: 377

Research article

- **Di Lorenzo G**, Velho RV, Winter D, Thelen M, Ahmadi S, Schweizer M, De Pace R, Cornils K, Yorgan TA, Grüb S, Hermans-Borgmeyer I, Schinke T, Müller-Loennies S, Braulke T, Pohl S (2018) Gnptg-dependent mannose 6-phosphorylation of arylsulfatase B limits glycosaminoglycan degradation. *Mol Cell Proteomics doi:10.1074/mcp.RA118.000720*

Review

- Velho RV, De Pace R, Klünder S, **Di Lorenzo G**, Schweizer M, Braulke T, Pohl S (2017) Site-1 protease and lysosomal homeostasis. *Biochim Biophys Acta* 1864: 2162-2168

8.2 Conference contributions

Oral presentations

- **Di Lorenzo G**. Role of the γ-subunit of GlcNAc-1-phosphotransferase in the pathogenesis of the lysosomal storage disorder mucolipidosis type III gamma, Retreat of the Research Training Group 1459, Travemünde, Germany (08.-10.10.2015)

- **Di Lorenzo G.** Role of the γ-subunit of GlcNAc-1-phosphotransferase in the pathogenesis of the lysosomal storage disorder mucolipidosis type III, Retreat of the Research Training Group 1459, Timmendorfer Strand, Germany (06.-08.10.2016)

- **Di Lorenzo G**. Role of the γ -subunit of GlcNAc-1-phosphotransferase in the pathogenesis of mucolipidosis type III, 21th Workshop and Student Course, European Study Group on Lysosomal Diseases, Lyon, France (13.-17.09.2017)

Poster presentations

- Schweizer M, Markmann, **Di Lorenzo G**, Pohl S, Braulke T. Neuropathology of a knock-in mouse model for the lysosomal disease mucolipidosis II (MLII), PANOS Spring Meeting, Hamburg, Germany (14.04-15.04.2016)

- Schweizer M, Markmann S, **Di Lorenzo G**, Pohl S, Braulke T. Neuropathology of a knock-in mouse model for the lysosomal disease mucolipidosis II, Meeting of the German Society for Neuropathology and Neuroanatomy, Hamburg, Germany (22.-24.9.2016)

- **Di Lorenzo G**, De Pace R, Schweizer M, Thelen M, Braulke T, Pohl S. *In vivo* expression of the γ-subunit of MLIII-related GlcNAc-1-phosphotransferase, 14th International Symposium on MPS and Related Diseases, Bonn, Germany (13.07-17.07.2016)

- **Di Lorenzo G,** Velho RV, Thelen M, Braulke T, Pohl S. Role of the γ-subunit of GlcNAc-1-phosphotransferase for selective mannose 6-phosphate formation on lysosomal enzyme, GlycoBioTec symposium, Berlin, Germany (07.02-9.02.2017)

- **Di Lorenzo G,** Velho RV, Schweizer M, Thelen M, Winter D, Yorgan T, Schinke T, Schauer K, Gieselmann V, Braulke T, Pohl S. Selective mannose 6-phosphate formation on lysosomal enzymes, Gordon Research Conference on Lysosomal Diseases, Lucca, Italy (04.03-10.03.2017)

- **Di Lorenzo G,** Velho RV, Schweizer M, Yorgan T, Thelen M, Winter D, Schinke T, Braulke T, Pohl S. Role of the γ-subunit of GlcNAc-1-phosphotransferase for selective mannose 6-phosphate formation on lysosomal enzymes, 4th International Symposium on Protein Trafficking in Health and Disease, Hamburg, Germany (07.-09.06.2017)

- Sachs W, **Di Lorenzo G**, Sachs M, Pohl S, Meyer-Schwesinger C. Proteasomal or lysosomal degradation system failures have different consequences on renal cell protein homeostasis, American Society of Nephrology, Kidney Week 2017, New Orleans, USA (31.10.-5.11.2017)

- Westermann L, **Di Lorenzo G**, Schweizer M, Schinke T, Rose-John S, Braulke T, Pohl S. Targeting of pro-osteoclastogenic interleukin-6 in mucolipidosis type II as potential corrective approach, Annual Conference of the Working Group for Paediatric disturbances, Fulda, Germany (07.-09.03.2018)

Conference (attendance only)

- 20th Workshop and Student Course, European Study Group on Lysosomal Diseases, Pozzuoli, Italy (30.9.-4.10.2015)

Awards

- Young Scientist Award for oral presentation, 21th Workshop of the European Study Group on Lysosomal Diseases, Lyon, France (13.-17.09.2017)
- Student Talk Award, 21th Student Course of the European Study Group on Lysosomal Diseases, Lyon, France (13.-17.09.2017)

Abbreviations

3D	three-dimensional
4-MU	4-methylumbelliferone
Acan	aggregan
Acp2	acid phosphatase 2
Acp5	acid phosphatase 5
Aga	aspartylglucosaminidase
APS	ammonium peroxydisulfate
Arsa	arylsulfatase A
Arsb	arylsulfatase B
Asah1	acid ceramidase
ATP	adenosine 5′-triphosphate
BSA	bovine serum albumin
BV/TV	bone volume per tissue volume
Calcr	calcitonin receptor
cDNA	complementary DNA
Cln5	ceroid-lipofuscin protein 5
CNS	central nervous system
Cpq	carboxypeptidase Q
CS	choindroitin sulfate
Ctbs	di-N-acetylchitobiase
C-terminal	carboxy-terminal
Ctsc	cathepsins C
Ctss	cathepsins S
Ctsz	cathepsins Z
DAPI	4′,6-diamino-2-phenylindol
DEAE	diethylaminoethyl
DEPC	diethylpyrocarbonat
dH_2O	destillated water
DMEM	Dulbecco's modified Eagle's medium
DMSO	dimethylsulfoxide
DNA	deoxyribonucleic acid
dNTP	deoxynucleoside triphosphate
Dpp7	dipeptidylpeptidase 7
DTT	dithiothreitol
ECL	enhanced chemiluminescence
EDTA	ethylenediaminetetraacetate
Epdr1	mammalian ependymin-related protein 1
ER	endoplasmic reticulum
ERT	enzyme replacement therapy
et al	and others
EtOH	ethanol

FCS	fetal calf serum
for	forward
Fuca1	α-fucosidase
GAG	glycosaminoglycan
Galc	galactocerebrosidase
Galns	N-acetylgalactosamine-6-sulfatase
Gba	β-glucocerebrosidase
Gds	glucuronate
Ggh	γ-glutamyl hydrolase
Glb1	β-galactosidase
GlcNAc	N-acetylglucosamine
Gnptab	GlcNAc-1-phosphotransferase (α/β-subunit precursor)
Gnptg	GlcNAc-1-phosphotransferase (γ-subunit)
Gns	N-acetylglucosamine-6-sulfatase
GP	growth plate
Gusb	β-glucuronidase
HEPES	4-(2-hydroxyethyl)-1-piperazineethanesulfonic acid
Hexb	β-hexosaminidase subunit B
HRP	horseradish peroxidase
HS	heparan sulfate
Ids	iduronate 2-sulfatase
Idua	iduronidase
IF	immunofluorescence microscopy
IgG	immunoglobulin G
LF	lysosome-enriched fraction
Lipa	lysosomal acid lipase
LSS	liquid scintillation spectrometry
M6P	mannose 6-phosphate
Man2b1	α-mannosidase class 2B member 1
Man2b2	α-mannosidase class 2B member 2
Manba	β-mannosidase
M-Csf	macrophage colony stimulating factor
MEF	mouse embryonic fibroblasts
MeOH	methanol
MLII	mucolipidosis type II
MLIII	mucolipidosis type III gamma
MPR	mannose 6-phosphate-receptor
MPS	mucopolysaccharidosis
mRNA	messenger RNA
MS	mass spectrometry
N.Ob/B.Pm	number of osteoblasts per bone perimeter
N.Oc/B.Pm	number of osteoclasts per bone perimeter
N.Ot/B.Ar	number of osteocytes per bone area
Naglu	α-N-acetylglucosaminidase

Neu1	sialidase 1
Npc2	Niemann-Pick type C2 protein
N-terminal	amino-terminal
Ob.S/BS	osteoblast surface per bone surface
Oc.S/BS	osteoclast surface per bone surface
OD	optical density
PBS	phosphate-buffer saline
PCR	polymerase chain reaction
PFA	paraformaldehyde
Pla2g15	phospholipase A2, group XV
Plbd2	phospholipase B domain containing 2
PNS	postnuclear supernatants
Ppt2	palmitoyl-protein thioesterase 2
Prcp	prolylcarboxypeptidase
Rankl	receptor activator of nuclear factor kappa-B ligand
rev	reverse
RNA	ribonucleic acid
RT	room temperature
SDS	sodium dodecyl sulfate
SDS-PAGE	SDS polyacrylamide gel electrophoresis
Sgsh	N-sulfoglucosamine sulfohydrolase
Siae	sialate O-acetylesterase
SILAC	stable isotope labeling by amino acids in cell culture
Sost	sclerostin
SRP	signal recognition particle
TAE	Tris-acetate-ethylenediaminetetraacetic acid
Taq	Thermus aquaticus
Tb.N	trabecular number
Tb.Sp	trabecular spacing
Tb.Th	trabecular thickness
TBS	Tris-buffered saline
TBST	Tris-buffered saline/tween 20
TEMED	NNN′N′-tetramethylethylenediamine
TGN	trans-Golgi network
Tpp1	tripeptidyl peptidase 1
Tris	Tris-hydroxymethyl-aminomethane
UDP	uridine diphosphate
UV	ultraviolet
wt	wild-type
μCT	Micro-computed tomography

Eidesstattliche Versicherung

Declaration on oath

Hiermit erkläre ich an Eides statt, dass ich die vorliegende Dissertationsschrift selbst verfasst und keine anderen als die angegebenen Quellen und Hilfsmittel benutzt habe.

I hereby declare, on oath, that I have written the present dissertation by my own and have not used other than the acknowledged resources and aids.

Hamburg, den   Untersch

Acknowledgments

I would like to thank all the people that help me in different ways during this doctoral thesis which is based on studies performed during May 2015 to July 2018 at the Department of Biochemistry, Children's Hospital, UKE, Germany. I am very thankful for these 3 years because they have been the opportunity to grow, not only as a scientist but also as a person. I would like to thank Prof. Dr. Thomas Braulke and Prof. Dr. Tim-Wolf Gilberger for evaluating this dissertation.

Many thanks to my thesis advisor Prof. Thomas Braulke, for giving me the possibility to work on an interesting project together with a very nice team. His support with stimulating discussions and criticism and his advises improved my research skills and prepared me for future challenges.

I would like to express my sincere gratitude to my supervisor Dr. Sandra Pohl for her guide in each step of my PhD, for being always available for all my questions and for teaching me, since the first day, that "there are no stupid questions"! Her support and suggestions were fundamental to accomplish this step of my life.

I am thankful for having been part of the Research Training Group and for having participated to several congresses, they were huge opportunities to interact with top class researchers, to share my experience with other PhD students and PI, and to professionally grow.

Thanks to Prof. Thorsten Schinke and Dr. Timur Yorgan (Department of Osteology and Biomechanics, University Medical Center Hamburg-Eppendorf), for helping me with the bone analyses and for aiding me each time I had questions concerning the bone field. Thank to Dr. Michaela Schweizer (ZMNH, University Medical Center Hamburg-Eppendorf) for the Lacz staining and the electron microscopy images and for her ability to always find out how to help me to perform some experiments. Thanks to Dominic Winter and Melanie Thelen (Institute of Biochemistry and Molecular Biology, University of Bonn) for all the Mass Spectrometry analyses. Thanks to the GRK1459 and DFG for the funding support and for the opportunity to work one month together with Dr. Kristine Schauer at Institute Curie in Paris which gave me the opportunity to experience another lab and another project.

I am very thankful to Dr. Renata Voltolini Velho for her contribution in this thesis for measuring the GlcNAc-1-phosphotransferate activity but especially for her fundamental

daily support, both scientific and personal, I am extremely grate that I could share with her this important piece of my life (obrigata!). Thanks to Raffa, Georgia and all my previous colleagues/friends. Thanks to Johannes for his constant help. Thank to Tatyana, together with me and Renata she is part of the Mädchen Büro, where it was possible to share everything at any time. A sincere thanks goes to all my friends, the special long-time friends and the new precious friends with who I shared my life in Hamburg, each of them has made an important contribution for my personal growth during this 3 years. Thanks to Paolo, his support was very important especially during the writing time of this thesis. I am grateful to my family, my beloved parents and my piccolo brother, their support was essential, anything would be possible without them, therefore I dedicate this thesis to them.

GRAZIE MILLE A TUTTI!

I could not resist to write all the names of the persons that in different manner, during these years, have contributed to let me became who I am. It will not be difficult to find your name!

```
L  E  N  A  H  T  E  B  A  S  I  L  E  M  H  T  F  F  S  W
O  A  N  A  N  N  C  A  N  I  T  R  A  M  S  N  R  C  A  M
R  O  I  K  R  I  N  L  Y  M  R  M  I  I  A  A  G  N  A
E  C  L  I  E  C  N  E  U  A  T  A  T  T  N  A  N  E  D  R
N  I  O  L  H  O  T  T  C  A  U  T  S  C  G  T  C  O  R  I
Z  N  R  E  P  L  A  S  I  C  A  R  O  T  P  A  E  R  A  A
O  E  A  G  O  E  L  R  N  B  E  A  A  A  I  N  S  G  V  E
S  M  C  N  T  T  E  O  A  K  A  M  T  G  L  E  C  I  A  L
M  O  A  A  S  T  S  H  T  A  N  R  B  P  I  R  A  A  L  E
A  D  L  I  I  A  S  T  A  I  I  N  E  L  E  U  U  R  E  N
R  A  E  S  R  A  A  S  N  Z  T  E  R  Y  L  J  L  O  R  A
I  L  M  S  H  K  N  B  I  N  R  I  N  C  I  O  J  I  I  O
O  E  R  E  C  I  D  A  E  I  A  R  A  I  S  H  M  L  A  L
L  A  A  L  J  M  R  R  L  C  M  A  R  N  A  A  E  I  A  R
I  H  C  A  C  L  A  U  D  I  A  M  D  I  B  N  L  G  C  A
N  C  R  A  F  F  A  E  L  L  A  A  O  M  E  N  A  R  I  C
A  I  E  V  P  A  O  L  I  N  O  S  W  O  T  E  N  I  S  N
N  M  Y  T  A  T  Y  A  N  A  P  I  F  D  T  S  I  V  S  A
O  N  A  H  P  E  T  S  P  A  O  L  O  J  A  F  E  R  E  I
M  J  E  N  N  I  F  E  R  W  G  I  U  S  E  P  P  E  J  G
```